



THE UNIVERSITY *of* EDINBURGH

This thesis has been submitted in fulfilment of the requirements for a postgraduate degree (e.g. PhD, MPhil, DClinPsychol) at the University of Edinburgh. Please note the following terms and conditions of use:

This work is protected by copyright and other intellectual property rights, which are retained by the thesis author, unless otherwise stated.

A copy can be downloaded for personal non-commercial research or study, without prior permission or charge.

This thesis cannot be reproduced or quoted extensively from without first obtaining permission in writing from the author.

The content must not be changed in any way or sold commercially in any format or medium without the formal permission of the author.

When referring to this work, full bibliographic details including the author, title, awarding institution and date of the thesis must be given.

Centralized Random Backoff for Collision Free Wireless Local Area Networks

Jinho D. Kim



A thesis submitted for the degree of Doctor of Philosophy.

The University of Edinburgh

- December 2017 -

Abstract

Over the past few decades, wireless local area networks (WLANs) have been widely deployed for data communication in indoor environments such as offices, houses, and airports. In order to fairly and efficiently use the unlicensed frequency band that Wi-Fi devices share, the devices follow a set of channel access rules, which is called a wireless medium access control (MAC) protocol. It is known that wireless devices following the 802.11 standard MAC protocol, i.e. the distributed coordination function (DCF), suffer from packet collisions when multiple nodes simultaneously transmit. This significantly degrades the throughput performance. Recently, several studies have reported access techniques to reduce the number of packet collisions and to achieve a collision free WLAN. Although these studies have shown that the number of collisions can be reduced to zero in a simple way, there have been a couple of remaining issues to solve, such as dynamic parameter adjustment and fairness to legacy DCF nodes in terms of channel access opportunity.

Recently, In-Band Full Duplex (IBFD) communication has received much attention, because it has significant potential to improve the communication capacity of a radio band. IBFD means that a node can simultaneously transmit one signal and receive another signal in the same band at the same time. In order to maximize the performance of IBFD communication capability and to fairly share access to the wireless medium among distributed devices in WLANs, a number of IBFD MAC protocols have been proposed. However, little attention has been paid to fairness issues between half duplex nodes (i.e. nodes that can either transmit or receive but not both simultaneously in one time-frequency resource block) and IBFD capable nodes in the presence of the hidden node problem.

In this regard, this thesis firstly proposes a new IBFD MAC protocol for WLANs, and its performance in the presence of hidden nodes is evaluated through simulations. The simulation results show that the proposed protocol maintains a high level of fairness in terms of channel access opportunities between half duplex and full duplex nodes, while the fairness when using a state of the art IBFD MAC is degraded in the presence of hidden nodes. Secondly, the thesis proposes a novel multiple access protocol, called centralized random backoff (CRB), for collision resolution in Wi-Fi networks. In CRB, after a successful reception of a data frame from a distributed station, the virtual backoff algorithm (VBA) operating in the access point (AP) generates a unique backoff state and allocates it to the station by means of the ACK frame. The performance of CRB with the VBA is evaluated through practical Monte Carlo simulations. Simulation results show that CRB significantly improves the throughput performance by reducing collisions to zero without dynamic parameter adjustment, conditioned on the fact that each of the distributed stations has a unique backoff count to each other in an initialisation phase.

Thirdly, the condition of the initialisation phase is relaxed, and all nodes operating using CRB with the VBA are assumed to be initially randomized. This assumption is more practical when the number of active nodes is dynamically varying. In this condition, the thesis presents a tractable numerical analysis to obtain the throughput performance of CRB with the VBA. The analysis results show that the maximum number of nodes that can operate in a collision free state increases (up to the maximum contention window size, i.e. 1024 by default) with time. When using the state of the art collision resolution technique, called deterministic backoff, the maximum number of nodes that can operate in a collision free state is limited to 8. Because of this, CRB with the VBA is more effective when the number of nodes varies with time. Furthermore, the

performance of CRB is tested in a number of situations such as overlapping APs, mixed nodes, and hidden nodes.


Lastly, the thesis proposes a novel adaptive algorithm for CRB, which significantly reduces the time period required for the wireless network to resolve collisions when the number of active nodes is large. The performance of CRB with the adaptive algorithm is theoretically analysed. In addition, results obtained through Monte Carlo simulation validate the numerical analysis results. Furthermore, when nodes using CRB with the adaptive algorithm coexist with the legacy DCF nodes, it provides a higher level of fairness to the legacy DCF nodes compared to using CRB without the adaptive algorithm. Because of the high level of fairness to the legacy DCF nodes, CRB can be easily adopted in the 802.11 standard. Moreover, since a network operating using the adaptive CRB automatically and quickly converges from a decentralized mode to a collision free centralized mode in the absence of legacy DCF nodes, it could be used for fair and efficient femtocell communications (or device to device communications) in unlicensed frequency bands where legacy Wi-Fi devices are expected to be occasionally operating.

Declaration of Originality

I hereby declare that this thesis and the work reported herein was composed and originated entirely by myself in the School of Engineering at the University of Edinburgh.

Jinho D. Kim

Edinburgh, December 2017

Jinho D. Kim 

Acknowledgements

I appreciate the University of Edinburgh for providing good environment to research, and scholarships for my PhD course. I would like to thank following people:

- my supervisors, John S. Thompson and David I. Laurenson, for their advice and guidance. I've learned a lot from my supervisors.
- my mother (Myung-Ok Son), my sisters (Min-Hee Kim and Ran Kim), my wife (Jihyun Kim), and my daughter (Nayul Kim) for their support and encouragement.
- Hogun Park, Jin Sam Kwak, Su-Khiong Yong, Hyukmin Son, Taka Minemura, Jae Kyun Jung, Brian Jung, Chan-Hyun Youn, and so on. They encouraged me when I was preparing to start the PhD course. I always learn a lot from good people around me.
- people in the IDCOR group, including Kimin, Christian, Eric, Miryam, Saurav, Yuki, Alan, Aryan, and so on. I think I'm lucky to have good friends around me.

Lastly, I'd like to thank my father, Dong-Ki Kim (May 1952 - April 2014), for good memories and priceless life lessons.

When I was a little boy about 5 years old, we lived in a small village, where beautiful flowers were growing naturally. One day, my father interestingly said to me that four o'clock flowers open in the early evening automatically. I became very curious about the fact, and the next day about three o'clock I hunkered down on the ground in front of four o'clock flowers and kept closely watching the flowers for hours to see how they actually open. My father brought a small mat to me to

sit comfortably. He might think me interesting. When the sky was getting dark, I finally observed a series of subtle movements of the flowers opening. Then, I ran to my father and talked about what I saw.

Contents

Abstract	ii
Declaration of Originality	v
Acknowledgements	vi
List of Figures	x
List of Tables	xiii
List of Acronyms and Abbreviations	xiv
Glossary	xvi
List of Symbols	xvii
1 Introduction	1
1.1 Contributions to Knowledge	4
1.2 Thesis Structure	6
2 Background Information about Wi-Fi Networks and Full Duplex Radios	8
2.1 Basic Knowledge of the IEEE 802.11 Standards	9
2.1.1 Connection Establishment	10
2.1.2 Modulation and Coding Schemes	11
2.1.3 Packet Structure and MAC Frame Formats	14
2.1.4 Clear Channel Assessment	17
2.1.5 Multiple Access Methods	18
2.2 Review of In-Band Full Duplex Radios	26
2.2.1 Self Interference Cancellation	28
2.3 Summary	30
3 Fair and Efficient Access Protocol for Full Duplex Radios	32
3.1 Review of IBFD MAC Protocols	33
3.2 System Model	35
3.3 Fairness of the Polite IBFD Protocol	36
3.3.1 Busytone Signal Solution for Fairness	39
3.4 Centralized Random Backoff for Collision Resolution in Wi-Fi Networks	41
3.4.1 Packet Collisions in WLANs	42
3.4.2 Review of Collision Free Wi-Fi Networks	44
3.4.3 System Model	47

3.4.4	Concept of Centralized Random Backoff	48
3.5	Simulation Results	53
3.5.1	Evaluation of Busytone Signal Solution	53
3.5.2	Evaluation of Centralized Random Backoff	59
3.6	Conclusion	63
4	Performance Analysis of Centralized Random Backoff	64
4.1	Benefits of Centralized Random Backoff	65
4.2	System Model	66
4.3	Numerical Analysis of CRB	67
4.3.1	Review of CRB	68
4.3.2	Probability of a Virtual Collision	70
4.3.3	Probability of a Collision	76
4.3.4	The Number of Synchronized CRB Nodes	82
4.3.5	Throughput Performance	86
4.4	Simulation and Numerical Results	90
4.4.1	Four Simulation Configurations	91
4.4.2	Simulation Results	93
4.5	Summary	97
5	Centralized Random Backoff with Adaptive Algorithm	99
5.1	Concept of the Adaptive Virtual Backoff Algorithm (A-VBA) . .	101
5.2	Numerical Analysis	103
5.2.1	Average Number of Virtual Collisions	103
5.2.2	Convergence Time for A-VBA	104
5.2.3	Fairness to Legacy Nodes	110
5.3	Simulation Results	119
5.3.1	Simulation Setup	120
5.3.2	Results in Setup-A	122
5.3.3	Results in Setup-B	124
5.3.4	Results in Setup-C	126
5.4	Conclusion	126
6	Conclusions	128
6.1	Summary of the Thesis	128
6.2	Limitations and Future Work	131
	Appendices	148
A	List of Publications	148
B	Proof of the Probability $D_i^l _{(1^{st} \text{ slot})}$	171
C	Proof of the Probability $b_{0,0}$	173

List of Figures

1.1	Wireless devices sharing one access point to access the Internet. .	2
2.1	Seven layers of the OSI reference model.	9
2.2	Infrastructure mode and ad hoc mode.	11
2.3	DSSS and OFDM waveforms.	12
2.4	802.11 modulation techniques.	13
2.5	Overview of the IEEE 802.11 packet structure.	15
2.6	SIFS delay time, DIFS delay time, and ACK frame format.	18
2.7	Operation of the DCF protocol, capture effect, and packet collision.	20
2.8	Operation of the PCF protocol.	22
2.9	Techniques proposed for collision resolution in random access wireless networks.	23
2.10	Interferences in IBFD communications.	27
2.11	An example of in-band full duplex radio diagram.	29
2.12	110 dB self interference cancellation at Rx.	30
3.1	Wi-Fi network configuration.	36
3.2	Unfairness to legacy half duplex nodes.	37
3.3	The polite full duplex MAC protocol.	38
3.4	Fairness issue in the polite full duplex MAC protocol in the presence of the hidden node problem.	38
3.5	The polite full duplex protocol, and the proposed full duplex protocol using a busytone signal.	39
3.6	The unfairness issue in the adaptive deterministic backoff.	46
3.7	A single BSS network configuration.	47
3.8	CRB field in ACK frame.	49
3.9	Allocation of backoff states from the AP.	50
3.10	Virtual backoff algorithm (VBA).	51
3.11	Layered architecture of the simulation.	53
3.12	A two-dimensional simulation setup for testing full duplex MAC protocols in the presence of hidden node problem.	56
3.13	Comparison of the number of accesses granted to each node.	58
3.14	Comparison of throughput elements.	60
3.15	A two-dimensional simulation setup for testing CRB.	61
3.16	Comparison of collision resolution performance.	62

4.1	Wireless local area network configuration.	67
4.2	The flow of frames in CRB. The backoff stage value x in step ⑤ is equal to the number of virtual collisions that have occurred during the VBA.	70
4.3	The pseudo-code of VBA.	70
4.4	The pseudo-code of the operation of a station.	71
4.5	Backoff stages, contention windows, and ranges.	71
4.6	An example of two consecutive time slots granted to a node. . . .	74
4.7	Analytical results and simulation results for N_i^l (i.e. the number of SBCs in Range i when the number of SCNs is l) given $W_0 = 16$ and $m = 6$	76
4.8	Analysis results on Q_i^l and P_i^l ($W_0 = 16$ and $m = 6$).	77
4.9	Markov chain representing the network states during a convergence time period.	77
4.10	Markov chain model of a node operating in CRB. When $l \in [0, n - 1]$, the model represents a collision prone state where ($0 < p < 1$). When $l = n$, the model represents a collision free state where $p = 0$	78
4.11	Markov chain model for analysis of the vector P^j	84
4.12	Analysis results of vector P^j ($W_0 = 16$ and $m = 6$).	85
4.13	Analysis results on the saturation throughput.	89
4.14	Two-dimensional simulation setups.	92
4.15	Simulation results on the throughput of CRB, SRB, and DCF in the single AP setup without hidden nodes ($W_0 = 16$ and $W_m = 1024$). . . .	94
4.16	Simulation results in the mixed nodes scenario.	96
4.17	Simulation results in the two overlapped APs setup (n per each AP=10).	97
5.1	The pseudo-code of A-VBA, where the minimum VBS value i in line 2 is equal to the value N_{vc}^l . The value N_{vc}^l increases with the number of CRB nodes.	102
5.2	CRB field when using A-VBA.	104
5.3	Absorbing Markov chain model of a network operating using CRB with A-VBA.	105
5.4	Analytical results for the number of SCNs over time when $n = 20$ and $\Delta t = 100$ ms. The number of SCNs at different time steps is shown for A-VBA.	108
5.5	Analytic results for the convergence time when $\Delta t = 10$ ms. . . .	109
5.6	Analytical results for throughput performance when $\Delta t = 100$ ms. . .	110
5.7	Markov chain model for the mixed network.	116
5.8	Analytical results for the distribution vector $P_{N(l)}^j$ in the mixed network.	117
5.9	Analytical results for the total throughput compared to the total throughput of the DCF only network.	120

5.10	Analytical results for the throughput per station.	120
5.11	Two-dimensional setups.	121
5.12	Results on total throughput performance.	123
5.13	Simulation results when the number of active nodes increases by 6 every 3 seconds (shown by dashed lines).	124
5.14	Simulation results when $n = 10$ in setup-B.	125
5.15	Total throughput in Setup-C, where the number of active stations connected to each AP is 10.	127

List of Tables

3.1	Simulation parameters for testing the busytone signal solution. . .	55
4.1	The value of Δl between two consecutive slot times.	83
4.2	Parameters used to obtain numerical analysis results.	87
4.3	Simulation parameters.	90
5.1	Parameters used to obtain numerical analysis results.	109
5.2	The values of Δl	115

Acronyms and Abbreviations

A-VBA	Adaptive Virtual Backoff Algorithm
AARF	Adaptive Autorate Fallback Algorithm
ADC	Analogue to Digital Convertor
AP	Access Point
ARF	Autorate Fallback Algorithm
ATIM	Announcement Traffic Indication Message
BCC	Binary Convolutional Code
BEB	Binary Exponential Backoff
BER	Bit Error Rate
BPSK	Binary Phase Shift Keying
BSS	Basic Service Set
CARA	Collision-Aware Rate Adaptation
CCA	Clear Channel Assessment
CDMA	Code-Division Multiple Access
CRB	Centralized Random Backoff
CSMA/CA	Carrier-Sense Multiple Access with Collision Avoidance
CTS	Clear to Send
DCF	Distributed Coordination Function
DIFS	DCF Inter Frame Space
DSSS	Direct-Sequence Spread Spectrum
EIFS	Extended Inter Frame Space
ETSI	European Telecommunications Standards Institute
FCC	Federal Communications Commission
FCS	Frame Correction Sequence
IBFD	In-Band Full Duplex
IBSS	Independent Basic Service Set
IFS	Inter-Frame Spacing
IoT	Internet of Things
ISM	Industrial, Scientific and Medical
ISO	International Organization for Standardization
ITU	International Telecommunication Union
JFI	Jain's Fairness Index
LLC	Logical Link Control

LTE	Long Term Evolution
LTF	Long Training Field
MAC	Medium Access Control
MSDU	MAC Service Data Unit
NS-3	Network Simulator version 3
OFDM	Orthogonal Frequency Division Multiplexing
OFDMA	Orthogonal Frequency-Division Multiple Access
OSI	Open Systems Interconnection
PLCP	Physical Layer Convergence Protocol
PRMA	Packet Reservation Multiple Access
PSDU	PLCP Service Data Unit
QAM	Quadrature Amplitude Modulation
QoS	Quality of Service
QPSK	Quadrature Phase Shift Keying
RBAR	Receiver-Based AutoRate
RTS	Request to Send
SIC	Self Interference Cancellation
SIFS	Short Inter Frame Space
SNR	Signal-to-Noise Ratio
STF	Short Training Field
TDMA	Time Division Multiple Access
UDP	User Datagram Protocol
VBA	Virtual Backoff Algorithm
WLANs	Wireless Local Area Networks

Glossary

- SBC Synchronized Backoff Count. The allocated backoff count from the AP to a SCN, which is being used by the SCN to access the channel.
- SCN Synchronized CRB Node. In CRB, when a source node has successfully received the ACK frame with the backoff state allocated by the AP and uses the backoff state for transmitting the next data frame, the source node is called a synchronized CRB node (SCN).
- UBC Unsynchronized Backoff Count. The independently generated backoff count by an UCN, which is being used by the UCN to access the channel.
- UCN Unsynchronized CRB Node. In CRB, when a source node fails to receive the ACK frame, then in order to start contention again for retransmission the source node independently generates a new backoff state by itself following the current IEEE 802.11 DCF. In this case, the source node is called an unsynchronized CRB node (UCN).

List of Symbols

$A_{N(L_i)}$	The absorbing Markov chain when all nodes are operating using CRB with A-VBA.
A_{mix}	The Markov chain model with respect to the number of synchronized CRB nodes l in a mixed network where CRB nodes coexist with legacy DCF nodes.
A	The absorbing Markov chain when all nodes are operating using CRB with VBA.
D_i^l	The probability of selecting a new non-zero SBC in Range i when the number of SCNs is l .
$E[P]$	Average packet payload size successfully transmitted.
$E[P^*]$	Average length of the longest packet payload involved in a packet collision.
$I_{N(L_i)}$	The vector that represents the network state where $l = L_i$.
L_i	The number of SCNs just before the $(i + 1)$ th adjustment of the minimum VBS value when using CRB with A-VBA.
N_i^l	The number of SBCs in Range i when the total number of SCNs is l .
N_{vc}^l	The average number of virtual collisions per allocated backoff state when the number of SCNs is l .
$P_{N(l)}^j$	The probability distribution of the value l at a time slot j when using CRB with A-VBA, where $N(l)$ denotes the average number of virtual collisions.
P^j	The probability distribution of the value l at a time slot j when using CRB with VBA.
P_i^l	The probability of selecting a unique SBC in virtual backoff stage i when the number of SCNs is l .
$P_{x,y}^{N(L_i)}$	Probability of a state transition from the state that $l = y$ to the state that $l = x$ when the minimum VBS value is equal to $N_{vc}^{L_i}$.
P_{tr}^d	The probability that there is at least one DCF node starting to transmit in a considered slot time.
$P_{tr}^{sn}(l)$	The probability that there is at least one SCN starting to transmit in a considered slot time when the number of SCNs is l .
P_s^d	The probability of a successful slot time with a packet sent by a DCF node.

$P_s^{sn}(l)$	The probability of a successful slot time with a packet sent by a SCN when the number of SCNs is l .
$P_s^{un}(l)$	The probability of a successful slot time with a packet sent by an UCN when the number of SCNs is l .
$P_s(l)$	The probability that a transmission occurring in a considered slot time is successful when the number of SCNs is l .
$P_{tr}(l)$	The probability that there is at least one node starting to transmit in a considered slot time when the number of SCNs is l .
$P_{tr}^{un}(l)$	The probability that there is at least one UCN starting to transmit in a considered slot time when the number of SCNs is l .
$P_{x,y}$	Probability of a state transition from the state that $l = y$ to the state that $l = x$.
S_{crb}^j	The throughput per CRB node at time slot j .
S_{dcf}^j	The throughput per DCF node at time slot j .
S^j	Saturation throughput at time slot j .
S_i	Saturation throughput when the number of SCNs, l , is equal to the value i .
S_k	Throughput per node k .
S	Saturation throughput.
T_c	Average time the channel is sensed busy where a packet collision is involved.
T_s	Average time the channel is sensed busy because of a successful transmission.
W_0	The minimum contention window size in the IEEE 802.11 DCF standard.
W_m	The maximum contention window size in the IEEE 802.11 DCF standard.
Z^l	The probability of selecting zero as a SBC when the number of SCNs is l .
δ	Propagation delay.
σ	Duration of an empty time slot.
τ	Transmission probability of each node in a considered time slot.
$b_{i,k}$	The probability of a backoff state with a backoff stage value i and a backoff count value k .
l^j	The number of SCNs at time slot j .
l	The number of SCNs.
m	The maximum backoff stage value in the IEEE 802.11 DCF standard.
n_c	The number of CRB nodes.
n_d	The number of DCF nodes.

n_{max}	The maximum number of active nodes that can operate in a collision free state.
n	The number of active nodes.
$p(l)$	Collision probability of a packet transmitted by each node when the number of SCNs is equal to l .
$p^{sn}(l)$	The probability of a collision seen by a packet transmitted by a SCN when the number of SCNs is equal to l .
p_c^{sn}	Collision probability of a packet transmitted by a SCN.
$p^{un}(l)$	The probability of a collision seen by a packet transmitted by an UCN when the number of SCNs is equal to l .
p_c^{un}	Collision probability of a packet transmitted by an UCN.
p_c	Collision probability of a packet transmitted by a CRB node.
p_d	Collision probability of a packet transmitted by a DCF node.
p	Collision probability of a packet transmitted by each node.
τ_c	Transmission probability of a CRB node in a considered time slot.
τ_d	Transmission probability of a DCF node in a considered time slot.

Chapter 1

Introduction

The communication capacity of a wireless medium in noise (e.g. thermal noise) is limited [1] whilst demands for wireless communications have increased rapidly in recent decades. In many cases a wireless medium needs to be shared by multiple devices. For example, Figure 1.1 shows a typical Wi-Fi network setup, where stations share the access point to access the Internet.

In order to fairly and efficiently share the medium between multiple devices, they need to follow a set of rules, which is called a wireless Medium Access Control (MAC) protocol. For example, wireless MAC protocols such as the ALOHA protocols [2–4], Packet Reservation Multiple Access (PRMA) protocols [5–8], Carrier-Sense Multiple Access with Collision Avoidance (CSMA/CA), Code-Division Multiple Access (CDMA), Time Division Multiple Access (TDMA), and Orthogonal Frequency-Division Multiple Access (OFDMA) have been studied. For a detailed description about wireless MAC protocols, the reader is referred to [9–13].

Wireless Local Area Networks (WLANs), also known as Wi-Fi networks, are defined by the IEEE 802.11 standards to support various purposes. For example,

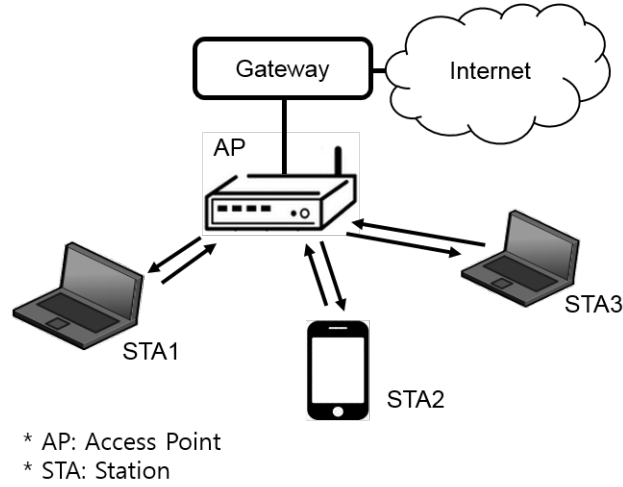


Figure 1.1: Wireless devices sharing one access point to access the Internet.

WLANs have been used for data communications in indoor environments such as offices, houses, and airports. In addition, Wi-Fi networks are also used for distributed sensor networks enabling the Internet of Things (IoT) scenarios [14–16]. Moreover, ad hoc communications defined in the IEEE 802.11 standards are considered to support vehicle to vehicle (and vehicle to infrastructure) communications for intelligent transportation systems [17–19]. This is because such vehicular communication systems require a very low latency (i.e. fast response for transmitted data), and the 802.11 standard techniques could support the requirement. According to [17, 18], random access channel access techniques defined by the 802.11 standard are used for vehicular communications. Furthermore, the ad hoc communications may also be necessary (or useful) in special cases such as natural disasters and battlefield environments [20, 21].

Wi-Fi devices following the IEEE 802.11 standards operate in unlicensed radio bands, called Industrial, Scientific and Medical (ISM) bands. The ISM radio bands are internationally reserved for industrial, scientific, and medical requirements, which is defined by the Article 5 of the International Telecommunication Union (ITU) radio regulations. Uses of the ISM bands may vary slightly subject to national (or regional) radio regulation. For example, in

Europe, use of the ISM bands is governed by the European Telecommunications Standards Institute (ETSI), and in the United States, use of the ISM bands is governed by the Parts 15 and 18 of the Federal Communications Commission (FCC) rules.

In WLANs, in order to fairly share a frequency channel, Wi-Fi devices follow the IEEE 802.11 Distributed Coordination Function (DCF) protocol before transmitting signals. The DCF protocol employs CSMA/CA with Binary Exponential Backoff (BEB), which implements random access to the channel by exponentially increasing the contention window size for each transmission failure in order to avoid consecutive collisions. Each Wi-Fi device operating using the DCF protocol independently selects a random number as its backoff count before transmitting; packet collisions can occur when two or more stations transmit simultaneously. Because of this, the throughput performance of Wi-Fi networks is known to be degraded as the number of contending nodes increases [22–24]. This packet collision issue will be addressed in detail in this thesis.

Wireless communication technologies, such as Wi-Fi and Long Term Evolution (LTE), currently operate in half duplex mode in a single channel. Half duplex communication means that in one time-frequency resource block, a node can either transmit or receive but not both simultaneously. The counterpart of half duplex communication is In-Band Full Duplex (IBFD) communication, where a node can simultaneously transmit one signal and receive another signal in the same band at the same time.

Compared to half duplex communication, IBFD communication has significant potential to improve the communication capacity of a radio band, which makes it an attractive feature for implementation future wireless communication devices [25–28]. However, in order to use IBFD communications in existing wireless networks, a number of MAC issues must be addressed, e.g. inter-node interference,

optimized selection of source and sink nodes, fairness to legacy nodes, uses of a busytone signal, and a residual hidden node problem [29, 30].¹

1.1 Contributions to Knowledge

The main contributions to knowledge of this thesis can be summarised as follows:

- A new IBFD MAC protocol for WLANs is proposed, and the performance of the proposed protocol is evaluated through simulations [31]. The simulation results show that the proposed protocol maintains a high level of fairness in terms of channel access opportunities between a legacy half duplex node using the DCF protocol and a full duplex node using the proposed protocol in the presence of the hidden node problem. In contrast, the fairness index when using the state of the art IBFD MAC proposed in [32] is degraded in the presence of the hidden issue.
- A novel channel access mechanism called Centralized Random Backoff (CRB) with Virtual Backoff Algorithm (VBA) is proposed to resolve packet collisions caused by the random backoff algorithm adopted in the IEEE 802.11 DCF standard [31]. The VBA operating in the access point is designed to mimic the standard DCF protocol for maintaining a high level of fairness (in terms of channel access opportunity) while reducing collisions. Simulation results show that the number of packet collisions between nodes operating using CRB converges to zero, and the throughput performance of the WLANs is significantly improved. In addition, although it does not achieve a collision free network in the presence of legacy DCF nodes, it

¹A node is a hidden node if another node in the same wireless network can neither decode nor sense carrier signals from the first when it communicates with the access point (or the base station).

provides a high level of fairness in terms of the number of channel accesses per node when nodes using CRB coexist with legacy nodes using DCF [33]. This is important because the legacy nodes using DCF have already been widely deployed.

- In order to demonstrate the operation of CRB with VBA, a network simulator based on the NS-3 software package has been developed.² Its source code was released for reference [34], which can be accessed at <http://dx.doi.org/10.7488/ds/2068>.
- A novel adaptive algorithm for CRB, called adaptive VBA (A-VBA), is proposed to resolve the issue that CRB with VBA becomes ineffective when the number of active nodes is large [35]. The performance of CRB with A-VBA is evaluated through numerical analysis and simulation, and the performance is compared to the DCF, CRB with VBA, and an adaptive deterministic backoff mechanism. Evaluation results show that CRB with A-VBA significantly improves the throughput performance by quickly reducing packet collisions regardless of the number of nodes. Since a network operating using CRB with A-VBA automatically and quickly converges to a collision free centralized mode in the absence of legacy DCF nodes, it could be used for fair and efficient femtocell communications (or device to device communications) in unlicensed frequency bands where legacy Wi-Fi devices are expected to be operating.

²NS-3 is an open source project available at <http://www.nsnam.org>.

1.2 Thesis Structure

The rest of this thesis is organized as follows. Following this introduction, Chapter 2 will provide background information about the IEEE 802.11 standard and WLANs in more detail. The IEEE 802.11 standard specifies a number of rules that Wi-Fi devices have to abide by. These rules include clear channel assessment, signal detection mechanism, packet formats, connection establishment, and multiple access methods. In addition, this chapter will also consider major principles in IBFD communication, e.g. interference introduced/caused by nodes capable of IBFD communication and various techniques for self interference cancellation.

Chapter 3 presents a review of existing IBFD MAC protocols for WLANs. Then, this chapter suggests a new IBFD MAC protocol and explains why the proposed protocol is fairer than the state of the art method in more detail. In the second half of this chapter, the packet collision issue in WLANs is described in more detail. After that, the concept of CRB with VBA is introduced for reducing packet collisions in WLANs.

Chapter 4 reviews various techniques devised for collision resolution in Wi-Fi networks, and explains limitations of the previous techniques. Then, this chapter describes how CRB with VBA operates in more detail, and the performance of CRB with VBA is evaluated through numerical analysis. Furthermore, to demonstrate practicality, the performance of CRB with VBA is evaluated in a number of situations such as overlapping APs, mixed nodes, and hidden nodes.

Chapter 5 reviews limitations of CRB with VBA. To resolve the limitations, this chapter suggests a novel adaptive algorithm for CRB, which is called CRB with

Adaptive Virtual Backoff Algorithm (A-VBA). The performance of CRB with A-VBA is evaluated through numerical analysis and practical simulations.

Finally, Chapter 6 summaries the research achievements presented throughout this thesis, and then a number of points remaining to be addressed in future years are described.

Chapter 2

Background Information about Wi-Fi Networks and Full Duplex Radios

In order to provide the preliminary knowledge for this thesis, this chapter introduces several major techniques adopted in the IEEE 802.11 standard. These include clear channel assessment, signal detection mechanism, packet formats, connection establishment, and multiple access methods. In addition, this chapter reviews recently published research about in-band full duplex (IBFD) communications, and describes some principles in IBFD communications.

2.1 Basic Knowledge of the IEEE 802.11 Standards

In the framework of the seven Open Systems Interconnection (OSI) layers of the standard communication model defined by the International Organization for Standardization (ISO) [36], the IEEE 802.11 standards specify a number of rules for the physical layer and the data link layer. As seen in Figure 2.1, the data link layer consists of two sublayers called the Medium Access Control (MAC) layer and the Logical Link Control (LLC) layer. The LLC layer lies above the MAC layer. The MAC layer is dependent on the physical layer, while the LLC layer is generally more independent of the physical layer. For background information to this thesis, some of the IEEE 802.11 standard technologies in the physical layer and the MAC layer are reviewed in this section. For a more detailed description about the IEEE 802.11 standards and WLANs, the reader is referred to [37].

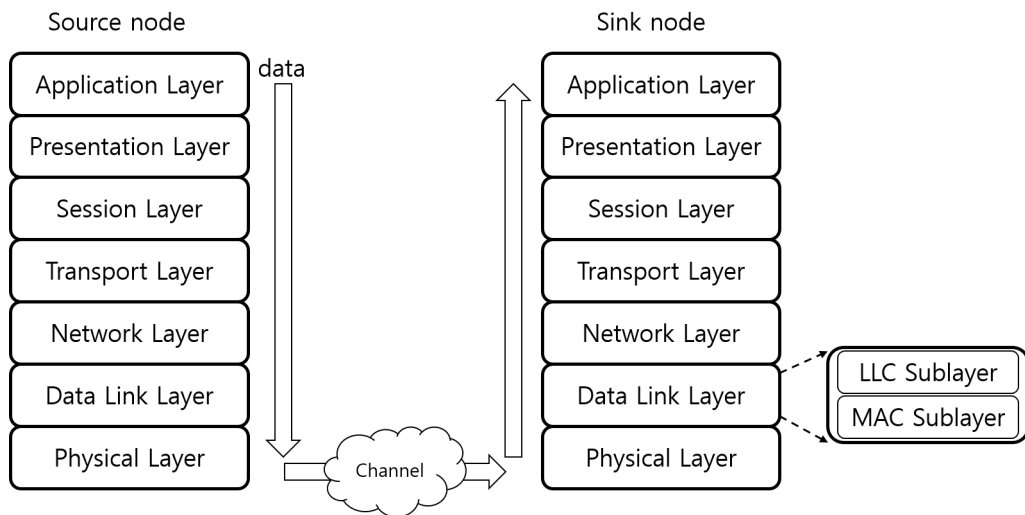


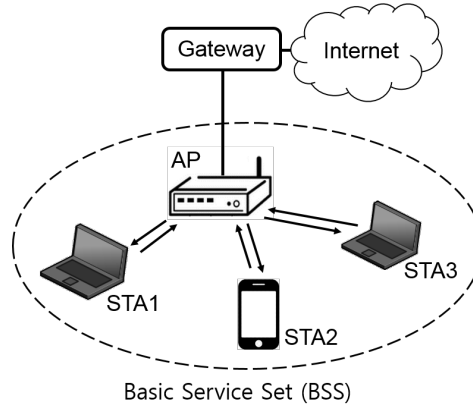
Figure 2.1: Seven layers of the OSI reference model.

2.1.1 Connection Establishment

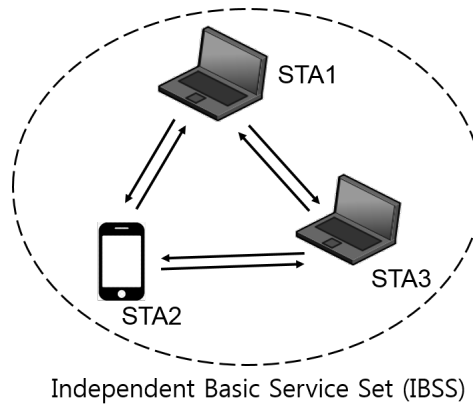
A station operating in the infrastructure mode in the IEEE 802.11 standard initially seeks an Access Point (AP) to make a connection establishment in order to transmit data packets addressed to somewhere over the Internet. The AP generally has a wired connection to the Internet through a backbone network. As shown in Figure 2.2a, such a single AP together with all connected stations is called a Basic Service Set (BSS). The counterpart of the infrastructure mode is the ad hoc mode, where stations placed near each other directly communicate with each other without an AP. The set of such stations is called an Independent Basic Service Set (IBSS), as shown in Figure 2.2b.

Stations discover APs through a *scanning* process, which seeks beacon transmissions from APs or sends out probe request frames which lead to probe response frames from those APs that heard the probe request. The first technique, which is a more generally applicable method, is called passive scanning. The second method is called active scanning. After the sensing or scanning process, stations become aware of basic attributes of the discovered APs. This is because a beacon frame (or a probe response frame) contains basic information about the AP, e.g. timestamp for synchronization, beacon interval, capability of data encryption, supported rates, service set identifier (SSID) for identifying the wireless network, and so on.

After choosing an AP, the station and the AP transmit authentication frames to each other to exchange their identity in terms of security. Then, the station sends an association request frame to the AP to deliver its detailed capability information, and the AP informs the station of specific operating parameters for the station within the BSS. For a detailed description about the connection establishment process, the reader is referred to [12].



(a) Infrastructure mode, where stations communicate through the AP.

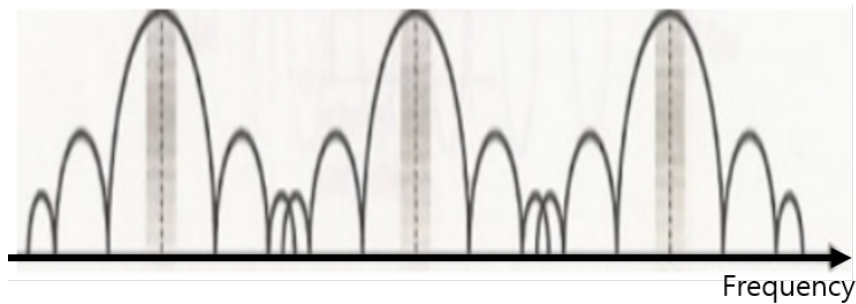


(b) Ad hoc mode, where stations directly communicate with each other.

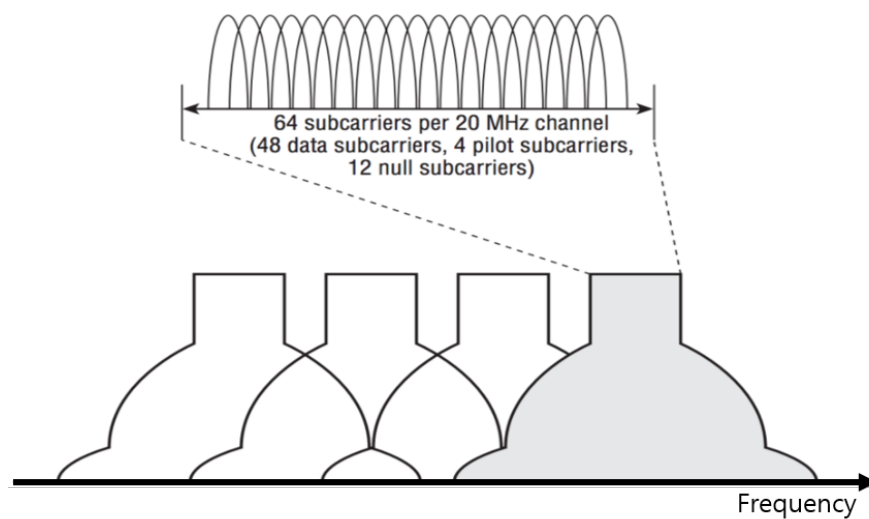
Figure 2.2: Infrastructure mode and ad hoc mode.

2.1.2 Modulation and Coding Schemes

The 802.11b standard introduced in 1999 employs Direct-Sequence Spread Spectrum (DSSS) modulation, while Wi-Fi devices following the 802.11a (introduced in 1999), the 11n (introduced in 2009), and the 11ac (introduced in 2013) transmit signals modulated by an Orthogonal Frequency Division Multiplexing (OFDM) technique to support higher data rates (Refer to Figure 2.3). For example, the maximum data rate supported in the 802.11b standard is 11 Mbps, while the maximum data rate that can be used by Wi-Fi devices following the 802.11a standard is 54 Mbps.



(a) 802.11b DSSS waveform.



(b) 802.11a OFDM waveform.

Figure 2.3: DSSS and OFDM waveforms.

The 802.11g standard introduced in 2003 employs both the DSSS technique (used in 802.11b) and the OFDM technique (used in 802.11a) in the 2.4 GHz band to maintain *backward compatibility* to devices supporting only the 802.11b standard (Refer to Figure 2.4). Implementation of the mandatory features of the 802.11b standard is a prerequisite for 802.11g devices. By doing so, a mobile device supporting 802.11g can communicate at up to 11 Mbps with an (old) AP supporting only 802.11b, while it can use the 54 Mbps data rate if the channel conditions are sufficiently good when it communicates with devices following the 802.11a/g standards. Because of this, the 802.11g standard was

rapidly adopted in the market. Likewise, Wi-Fi devices following the 802.11n standard can communicate with (old) Wi-Fi devices supporting only 802.11g in the 2.4 GHz band. However, the 802.11ac standard published in 2013 employs only the OFDM method, which can support up to 346 Mbps data rate in a 20 MHz channel in the 5 GHz band.

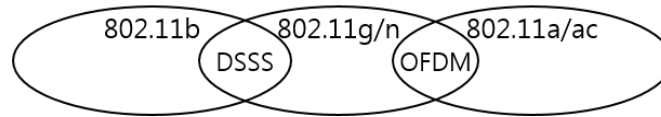


Figure 2.4: 802.11 modulation techniques.

In the OFDM method adopted in the 802.11 standards, an available radio band is divided into a number of sub-channels in frequency, each of which is used to transmit a *subcarrier* signal (Refer to Figure 2.3b). In the case of the 802.11a, a 20 MHz band is evenly divided for 64 orthogonal subcarriers, where the centre subcarrier is always null; the lowest six subcarriers and the highest five subcarriers are also not used as they are guard bands to reduce interference between adjacent channels. Among the remaining 52 subcarriers, four are reserved for transmitting pilot signals (for phase and frequency tracking), and the other 48 subcarriers are used to transmit data. In the 802.11a standard, the duration of each OFDM symbol is fixed at 4 μ s.

In the case of the 802.11a standard, data bits are first scrambled and then encoded before being transmitted. For data encoding, one of the three different coding rates, i.e. a rate $\frac{1}{2}$ code, a rate $\frac{2}{3}$ code, and a rate $\frac{3}{4}$ code, can be applied. Implementation of a rate $\frac{1}{2}$ Binary Convolutional Code (BCC) is mandatory for devices following the 802.11a standard. Then, the coded data bits are grouped into symbols, which consist of the subcarriers (of each 4 μ s duration) modulated by one of the modulation techniques such as Binary Phase Shift Keying (BPSK), Quadrature Phase Shift Keying (QPSK), 16-Quadrature Amplitude Modulation (QAM), and 64-QAM. Implementation of BPSK, QPSK,

and 16-QAM are mandatory for devices following the 802.11a standard, while implementation of 64-QAM is optional.

When BPSK modulation with a rate $\frac{1}{2}$ code is used to transmit a signal, the data rate becomes 6 Mbps (which is the slowest and the most robust format among the available data rates supported in the 802.11a standard), whereas when 64-QAM modulation with a rate $\frac{3}{4}$ code is used, the data rate becomes 54 Mbps (which is the fastest format among the available data rates). A timely selection of a proper combination of a modulation method and a coding scheme, i.e. dynamic rate adjustment, generally depends on the channel conditions. The channel conditions may vary over time and frequency.¹ So, automatic rate adaptation algorithms, such as the Autorate Fallback Algorithm (ARF) [39], the Receiver-Based AutoRate (RBAR) [40], the Adaptive Autorate Fallback Algorithm (AARF) [41], the Collision-Aware Rate Adaptation (CARA) [38], and Minstrel [42], are necessary for efficient transmission in WLANs. However, because it is not regarded as an interoperability (or a compatibility) issue between devices, algorithms for dynamic (and automatic) rate adaptation to the channel condition are device specific and beyond the scope of the 802.11 standards.

2.1.3 Packet Structure and MAC Frame Formats

Recently the OFDM method adopted in the 802.11a/g/n/ac standards has been widely used in Wi-Fi networks, because it can support higher data rates compared to the DSSS technique adopted in the 802.11b standard. In the case of 802.11a/n/ac standards, the waveform of the first 16 μ s portion of a valid signal transmission is completely specified, and is called a *preamble* signal. The first 8 μ s portion of the preamble signal is the Short Training Field (STF) signal

¹The choice of modulation and coding schemes should not be affected by transmission failures caused by packet collisions [38].

as shown in Figure 2.5. This signal is mainly used for packet detection, time synchronization, and automatic gain control tasks. The latter $8 \mu\text{s}$ portion of the preamble signal is the Long Training Field (LTF) signal, which is mainly used for channel estimation.

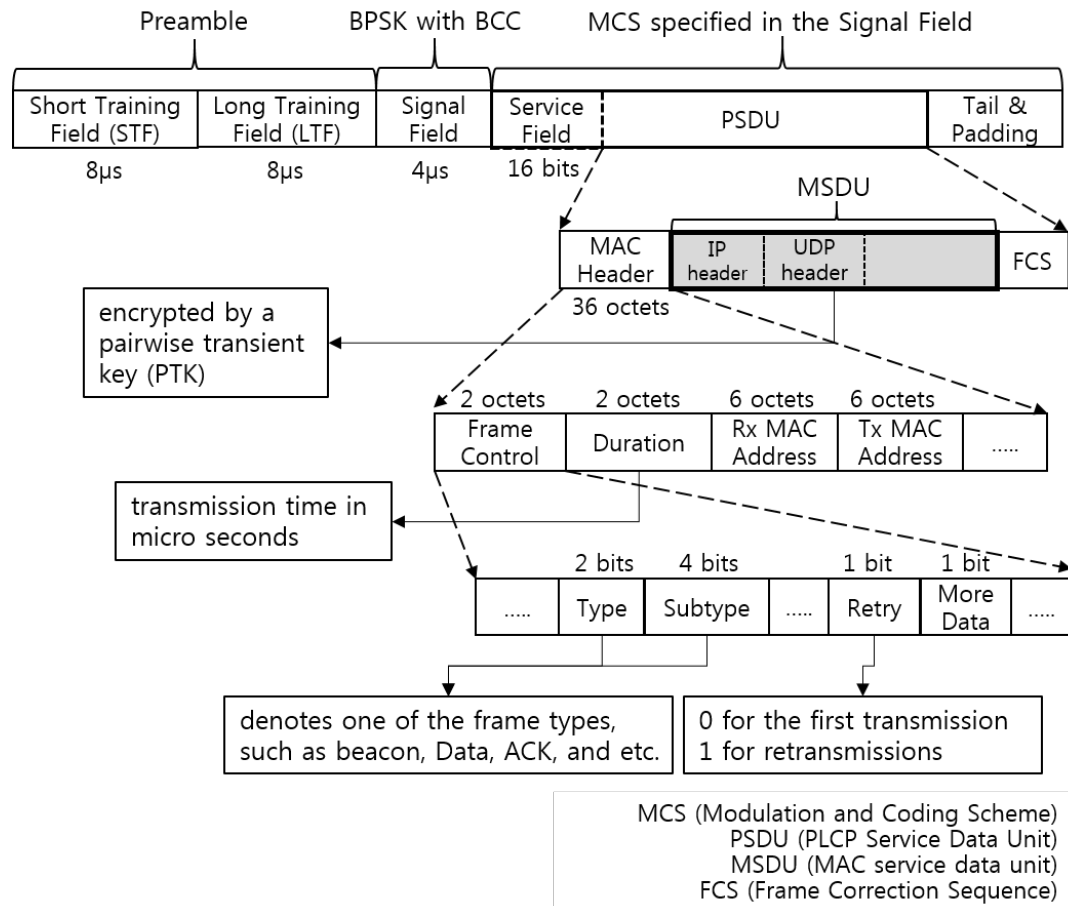


Figure 2.5: Overview of the IEEE 802.11 packet structure.

The LTF signal is followed by the *Signal* field, which is a single OFDM symbol that is used to carry 24 bits of information. The most robust modulation scheme (i.e. BPSK) and the most robust coding scheme (i.e. rate $\frac{1}{2}$ coding) are applied to transmit the signal field. This data conveys the length of the transmission to receiver devices, and it also indicates the modulation and coding schemes applied for the remaining OFDM symbols following the signal field.

These OFDM symbols deliver a PSDU (PLCP² Service Data Unit) and tail bits. As seen in Figure 2.5, a PSDU, which is usually called a *MAC frame*, includes a MAC header, a MAC Service Data Unit (MSDU), and a Frame Correction Sequence (FCS). A MAC header, which is 36 octets in length, includes information such as the frame type, the duration, the source address, the destination address, and so on. The duration field is variable but limited to 32,768 according to the 802.11 standard. This field can be used by neighbouring nodes to set the network allocation vector.

The MSDU contains information specific to the frame type. For example, beacon frames (which are periodically broadcasted by APs) include information about capabilities of the AP, while a normal data frame includes data received from the LLC sub-layer. (MSDUs with data received from the LLC sub-layer are usually encrypted for security purposes). FCS is a code of 4 octets for detecting bit errors, and it is used for checking the integrity of the received frame. In the case of a data frame transmission which requires a positive acknowledgement from the receiver, if a bit error is detected, then the receiver does not transmit an acknowledgement (ACK) frame. If the source node fails to successfully receive the ACK frame, it will retransmit the data frame, as long as the number of retransmissions is less than or equal to the maximum number of retransmissions allowed in the network.

MAC frames can be categorized into three types: management frames, control frames, and data frames. Management frames are generally used for device discovery, connection establishment, and connection termination. Management frames include Beacons, Association Request/Response, Probe Request/Response, Authentication/Deauthentication, Announcement Traffic Indication Message (ATIM), and so on [37]. Control frames are used to assist with the delivery of data frames, and they must be received by all the nodes in

²Physical Layer Convergence Protocol (PLCP)

the network. This means they have to be transmitted by one of the mandatory modulation techniques (i.e. BPSK, QPSK, or 16-QAM) with rate $\frac{1}{2}$ coding. Control frames include ACK, Block ACK, Block ACK Request, Request to Send (RTS), Clear to Send (CTS), Beamforming Report Poll, and so on [37]. The format of ACK frame is shown in Figure 2.6. Data frames, which are generally used to transmit data, include normal best effort Data frames not related with Quality of Service (QoS), Data frames (related with QoS), Null frames, and so on [37].

A time gap between two consecutively transmitted frames is specified by the 802.11 standard, which is called Inter-Frame Spacing (IFS) [37]. For example, in the 802.11a/n/ac standards, when a data frame sent by a source node is successfully received, the receiver has to transmit an ACK frame within a $16\mu\text{s}$ time period. This standardized idle time interval between the end of the signal delivering the data frame and the start of the signal delivering the ACK frame is called the Short Inter Frame Space (SIFS) delay time, which is required for a wireless interface to process a received frame and to decide whether to send an ACK frame or not (Refer to Figure 2.6).

If the channel is sensed idle for the DCF Inter Frame Space (DIFS) time period, each source node with packets to transmit starts the random backoff procedure. The DIFS time period is the standard wait time required before starting the random backoff procedure. In the cases of the 802.11a/n/ac standards, the DIFS time period is $34\mu\text{s}$; in the case of the 802.11b standard, the DIFS time is $50\mu\text{s}$.

2.1.4 Clear Channel Assessment

In order to assess if the channel is occupied or not, Wi-Fi devices have to follow the Clear Channel Assessment (CCA) mechanism specified in the 802.11 standard.

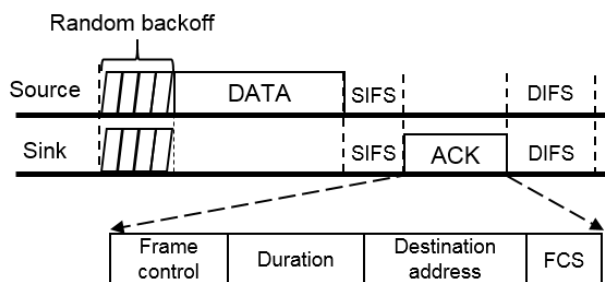


Figure 2.6: SIFS delay time, DIFS delay time, and ACK frame format.

According to the 802.11 standard, the preamble signal at a receive level equal to or greater than the minimum sensitivity level (i.e. -82 dBm for 20 MHz channel spacing) shall indicate that the channel is occupied for the packet transmission time with a probability equal to or greater than 0.9 within $4 \mu\text{s}$ [37]. If the preamble signal was missed, then the receiver shall indicate that the channel is busy for any signal 20 dB above the minimum sensitivity level. Otherwise, the receiver assumes that the channel is clear for it to transmit.

2.1.5 Multiple Access Methods

Distributed Coordination Function

A WLAN consisting of a single AP together with the connected stations usually operates in a single frequency band, and each of the stations (sharing the AP) follows the DCF protocol in order to transmit data frames to the AP. In other words, the stations perform contention (in a distributed manner) to get access to the channel by means of the DCF protocol. The DCF protocol employs CSMA/CA with binary exponential backoff (BEB). Fig. 2.7a describes operation of the DCF protocol. The operation of DCF is as follows. First, each station with data packets in its transmission queue performs the CCA method to check if the channel is being used or not. If the channel is busy (i.e. occupied by other signals), then the station waits for the channel to become idle (e.g. STA2

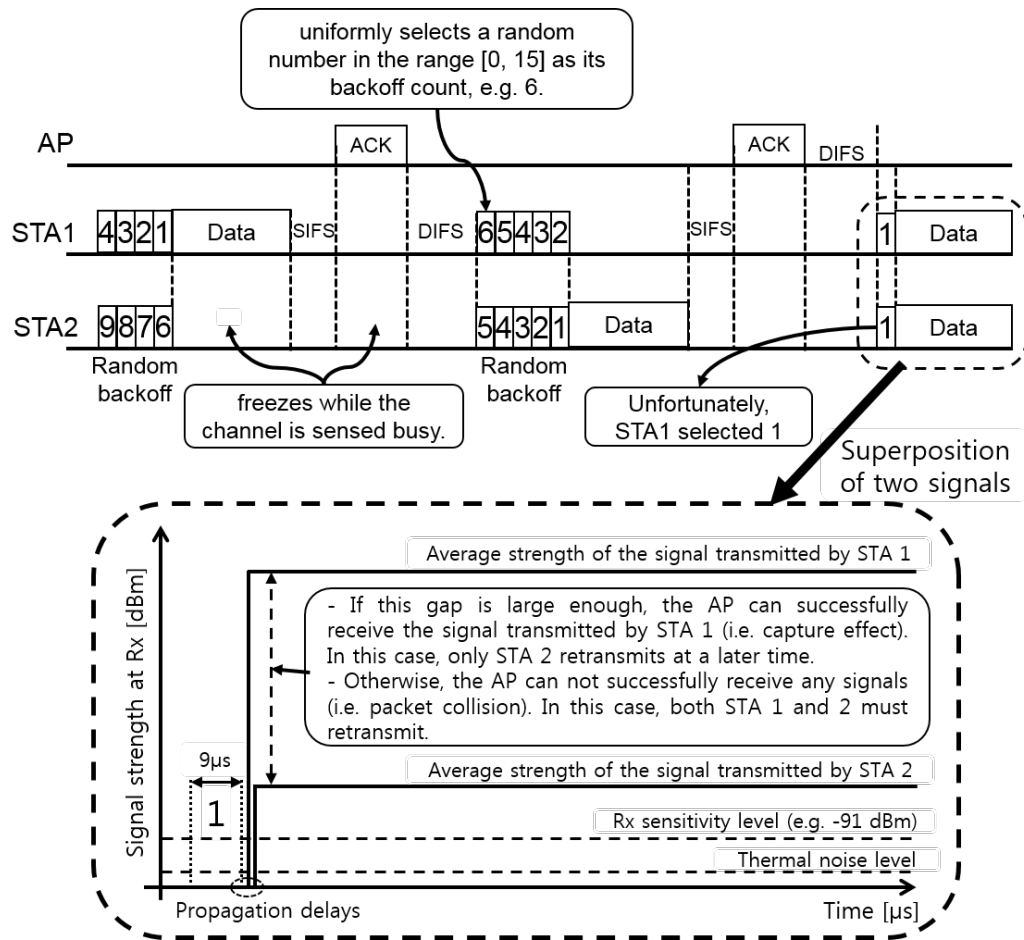
in Fig. 2.7a freezes, while STA1 is transmitting).³ If the channel is sensed idle for the DIFS time, then the station waits for a random backoff time by counting down a random number called a *backoff count* (e.g. the time period denoted by "Random backoff" in Fig. 2.7a). The station uniformly selects a random number from the specified range called the *contention window*, and then it reduces the number by one every *empty time slot*.⁴ When the value reaches zero, the station starts transmitting a signal to the AP. By doing so, multiple stations perform random access to the shared channel.

In DCF, each station in the saturation condition⁵ independently selects a random number as its backoff count before transmitting and it follows the BEB algorithm to increase the contention window size for each transmission failure. Since one of the stations can choose a random number that is equal to one of the backoff counts of the other stations, a superposition of two signals can occur when two or more stations simultaneously contend to transmit (Refer to Fig. 2.7a). For example, in Fig. 2.7a and Fig. 2.7c, if none of the signals are successfully received by the AP, then both the stations must retransmit the data. The event that none of the signals involved in the superposition is successfully received is called packet collision in this thesis. The event that one of the signals involved in the superposition is successfully received is called capture effect (Refer to Fig. 2.7b, where Data signal transmitted by STA1 is successfully received by the AP, and the AP sends ACK frame to STA1.).

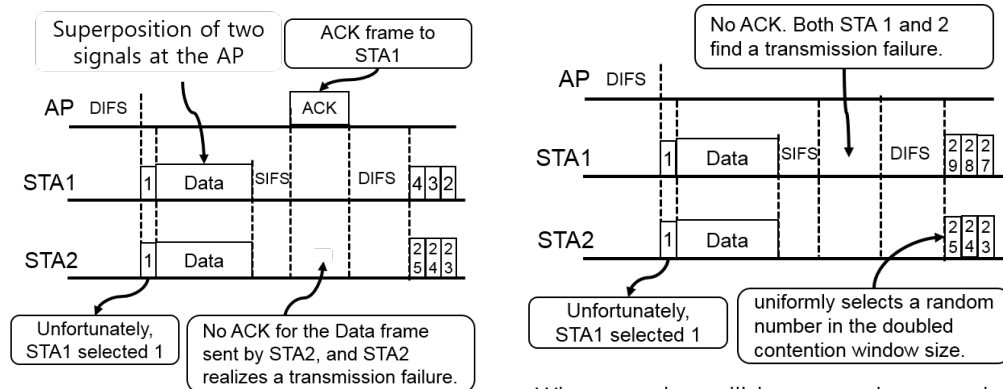
³As shown in Fig. 2.5, the MAC header of each Data frame delivers *Duration* information. This value can be used for neighbouring stations to quickly know/compute the whole waiting time instead of persistently sensing the channel state until it becomes idle. The transmission time protected from the neighbouring stations overhearing the duration information is called network allocation vector (NAV) in the 802.11 standard. Since continuously measuring the channel state consumes much energy, waiting for the channel to become idle based on the overheard duration information is generally more efficient.

⁴In the DCF protocol with the 802.11a/n/ac standards, a 9 μ s of channel idle time is called an empty time slot; in the DCF protocol with the 802.11b standard, a 20 μ s of channel idle time is called an empty time slot.

⁵where the transmission queue of each station is assumed to be always non-empty and each station immediately attempts to transmit a packet after the completion of each transmission.



(a) An example of two stations following the DCF protocol.



When the Data frame sent by STA1 is captured.

When a packet collision occurs between the two Data frames at the AP.

(b) Capture effect when superposition of the two signals occur. (c) Packet collision when superposition of the two signals occur.

Figure 2.7: Operation of the DCF protocol, capture effect, and packet collision.

As the number of contending nodes increases, the number of transmission failures due to packet collisions increases. This significantly degrades throughput performance [22–24, 43–45]. For example, according to the performance analysis model presented in [22], it is known that when the number of contending nodes is 20, the collision probability for a packet becomes 0.47, and because of this, the total throughput is reduced by 20%.

Point Coordination Function

As an optional function in the IEEE 802.11 standard, the AP together with all connected stations can use the point coordination function (PCF) protocol.⁶ In PCF, the point coordinator (PC) running in the AP announces a periodic contention free period (CFP) during which contention free access to the channel is scheduled by the PC (Refer to Figure 2.8). For a detailed description about PCF, the reader is referred to [12]. By doing so, the number of packet collisions can be reduced. However, the PCF protocol has not been widely used due to a couple of limitations [12]. First, traffic to be sent under DCF during a contention period (CP) must wait until the end of the CFP before channel access can be gained. This can severely impact delay sensitive applications. Second, optimization of the ratio between CFP and CP may be too slow to cope with the variation of the number of active stations.

Quality of Service Mechanism

According to the IEEE 802.11e standard, a data packet can be categorized into one of four types: voice data packet, video data packet, best effort data packet, and background data packet. Voice data packets are given the highest channel access priority, because users are sensitive to delays on voice data packets. In

⁶According to the IEEE 802.11 standard, implementation of the DCF protocol is mandatory, while supporting the PCF protocol is optional.

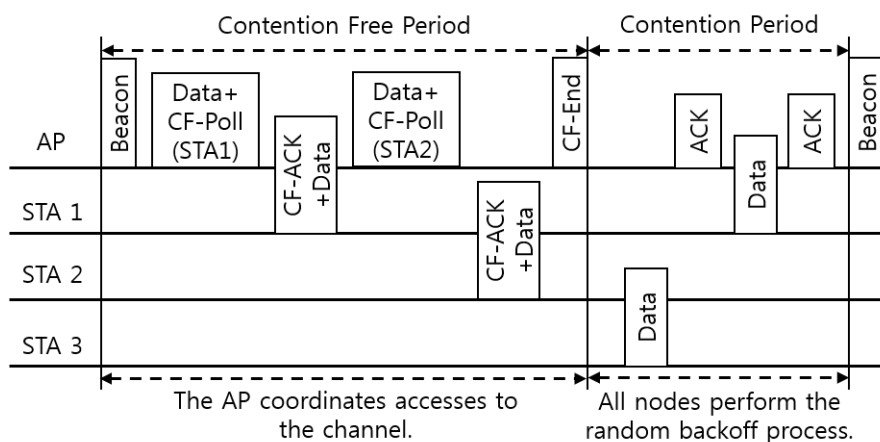


Figure 2.8: Operation of the PCF protocol.

contrast, background data packets are given the lowest channel access priority. This access prioritization, which is also known as the enhanced distributed channel access (EDCA) method, is implemented by adjusting the contention window size and the IFS for each data packet. In addition, the 802.11e standard also provides contention-free access to the channel for a period called a Transmit Opportunity (TXOP). A TXOP is a time interval during which a station can send voice or video data packets without contention. By doing so, the QoS of WLANs in Wi-Fi users' perspective can be improved. However, the fact that the number of packet collisions increases with the number of active nodes is still a feature of such a system, causing throughput degradation.

Various Methods Proposed for Collision Resolution

Collision avoidance or collision resolution techniques have been studied to improve spectral efficiency and energy efficiency while maintaining fairness in terms of channel access opportunity in wireless local area networks. Figure 2.9 shows various techniques proposed for collision resolution in random access wireless networks. The ALOHA protocol presented in [2] in 1970 introduced a random access mechanism for fair multiple accesses from independent (and distributed)

nodes in wireless local area networks. After that, the Slotted ALOHA (S-ALOHA) protocol proposed in [4] introduced discrete time slots, and it increased the maximum throughput. S-ALOHA protocol is used in satellite communications and in contactless radio-frequency identification (RFID) technologies. In addition, the Reservation ALOHA (R-ALOHA) protocol [3] demonstrated that dynamic resource reservation can be achieved by transmitting in a time slot that follows a deterministic number of slots later. By doing so, the collision probability in the reserved time slots can be reduced.

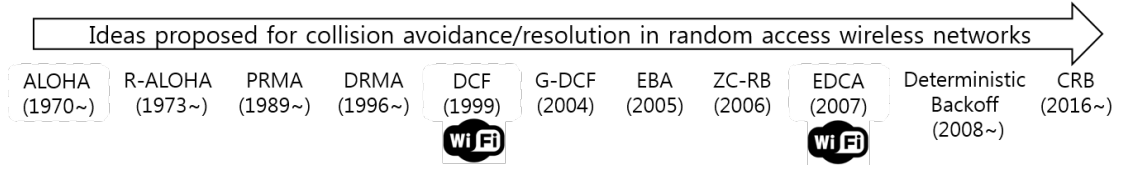


Figure 2.9: Techniques proposed for collision resolution in random access wireless networks.

In the Packet Reservation Multiple Access (PRMA) protocol [5], data packets are divided into two types: periodic information packets and random information packets. Packets delivering voice data are always classified as periodic information packets. When a node successfully transmits a periodic information packet, it explicitly reserves that time slot for the next periodic packet, and the number of subsequent collisions with packets from other nodes is reduced. In order to transmit random information packets, nodes perform the S-ALOHA protocol [4]. By doing so, the quality of voice data communication was improved. In addition, Centralized PRMA (C-PRMA) [8] proposed a combined access method, which employs both a random access and a centralized polling scheme to support the prioritized classes of services and to allow prompt retransmission of corrupted packets to enhance quality of service. However, because of the random access method used in both the PRMA and C-PRMA protocols, the fact that the number

of packet collisions increases with the number of active nodes is still a feature of such a system, causing throughput degradation.

In 1999, the DCF protocol was approved as a standard MAC protocol for Wi-Fi devices, and the DCF protocol has been widely deployed so far. However, since each Wi-Fi device operating using DCF protocol independently selects a random number as its backoff count, packet collisions can occur when two or more stations transmit simultaneously. The collision probability was analysed in a number of studies [22–24]. In addition, the fact that an optimum value of the minimum contention window size exists for a given number of active nodes was explained with a Markov chain model in [22]. However, timely adjustment of the minimum contention window size value when the number of active nodes varies over time is still a complex issue. Moreover, the collision probability increases with the number of active nodes, causing throughput degradation.

In 2005, the *Gentle* DCF (G-DCF) protocol [46], which is based on the standard DCF protocol, proposed that nodes halve their contention window size after a specific number of consecutive successful transmissions. By doing so, the contention window size of the active stations automatically adapts to the number of active nodes, and the collision probability can be maintained at a low value regardless of the number of active nodes. However, the collision probability is still larger than zero, causing throughput degradation.

More recently, dynamic reservation techniques based on the standard DCF protocol were reported in [47–50] in order to reduce the number of packet collisions to zero. In Early Backoff Announcement (EBA) [47], a station announces its future backoff count using the MAC header of its transmitted data frame. All the neighbouring stations that receive the backoff count avoid collisions by excluding the same backoff count when selecting their future backoff value. By doing so, a collision free Wi-Fi network can be achieved. However, the performance of EBA

is significantly limited in practice, because some of the neighbouring stations may not be able to overhear the announced backoff count in the data frame. This is because different data rates have a different transmission coverage to each other. For example, the coverage of a station using a 54 Mbps data rate is much smaller than that of a station using a 6 Mbps data rate.

The operation of Zero Collision Random Backoff (ZC-RB) [48] is similar to that of R-ALOHA, and it is known that ZC-RB also achieves a collision free mode of operation under certain conditions such as fixed number of active nodes. However, in most cases the number of active nodes varies over time, and timely adjustment of the size of each round when the number of active nodes varies over time is still a complex issue.

According to [49, 50], a collision free Wi-Fi network can be achieved by each active node setting its backoff counter to a deterministic value upon a successful packet transmission. This deterministic backoff mechanism, based on the standard DCF protocol, is called CSMA/ECA (Carrier Sense Multiple Access with Enhanced Collision Avoidance) in [49] and also called semi-random backoff (SRB) in [50]. In the case of a failed packet transmission, the station reverts to the standard random backoff procedure of DCF. The performance of the deterministic backoff was experimentally demonstrated in [51]. However, the maximum value number of active nodes that can operate in a collision free state is limited to half of the minimum contention window size. So, to support a larger number of nodes in a collision free state, the minimum contention window size has to be increased.⁷ However, the channel idle time also tends to increase with the window size. Because of this, when the number of active nodes is assumed to change over time, deterministic backoff requires dynamic adjustment of the optimum value of

⁷According to the 802.11 standard, the minimum contention window size is 16 by default.

the contention window size. However, timely adjustment of the value is still a complex issue.

2.2 Review of In-Band Full Duplex Radios

Most wireless devices such as access points, laptops, smart phones need to work as both transmitters and receivers. For example, when a smart phone user makes a video-telephone call to another user, the smart phone needs to function as both a transmitter and a receiver during the call time. In this case, simultaneous transmission and reception by IBFD radios offers the opportunity to significantly improve (or to potentially double) the spectral efficiency. On the other hand, IBFD communication may not be so valuable for a wireless device that generally functions as either a transmitter or a receiver (e.g. wireless sensors, surveillance cameras, wireless displays, and wireless speakers). However, IBFD communications can also be beneficial for such wireless devices. For example, a transmitter device that supports IBFD communication could quickly detect collisions while transmitting, or quickly receive feedback from the receiver device for fast adaptation to the channel [26].

The operation of half duplex radios can be understood from Figure 2.10a, where a node can either transmit or receive but not both at the same time. However, simultaneous transmission and reception in IBFD communications causes the transmitted signal to strongly interfere with the signal being received, which is called self interference (See Node 1 and 2 in Figure 2.10b, and Node 2 in Figure 2.10c). Since the signal of interest being received is typically several orders of magnitude (50-100 dB) weaker than the self interference signal [26, 52, 53], successfully receiving a weak signal of interest in the presence of a strong self interference signal is one of key requirements to enable IBFD radios. Section 2.2.1

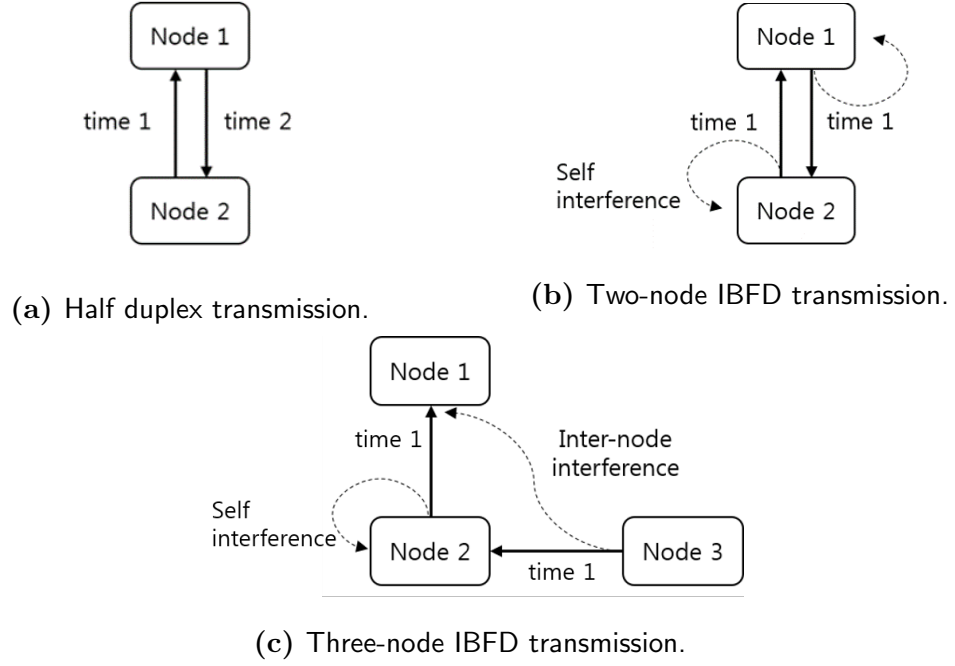


Figure 2.10: Interferences in IBFD communications.

will briefly introduce Self Interference Cancellation (SIC) techniques for enabling IBFD communications.

Figure 2.10b shows a two-node IBFD communication, in which the two nodes transmit and receive simultaneously. The two-node IBFD communication will increase throughput only when both nodes have data packets to send to each other. Figure 2.10c shows a three-node IBFD communication as presented in [26, 28, 54], in which only Node 2 transmits and receives at the same time, while Node 1 receives and Node 3 transmits. In this case, Node 1 will suffer from the inter-node interference signal from Node 3. Supporting three-node IBFD communication along with two-node IBFD communication will increase full duplex transmission opportunities.

A recent surge of interest in IBFD communication may be partly attributed to

the trend of shrinking cell sizes (e.g. femtocells⁸) [26, 57]. In order to achieve a target received Signal-to-Noise Ratio (SNR), the transmit power should scale with pathloss, which increases with distance. Thus, as the spatial coverage becomes smaller, the strength of the self interference signal is reduced with decreased transmit power. According to [52], Wi-Fi devices transmit signals at about 20 dBm (i.e. 100 mW), and the noise floor is assumed to be around -90 dBm. In this case, about 110 dB self interference cancellation is required for a wireless device to isolate its transmitted signals from signals being received from a remote device.

2.2.1 Self Interference Cancellation

Recent research has attempted to reduce self interference by developing novel SIC techniques. Most of the SIC techniques contain some combination of passive suppression, active analog cancellation, and digital cancellation.

Passive suppression methods include antenna separation and circulator isolation. The antenna separation method in [52] uses a circulator to isolate the transmit path and the receive path of a single antenna operating in IBFD (Refer to Figure 2.11). The research in [58] proposed three different methods for reducing self interference signals: cross polarization, directional isolation, and absorptive shielding. This research showed that the passive suppression techniques could achieve more than 70 dB of passive suppression in certain environments. However, the research also described key limitations such as reflection signals from environment and the frequency selectivity in the passive suppression method.

Active analog cancellation means reducing self interference by injecting a cancelling signal into the received signal in the analog domain, which can be

⁸A femtocell refers a small, low power cellular base station, typically designed for use in a home or small business [55, 56].

performed either at the carrier frequency or at analog baseband. Most active analog cancellers work at the carrier frequency [27, 52, 59, 60].

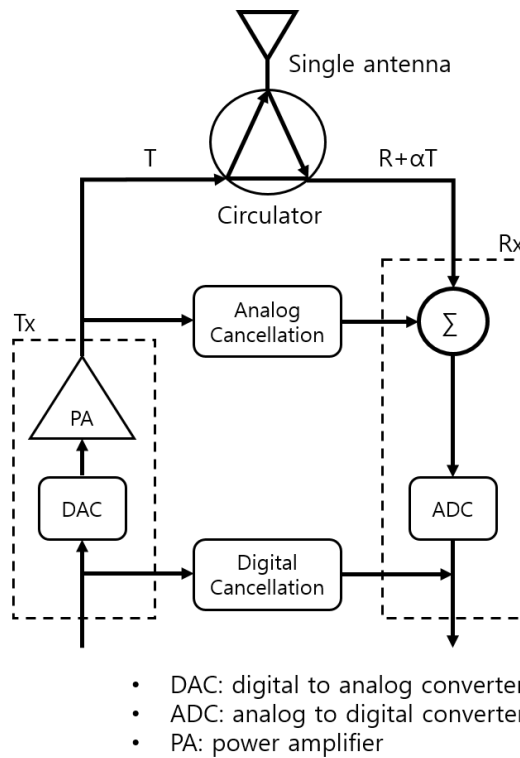


Figure 2.11: An example of in-band full duplex radio diagram.

Digital cancellation occurs in the digital domain after the received signal has been quantized by an Analogue to Digital Convertor (ADC). For example, [52] presented a digital cancellation method for both linear components of self interference and non-linear components of self interference. Reflections from the environment constitute the linear components, while harmonics caused by circuit characteristics contribute to the non-linear components.

The research in [52] presented a new design of full duplex Wi-Fi radios, and maintained that the strength of self interference signals can be reduced to the noise floor level. This result can be described as Figure 2.12. The research in [32] proposed a new design of a full duplex multi-antenna system, and the evaluation

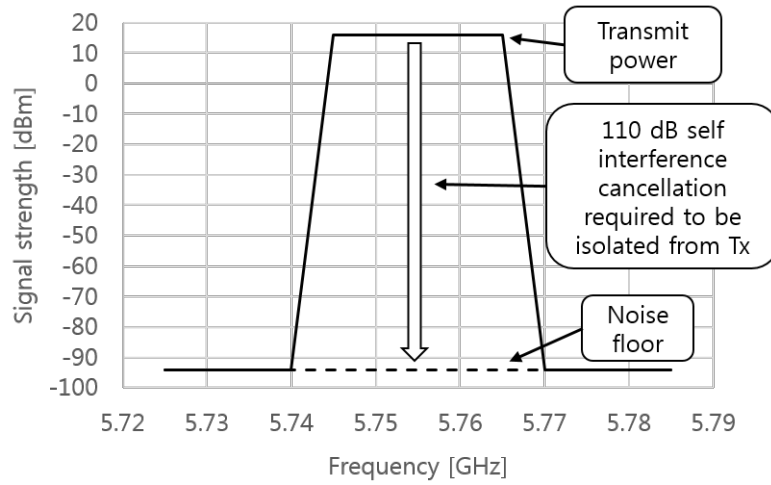


Figure 2.12: 110 dB self interference cancellation at Rx.

results in the research suggested that significant benefits could be gained from using full duplex communications in Wi-Fi networks. In this thesis, it is assumed that each node performs ideal cancellation of the transmitted signal, i.e. cancelling its transmitted signal by 110 dB in its receiver. However, this assumption may not be practical at the moment.

2.3 Summary

This chapter provided basic knowledge about WLANs and full duplex radios. The technical terms and fundamental concepts reviewed in this chapter will be used in the remainder of the thesis.

The performance of collision resolution techniques reviewed in this chapter is significantly limited in practice. This is because the number of active nodes is unknown, and it varies over time. This is because it is difficult to anticipate traffic patterns in WLANs. Moreover, legacy Wi-Fi devices using the DCF protocol have already widely been deployed, and the performance of a collision resolution technique should also be evaluated in a mixed network where nodes using the

DCF protocol coexist with nodes using a collision resolution technique. Channel access opportunities should be fairly distributed between the two different types of nodes operating in the mixed network. Little attention has been paid to this fair coexistence issue. In addition, this thesis will also address a fairness issue when an IBFD radio node coexists with a legacy half duplex node using the DCF protocol in the presence of a hidden node issue. Little attention has been paid to this issue.

Chapter 3

Fair and Efficient Access Protocol for Full Duplex Radios

In order to maximize the performance of IBFD communication capability and to fairly share access to the wireless medium among distributed devices in WLANs, a number of IBFD MAC protocols have been proposed. Recently in [32], a practical IBFD MAC protocol operating with RTS and CTS frames was presented. Based on the IEEE 802.11 DCF standard, the protocol was designed to support IBFD transmission between two nodes when both the AP and a station have data packets to send to each other. However, little attention has been paid to fairness issues between half duplex nodes and IBFD capable nodes in the presence of the hidden node problem. In the first half of this chapter, the fairness of the state of the art protocol will be addressed. In the second half of this chapter, a novel channel access protocol, called CRB, will be proposed to resolve packet collisions in WLANs operating using the DCF. By doing so, the throughput performance is improved. Based on these two contributions, this chapter proposes a fair and efficient IBFD MAC protocol for WLANs.

3.1 Review of IBFD MAC Protocols

IBFD MAC protocols need to support a self interference cancellation mechanism operating of the physical layer to implement simultaneous transmission and reception. For example, in [32, 54, 61–66], RTS/CTS frames are transmitted (following the IEEE 802.11 DCF standard) in a half duplex transmission format before simultaneous transmission and reception of data frames. This allows the 802.11 preamble signals, such as the STF and the LTF, to be used for training the self interference cancellation mechanism in the physical layer.

In [60], a backoff count sharing scheme, called shared random backoff (SRB), was proposed to perform efficient IBFD communications and to prevent neighbouring half duplex nodes being starved by the IBFD communication. However, in this protocol, nodes perform half duplex transmissions when they have only one data packet to send. In addition, since the full duplex nodes do not follow the standard random access (i.e. the 802.11 DCF) for each data frame transmission, the full duplex nodes would cause a fairness issue (in terms of the number accessing the channel) when they coexist with legacy DCF nodes.

After an exchange of RTS/CTS frames in [32, 61, 64, 65], the two nodes involved the IBFD communication simultaneously start to transmit data frames to each other. Meanwhile, in [54, 62, 63, 66, 67], one of the two nodes involved an IBFD communication starts to transmit first, and after a short time interval the other node starts to transmit while receiving the first signal. According to [62, 63, 66], the first (which is transmitting first) captures the signal from the second in the presence of residual self interference, which enables the IBFD communication establishment. In [54], the first (i.e. the AP transmitting first) includes additional information in the header of the data frame being transmitted (to the second) to inform the second of the optimum transmit power to be used when it transmits

to the first. By doing so, the wireless network reduces the inter-user interference, and this optimizes the throughput performance.

In half duplex communications, use of RTS/CTS frames can resolve hidden node problems. This is because hidden nodes set their network allocation vector when they overhear CTS frames. The duration of a network allocation vector is computed based on the duration of the Data frame to be transmitted following a CTS frame. In full duplex communications, two Data frames are transmitted at the same time, but the duration of each Data frame may not be equal to each other. Because of this, the duration of network allocation vector for a successful full duplex communication can not be obtained/computed by means of overhearing RTS/CTS frames. This means that use of RTS/CTS frames could not resolve hidden node problems in full duplex communications.

In the past, uses of a busytone signal would be considered to resolve hidden node problems in half duplex communications [68–70]. In [62, 71–76], techniques using a busytone signal were proposed to prevent nodes involved an IBFD communication from hidden node problems. For example, in a format of simultaneous transmission and reception in IBFD communications, the node that finishes data frame transmission starts to transmit a busytone signal until the other node finishes its transmission. By doing so, the IBFD node sending out a busytone signal avoids a transmission collision by another node which is hidden to the IBFD node that is still transmitting the data frame. In this thesis, a busytone signal is assumed to be a single subcarrier known to nodes in the considered wireless network.

After successful simultaneous transmission and reception of data frames, the nodes transmit ACK frames to each other. In [62], the two IBFD nodes involved in a symmetric dual links transmit ACK frames simultaneously to each other, while two sink nodes of the three nodes involved in an asymmetric dual links send ACK

frames one by one in a half duplex format. This pattern can also be found in other studies; for example, according to [32, 61, 71, 73, 74, 77] the two IBFD nodes involved in a symmetric dual links transmit ACK frames simultaneously to each other, while in [54, 60, 72, 78] the two sink nodes among the three transmit ACK frames one by one in a half duplex format. This is because one of the two source nodes which successfully transmitted a data packet could not receive the ACK frame, if the two sink nodes send ACK frames simultaneously.

3.2 System Model

A network model shown in Figure 3.1 is considered, which includes a single AP, a gateway wired to the AP, wired nodes behind the gateway, and two Wi-Fi stations connected to the AP. All the Wi-Fi nodes operate using the infrastructure mode specified in the IEEE 802.11 standard. In the infrastructure mode, a single AP together with all connected stations (STAs) is called a single BSS (Basic Service Set). The AP and one of the Wi-Fi stations are assumed to support both half duplex and IBFD communications, while the other Wi-Fi station is assumed to support only half duplex communication. (i.e. in this network model, a legacy half duplex user coexists with an IBFD user.) In addition, it is assumed that the AP and the half duplex node use the RTS/CTS protocol to transmit packets to each other.

We assume that the AP and the connected STAs transmit signals with a constant transmission power ($=16$ dBm). In addition, for simplicity, all the Wi-Fi nodes are assumed to support only the 802.11a physical layer (PHY), and the Wi-Fi stations remain stationary (i.e. no mobility). The log distance propagation loss model (exponent=3) in [79] is assumed to apply to the transmitted signals. This loss model predicts the received signal power as a deterministic function of distance.

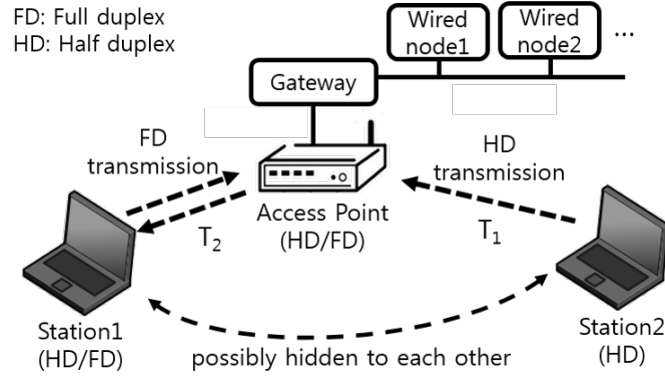


Figure 3.1: Wi-Fi network configuration.

We focus on a single BSS environment, where interference from adjacent wireless networks is assumed to be negligible.

In order to evaluate the throughput performance in saturation conditions (where the transmission queue of each node is assumed to be always non-empty and each active node immediately attempts to transmit a packet after the completion of each transmission), User Datagram Protocol (UDP) data packets are used in this network model, and it is assumed that a real time streaming application is being used by each user. The wired nodes transmit UDP data packets of a constant size to Wi-Fi stations through the gateway and the AP. In a symmetric fashion, the Wi-Fi stations transmit UDP data packets of the same size to the wired nodes.

3.3 Fairness of the Polite IBFD Protocol

In the IEEE 802.11 standard, nodes use a longer wait time called Extended Inter Frame Space (EIFS) rather than the standard wait time (i.e. DIFS¹), if they receive an erroneous packet. The extended wait time, EIFS, is used to allow some

¹The standard wait time required before starting the random backoff procedure in the saturation condition. In the cases of 802.11a/n/ac standards, the DIFS time is 34 μ s.

3.3.1 Busytone Signal Solution for Fairness

In order to solve the fairness issue shown in Figure 3.4, a use of a busytone signal is proposed as described in Figure 3.5. This is designed to require minimal changes to the current Wi-Fi standard. It is assumed that the full duplex transmission opportunity discovery process in [32] is reused. After the discovery process, the AP and the IBFD station transmit a data frame to each other simultaneously. The AP then transmits the ACK1 frame to the IBFD station first, and then the IBFD station transmits the ACK2 frame to the AP.

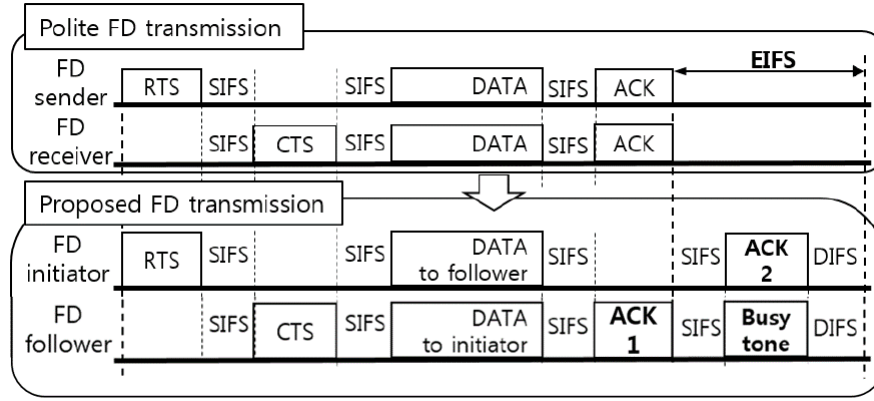


Figure 3.5: The polite full duplex protocol, and the proposed full duplex protocol using a busytone signal.

The *initiator*, one of the two nodes involved in an IBFD communication, initiates the communication by transmitting the RTS frame. The other node becomes the IBFD *follower* when it performs the IBFD transmission with the initiator. After transmitting the RTS frame and receiving the CTS frame, the initiator transmits a data packet at the head of its transmission queue, or transmits a data packet that needs to be retransmitted to the follower. The initiator will conduct a retransmission if it fails to receive an ACK frame for the transmitted data frame.

After transmitting the CTS frame, the IBFD follower waits for the SIFS (Short Inter Frame Space) delay time (required for the wireless interface to process the

received frame and to respond with a response frame), and transmits a data packet to the initiator in IBFD transmission when it has a packet for that node. Unlike the initiator, the follower does not retransmit after it fails to receive an ACK frame for the transmitted data frame, due to its follower status. Any data packet that is not delivered successfully by a station while it is an IBFD follower can be transmitted again when it becomes an IBFD initiator.

If it is assumed that Station1 in Figure 3.1 becomes an IBFD follower, it transmits a packet at the head of its transmission queue or a packet that needs to be retransmitted. However, if the AP becomes an IBFD follower while it is connected to multiple clients, the AP looks for a data packet to send to the initiator nearest to the head of the transmission queue. That is because the data packet at head of the transmission queue may not be addressed to that node. If the AP as an IBFD follower fails to receive an ACK frame for a transmitted data packet, it does not conduct a retransmission for that data packet but places it back into the original order in the transmission queue in order to maintain the order of arrival in the queue.

The two ACK frames presented in Figure 3.5, ACK1 and ACK2 frames, are transmitted at different times. ACK1 is transmitted first in half duplex transmission by the AP. After that, ACK2 is transmitted by an IBFD station. While receiving the ACK2 signal, the AP transmits a *busytone signal* in order to resolve the hidden node problem. The use of a busytone signal in IBFD communications was also introduced in [62, 71, 73] for early detection of a collision of data frames and for alleviating the hidden node problem while transmitting data frames. However, it has not been used before for alleviating the hidden node problem occurring while transmitting ACK frames. It is assumed that the busytone signal is a single subcarrier known by the AP to all stations in the wireless network.

After simultaneous transmission of the ACK2 frame and the busytone, the two IBFD nodes will wait for the *DIFS* delay time rather than the *EIFS* delay time. The ACK1 frame transmitted in half duplex mode by the AP, and it can be successfully received at the hidden legacy node. This means that the hidden legacy node will wait *DIFS* delay time, not *EIFS* delay time. By doing so, all nodes (hidden or not) in the wireless network will wait for the *DIFS* delay time as well. In this way, it is expected that channel access opportunities are evenly distributed between a legacy half duplex station and an IBFD station even though they are hidden from each other. Moreover, in the IEEE 802.11 standard, the *EIFS* time is specified as *SIFS wait time plus ACK transmission time plus DIFS wait time*. This means that the IBFD transmission time of the proposed protocol is equal to that of the polite FD protocol. This implies that the throughput performance of the proposed protocol will be more or less the same as that of the polite FD protocol.

3.4 Centralized Random Backoff for Collision Resolution in Wi-Fi Networks

Wi-Fi devices operate following the IEEE 802.11 DCF in order to fairly use the channel that the devices share. However, the throughput performance of the Wi-Fi networks is known to be degraded due to packet collisions. So, we propose a novel multiple access protocol, called centralized random backoff (CRB) for collision-free Wi-Fi networks. In CRB, after a successful reception of a data frame from a station, the access point allocates a unique backoff state to the station by means of the ACK frame. We evaluate its performance through simulation.

Section 3.4.1 reviews the packet collision issue in WLANs, and Section 3.4.3 describes the system model to be discussed in this section. After that, Section

3.4.4 explains the concept of CRB. Lastly, Section 3.5.2 presents evaluation results on the performance of CRB through simulations.

3.4.1 Packet Collisions in WLANs

In order to fairly use the frequency channel that Wi-Fi devices share, they generally perform the 802.11 DCF before transmitting signals. The DCF protocol employs the CSMA/CA multiple access method with the binary exponential backoff (BEB) algorithm. The BEB algorithm increases the contention window size for each transmission failure. The DCF protocol implements random access by exponentially increasing the contention window size for each transmission failure in order to avoid consecutive collisions. Each station operating using the DCF independently selects a random number as its backoff count before transmitting, and packet collisions can occur when two or more stations contend to transmit simultaneously. It is known that the probability of a collision ($=p$) increases with an increasing number of active (i.e. contending) nodes n [22–24]. Because of this, the throughput performance of Wi-Fi networks is degraded as the number of contending stations increases.

Maximizing network throughput while maintaining fairness between users in terms of channel access opportunity is one of the key goals of wireless MAC protocols [9]. The throughput performance of Wi-Fi networks following the 802.11 DCF protocol decreases due to packet collisions. In the 802.11 DCF, given a number of active nodes n the collision probability p tends to decrease as the minimum (or the initial) contention window size W_0 increases. However, the channel idle time (i.e. empty time slots) also increases with the value W_0 . The fact that an optimum value of W_0 exists for a given value n was explained with a Markov chain model in [22].

The Markov chain model presented in [22] was further developed for more practical conditions, such as a finite retry limit [43], imperfect channel conditions [24, 44, 80–82], multiple data rates [83, 84], QoS prioritization [85, 86], WLANs with multi-hop links [87–89], unsaturated traffic conditions [23, 24], decorrelation between consecutive time slots [90], use of a power saving mode [91], and vehicular ad-hoc networks [92, 93]. In addition, several ideas were proposed to dynamically estimate the value n for timely adjustment of the optimum value of W_0 [94, 95]. However, when the value n varies over time, fast estimation of the value of n and fast adjustment of the optimum value of W_0 (to the estimated value) is still a complex issue in practice.

In order to improve the throughput performance of WLANs by reducing the number of packet collisions, various mechanisms were proposed in [46, 96–100]. It was discussed in [46] the fact that nodes operating using the 802.11 DCF decrease their contention window size to the minimum value (i.e. W_0) after a successful transmission has been based on the assumption that a successful transmission implies that the network is not in a heavily saturated condition. Moreover, [46] proposed the *gentle* DCF (GDCF) protocol, where nodes halve their contention window size after a specific number of consecutive successful transmissions. By doing so, the contention window size of the active stations automatically adapts to the number of active nodes, and the collision probability of WLANs is maintained at a low value regardless of the number of active nodes. However, the collision probability in the WLANs operating using GDCF (or using one of the mechanisms in [96–100]) is still larger than zero, causing throughput degradation.

Recently the IEEE 802.11ax project [101] has been tackling the challenging goal of improving average throughput in WLANs with high density user environments. However, the fact that packet collisions increase with the number of active nodes n is still a feature of such systems, causing throughput degradation.

The number of collisions between Data frames can be reduced by exchanging RTS/CTS frames before transmitting Data frame. Stations overhearing RTS/CTS frames set their network allocation vector (NAV), and do not attempt to access the channel for the duration time specified in the overheard RTS/CTS frames. However, the throughput performance is reduced by the transmission time required for exchanging RTS and CTS frames. Moreover, RTS frames are transmitted following the IEEE 802.11 DCF standard, and collisions still occur between RTS frames. The number of collisions between RTS frames increases with the number of active nodes. Because of this, the throughput performance when using RTS/CTS frames is reduced again.

3.4.2 Review of Collision Free Wi-Fi Networks

Techniques to enable a *collision free* Wi-Fi network, where the probability of a collision p is zero, have been studied for several decades. First of all, the IEEE 802.11 PCF (Point Coordination Function) protocol, which is based on a centralized polling method, was proposed to reduce the number of packet collisions. However, as mentioned in Section 2.1.5 in Chapter 2, it is known that the PCF has several limitations. In contrast to the PCF, each time slot in CRB is randomly reserved by the VBA running in the AP. In order to select a time slot to be reserved, VBA mimics the standard DCF protocol. This results in randomly distributed empty time slots over time (like empty time slots when using DCF), which is necessary to support new entrants using delay sensitive applications.

Review of Collision Resolution Techniques

More recently, dynamic reservation techniques were reported in [47, 49–51, 102–104]. For example, in Early Backoff Announcement (EBA) [47], a station

announces its future backoff count using the MAC header of its transmitted data frame. All the neighbouring stations that receive the backoff count avoid collisions by excluding the same backoff count when selecting their future backoff value. However, the performance of EBA is significantly limited in practice, because some of the neighbouring stations may not be able to overhear the announced backoff count in the data frame. This is because different data rates have a different transmission coverage to each other. For example, the coverage of a station using a 54 Mbps data rate is much smaller than that of a station using a 6 Mbps data rate.

According to [49–51, 102–104], a collision free Wi-Fi network can be achieved by each active node setting its backoff counter to a deterministic value upon a successful packet transmission. This deterministic backoff mechanism is called CSMA/ECA (Carrier Sense Multiple Access with Enhanced Collision Avoidance) in [49, 102] and also called semi-random backoff (SRB) in [50]. In the case of a failed packet transmission, the station reverts to the standard random backoff procedure of the DCF. The performance of the deterministic backoff was experimentally demonstrated in [51], and it was also evaluated with non-saturated traffic, an imperfect channel, and in the presence of legacy DCF nodes [103]. More recently, in [104] a deterministic backoff was also considered to enable collision free multi-hop wireless networks.

The maximum value n that can operate in a collision free state achieved by the deterministic backoff ($=n_{max}$) is limited to the value $\frac{W_0}{2}$. The notation W_0 denotes the minimum contention window size in the 802.11 standard. So, to support a larger number of nodes in a collision free state, the value W_0 has to be increased.² However, the channel idle time also tends to increase with the value W_0 . Because of this, when the value n is assumed to change over time, deterministic backoff

²According to the 802.11 standard, the value of W_0 is 16 by default.

requires dynamic adjustment of the optimum value of W_0 . Timely adjustment of the value W_0 is still a complex issue.

In order to dynamically adjust the minimum contention window size value W_0 , CSMA/ECA [49] proposed a centralized (and explicit) adjustment method using beacon frames, and SRB [50] suggested a distributed (and implicit) adjustment method counting empty time slots. Due to the beacon interval (i.e. 100 ms by default in the IEEE 802.11 standard), the first approach may not be fast enough for timely adjustment of W_0 . The second approach may not be fair when the value n varies over time, because one of the stations may use a different estimate of n to that of the other stations. The unfairness issue between nodes operating using the adaptive deterministic backoff in the second approach can be seen in Figure 3.6, where nodes 1, 2, and 3 are granted a larger number of channel access than that for node 4, when the threshold values α and β on the congestion index are 0.25 and 0.6 respectively as given in [50].

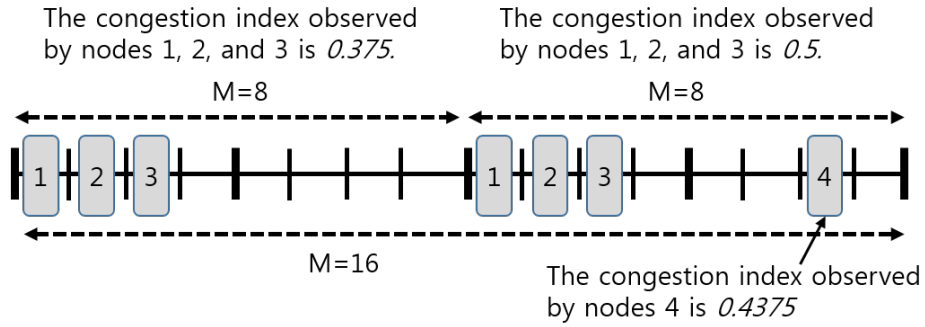


Figure 3.6: The unfairness issue in the adaptive deterministic backoff.

In addition, since legacy Wi-Fi devices perform random access following CSMA/CA to transmit signals, a deterministic TDMA scheduling approach would not be compatible with existing Wi-Fi networks due to interference with the signals transmitted by the legacy devices. Specifically, deterministic TDMA scheduling would cause a fairness issue between the stations using a deterministic TDMA and the legacy stations, when the number of active legacy nodes changes

over time; otherwise, it will require a dynamic parameter adjustment to the distributed stations to maintain fairness. However, the dynamic parameter adjustment is still a very complex issue when the number of users varies over time.

3.4.3 System Model

Figure 3.7 shows a network model to be considered, which includes a single AP, a gateway wired to the AP, and Wi-Fi stations connected to the AP. We first consider CRB in the case where all the nodes transmit in the basic half duplex mode (i.e. half duplex mode not using RTS/CTS frames). After that we evaluate CRB in the case where all the nodes transmit in the proposed IBFD mode using the RTS/CTS frames. We assume ideal channel conditions, and there are no hidden nodes.³

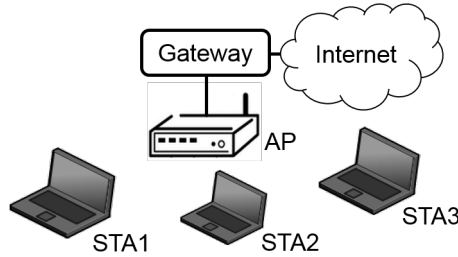


Figure 3.7: A single BSS network configuration.

In order to evaluate the throughput performance in saturation conditions, UDP (User Datagram Protocol) data packets are used in this network model, and it is assumed that a real time streaming application is being used by each user. Unlike when sending TCP (Transmission Control Protocol) data packets, each station sending UDP data packets immediately attempts to transmit a data frame after the completion of each transmission. Because of this, stations with UDP data

³A node is a hidden node if another node in the same BSS can neither decode nor sense carrier signals from the first when it communicates with the AP.

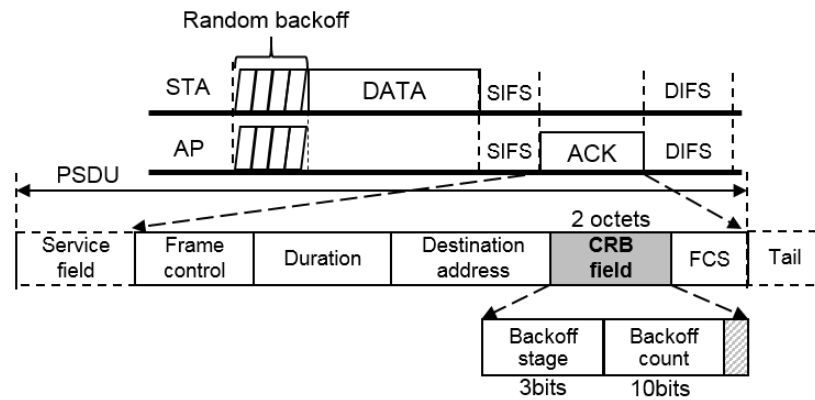
packets in the considered network model remain active continuously, and the number of active nodes, n , can be controlled in simulation.

3.4.4 Concept of Centralized Random Backoff

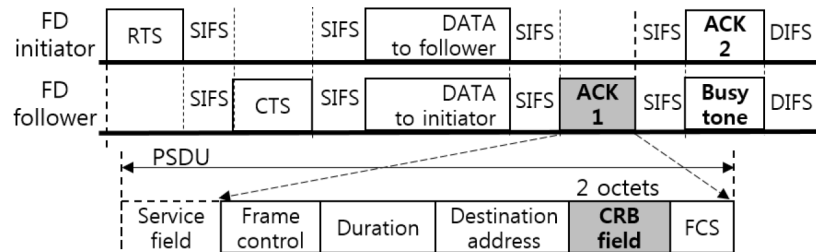
In the CRB mechanism, the AP allocates backoff information to each active node by means of the ACK frame, when the AP has received a successful data frame from a node and discovered that the node has more data packets to send. As seen in Figure 3.8, two octets of the CRB field are added in ACK frames to carry the backoff information. The backoff information means the backoff state to be allocated to the node, which includes two numbers: a backoff stage (BS) and a backoff count (BC). This is generated by the AP before transmitting the ACK frame, and then it is delivered to the node (Refer to steps ② and ⑤ in Figure 3.9). If the data frame is unsuccessfully received (and the node fails to receive the ACK frame before starting contention again), then the node generates a new backoff state by itself following the current IEEE 802.11 DCF.

The AP generates a unique backoff state for each node as described below. After successfully receiving a data frame from STA2 (i.e., after step ④ and before step ⑤ in Figure 3.9), the AP picks a random number (which is a candidate backoff count to be allocated) from the range $[0, 15]$ (*virtual backoff stage 0*) to send to STA2. This internal operation of the AP can be described by the state transitions denoted by ⑨ in Figure 3.10, where p denotes the probability of a collision and the value of W_0 is equal to 16. The notations m and W_m represent the maximum backoff stage value and the maximum contention window size in the IEEE 802.11 DCF specification respectively.

However, if the selected number from the range $[0, 15]$ is the same as the backoff count of another station (*a virtual collision*), for example the backoff count of



(a) CRB field in ACK frame in the legacy half duplex communication.



(b) CRB field in ACK frame in the proposed full duplex communication.

Figure 3.8: CRB field in ACK frame.

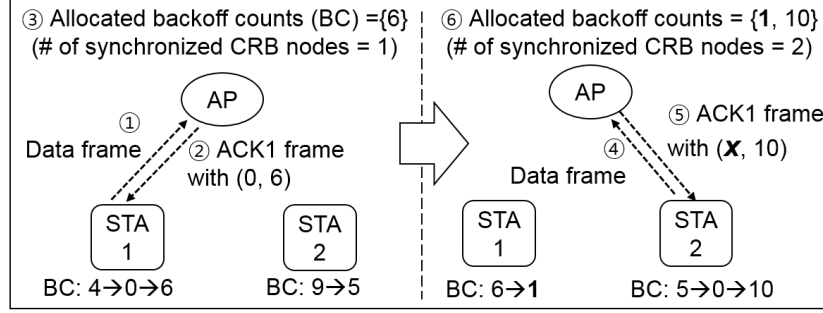


Figure 3.9: Allocation of backoff states from the AP.

STA1 (=1) as shown in Figure 3.9, the AP again picks another random number in the doubled range $[0, 31]$ (*virtual backoff stage 1*). This operation can be described by the state transitions denoted by ⑥ in Figure 3.10, where $W_1 = 32$. (The event where the selected number is the same as one of the existing allocated backoff counts is called a *virtual collision*.) If the newly selected number is unique compared to the backoff count of STA1, then the backoff state is allocated to STA2. (This allocation can be described by the state transitions denoted by ③ in Figure 3.10.) However, if the number selected in $[0, 31]$ is equal to the backoff count of STA1 again, then the AP picks again a random backoff count in the doubled range $[0, 63]$ (*virtual backoff stage 2*). This can be described by the state transitions denoted by ④ in Figure 3.10. The process continues to the point where the range is $[0, 1023]$ (*virtual backoff stage m* which is 6 by default in the 802.11 standard), whereupon random numbers (as backoff counts) are selected in this range until a unique value is obtained. We call this a virtual backoff algorithm (VBA) in the AP. In addition, we allow the AP to allocate a unique backoff state to itself (by referring to the allocated and synchronized backoff counts). In this way, nodes contending at the same time to access the channel can be allocated a unique backoff count.

Note that since the maximum contention window size is given as $[0, 1023]$ by default in the 802.11 standard, no more than 1023 stations can be allowed to establish a simultaneous connection with the AP.

Note that the backoff stage value x in step ⑤ in Figure 3.9 is equal to the number of virtual collisions that have occurred during the VBA.

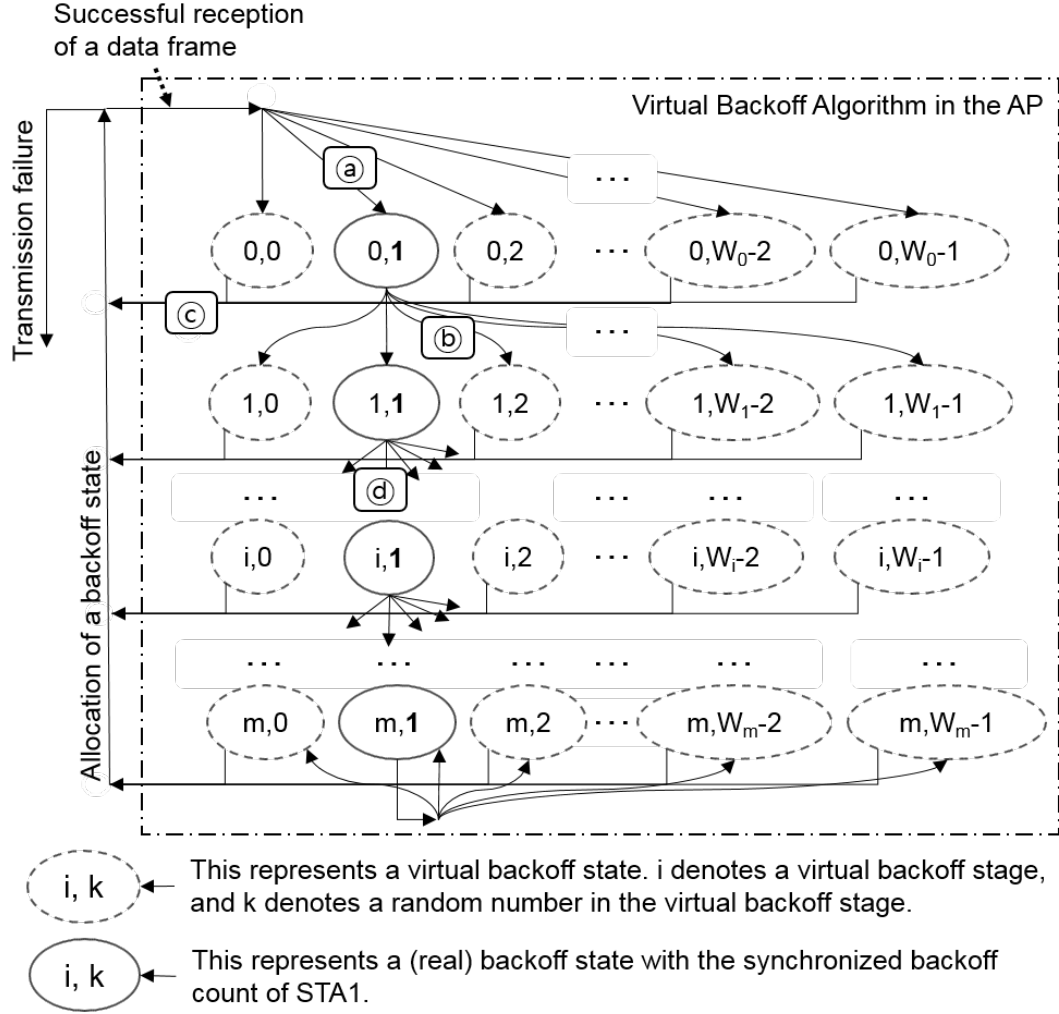


Figure 3.10: Virtual backoff algorithm (VBA).

According to the IEEE 802.11a standard, although it supports eight different data rates in the range from 6 Mbps upto 54 Mbps, only three data rates (i.e. 6 Mbps, 12 Mbps, and 24 Mbps) are mandatory. This means that in order to support backward compatibility to 802.11a devices, one of the three data rates must be used for transmitting control frames such as ACK frames. When 6 Mbps data rate (i.e. BPSK modulation with a rate 1/2 coding) is used for transmitting ACK frames, an OFDM symbol is encoded to carry three octets. A legacy ACK frame

contains 16 octets in its PLCP Service Data Unit (PSDU), which is followed by six tail bits. Therefore, 6 OFDM symbols are required to carry the PSDU and the tail bits. This means that adding two additional octets for including the CRB field in a legacy ACK frame will require an additional OFDM symbol. However, if a data rate of 24 Mbps (i.e. 16-QAM modulation with a rate 1/2 coding) is used for transmitting ACK frames, an OFDM symbol is encoded to carry 12 octets. This means that adding two additional octets for including the CRB field in a legacy ACK frame will not require an additional symbol.

A 6 Mbps constant rate is used to transmit ACK frames in the evaluation in this chapter. Although use of the 6 Mbps or the 12 Mbps options require one additional OFDM symbol, the impact of the additional OFDM symbol is very small compared to the significant throughput gain from using CRB.

Figure 3.10 shows the VBA algorithm doubling the virtual contention window size in every virtual collision until the virtual contention window size becomes equal to the maximum contention window size, W_m . This algorithm was designed to mimic the operation of legacy nodes following the binary exponential backoff (BEB) algorithm in DCF standard protocol, in which legacy nodes double their contention window size after every collision until the contention window size becomes the maximum contention window size, W_m . By doing so, it is expected that a high level of fairness in terms of channel access opportunity between nodes using CRB method and nodes using DCF method would be maintained when they coexist with each other.⁴

⁴In stead of doubling the virtual contention window size in every virtual collision, VBA algorithm could increase the virtual contention window size more rapidly or more slowly. If it increases the virtual contention window size more rapidly, e.g. tripling the virtual contention window size in every virtual collision, then collisions could be resolved more rapidly when CRB nodes do not coexist with DCF nodes. However, it may not achieve a high level of fairness when they coexist with legacy nodes following the BEB algorithm. If it increases the virtual contention window size more slowly, e.g. double the virtual contention window size in every two or three virtual collisions, then collisions could not be resolved rapidly even when CRB

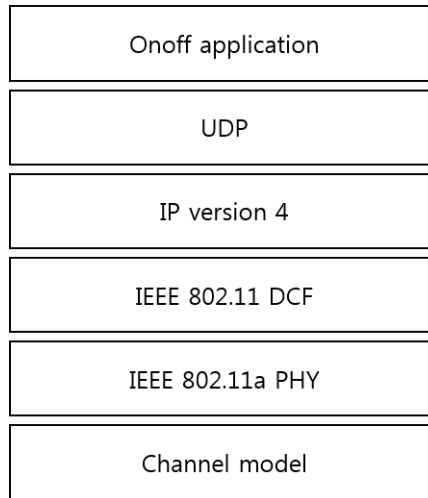


Figure 3.11: Layered architecture of the simulation.

3.5 Simulation Results

A network simulator has been developed based on the Network Simulator version 3 (NS-3) source code in order to evaluate the proposed solutions in this chapter.⁵ Figure 3.11 shows a layered architecture of the simulation implemented. This section presents simulation results on the busytone signal solution and the CRB mechanism.

3.5.1 Evaluation of Busytone Signal Solution

Detailed simulation configurations are described first, and then the simulation results are presented.

nodes do not coexist with DCF nodes. A dynamic adaptation method of the virtual contention window size is discussed in Chapter 5.

⁵NS-3 version 3.22. This is an open source project available at <http://www.nsnam.org>.

Simulation Setup

Simulation parameters are presented in Table 3.1. Each of the repeated simulations runs for 30 seconds, where the first 10 seconds is omitted to remove the effect of traffic generated in connection establishment procedures. It is assumed that the network becomes a statistically stationary network state, and such simulation time was chosen to collect a sufficient number of data. The simulation was repeated 100 times to obtain average values.

In this simulation, the bit error rate (BER) model presented in [105] is applied to decide if a MAC frame is successfully received or not. According to the BER model, each node first obtains the signal-to-interference-plus-noise ratio (SINR) values based on the received signal strength. Then, it computes the BER values, and obtains the PER (Packet Error Rate) value. Lastly, the PER value is compared to a uniformly selected random number between zero and one. If the PER value is smaller than the random number, then the simulation decides the MAC frame is successfully received. Otherwise, the transmission of the MAC frame is failed, and the MAC frame must be retransmitted.

It is assumed that each node performs ideal cancellation of the transmitted signal, i.e. cancelling its transmitted signal by 110 dB in its receiver, (Refer to Figure 2.12).

In order to evaluate the busy tone signal solution, a two-dimensional simulation setup with three wireless nodes shown in Figure 3.12 is considered. The AP and the legacy half duplex STA use the RTS/CTS protocol to transmit packets to each other, and the AP and the IBFD STA use the proposed full duplex MAC protocol to each other. The legacy half duplex STA and the IBFD STA in Figure 3.12 are symmetrically located at a distance ($=d$) from the AP at opposite sides of the cell. So, it is expected that the legacy half duplex STA and the IBFD STA will cause and suffer hidden node problems to each other if the value of d is large

Table 3.1: Simulation parameters for testing the busytone signal solution.

Parameters	Value
Wireless standard	IEEE 802.11a PHY and DCF MAC
Frequency channel	5.0 GHz
Bandwidth	20 MHz
Simulation time	30 seconds
Propagation loss model	Log distance model (exponent=3)
Transport layer protocol	UDP
UDP payload length	1400 bytes
Modulation & coding for ACK frame	BPSK with a rate $\frac{1}{2}$ coding
Available data rates	6, 9, 12, 18, 24, 36, 48, and 54 Mbps
Transmission queue	Single queue
Traffic model	Full buffer
Tx power	16 dBm
Rx sensitivity	-91 dBm
Noise floor	-94 dBm
Self interference	-94 dBm
CW_0	16
$CW_{m=6}$	1024
empty time slot interval	9 μs
SIFS time interval	16 μs
DIFS time interval	34 μs
Bit Error Rate (BER) model	Reference [105]

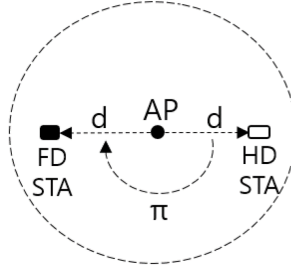


Figure 3.12: A two-dimensional simulation setup for testing full duplex MAC protocols in the presence of hidden node problem.

enough. In this setup, the number of channel accesses granted to each node to transmit the RTS frames is investigated.

In this simulation, Data packets are transmitted following UDP protocol in the transport layer, and the number of active nodes, n , is controlled by saturating each node. The value n when using TCP protocol might not be controlled because of the retransmission mechanism implemented in TCP protocol. However, it is expected that CRB method would also be beneficial for reducing packet collisions when using TCP protocol.⁶ The performance of CRB method with TCP protocol could also be tested in NS-3, but this issue is beyond the scope of this thesis.

Simulation Results

Figure 3.13 shows that as the distance d increases, the number of accesses granted to each node to transmit the RTS frames (i.e. the number of backoff counter expirations per second) tends to decrease. That is because the simulation runs for 30 s (constant time), while the three nodes lower their data rate as the value of d increases. The figure also shows that as the distance d increases above 60 metres, the legacy half duplex STA and the IBFD STA become hidden nodes to each other. This results in a dramatic increase in the number of accesses granted

⁶This is because the AP when using TCP protocol becomes very active to send TCP ACK packets, and packet collisions still occur between the AP and stations. Note that TCP ACK packets are categorized as Data frames in the MAC layer.

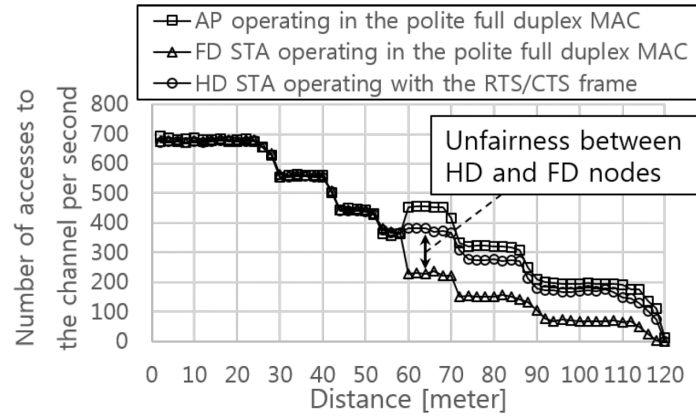
to the AP compared to those for the legacy half duplex STA and the IBFD STA, which can be seen in both Figure 3.13a and Figure 3.13b.

In the hidden node scenario, after a successful polite full duplex transmission between the IBFD STA and the AP, the IBFD STA waits for *EIFS* time while the legacy half duplex STA waits for *DIFS* time. That explains the difference (unfairness) between the number of accesses granted to the legacy half duplex STA and the IBFD STA shown in Figure 3.13a. A fair MAC protocol should not penalize some users of the system arbitrarily. In this regard, Jain's Fairness Index (JFI) is computed in equation (3.1), and compared between the polite full duplex protocol and the proposed protocol.

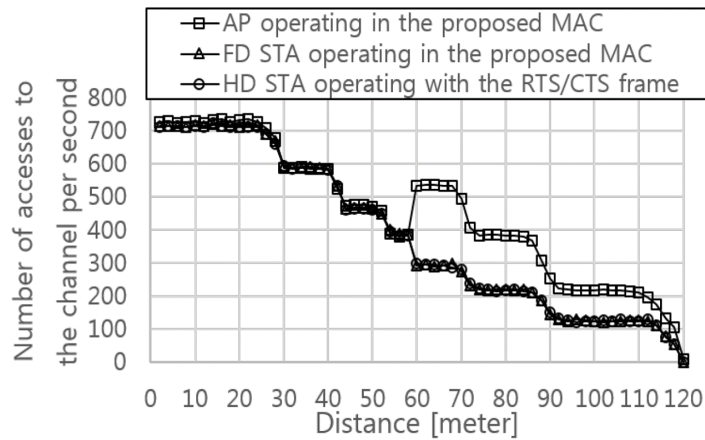
$$\text{Jain's Fairness Index} = \frac{(x_{HD} + x_{FD})^2}{2 \cdot (x_{HD}^2 + x_{FD}^2)} \quad (3.1)$$

The notations x_{HD} and x_{FD} represent the average number of accesses granted to the legacy half duplex node and the IBFD node, respectively. When they are randomly placed in the range of 1 to 110 metres from the AP, the average value of the fairness index is calculated as 0.92. However, when the AP and the IBFD STA operate in the proposed MAC protocol, the IBFD STA has more or less the same number of granted accesses to the channel compared to that of the legacy half duplex STA even though they are placed in a hidden node configuration, which is shown in Figure 3.13b. In this case, when they are randomly placed in the range of 1 to 110 metres from the AP, the average value of the fairness index is calculated as 1.00.

Figure 3.14 shows a comparison of the throughput performance of the polite full duplex and the proposed full duplex protocols for two different values of d . All the three nodes in the figure use 18 Mbps constant data rate. A thick arrow in the figure represents the traffic flow from a half duplex node or from a full duplex initiator. A thin arrow inside the thick arrow between the AP and the



(a) Polite full duplex MAC protocol. The average of Jain's fairness index between the IBFD station and the legacy half duplex station is equal to 0.92.



(b) Proposed full duplex MAC protocol. The average of Jain's fairness index between the IBFD station and the legacy half duplex station is equal to 1.0.

Figure 3.13: Comparison of the number of accesses granted to each node.

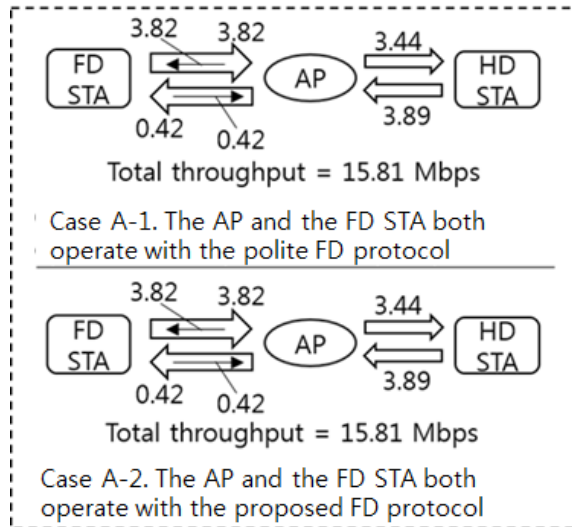
IBFD STA represents the traffic flow from the full duplex follower to the full duplex initiator. The figure shows that the data rate from the AP to the half duplex STA is much larger than that from the AP (as a full duplex initiator) to the IBFD STA. For example, in Case A-1, the data rate from the AP to the half duplex STA is 3.44 Mbps while that from the AP (as a full duplex initiator) to the IBFD STA is only 0.42 Mbps. This is because the AP has a single transmission queue, and a packet addressed to the half duplex STA is usually placed at the head of the AP's transmission queue. Packets addressed to the IBFD STA and placed near the head of the AP's transmission queue are transmitted to the IBFD STA from the AP when the AP is a full duplex follower. This characteristic of the mixed network where legacy half duplex nodes coexist with IBFD nodes was also reported in [106].

In addition, Figure 3.14a shows that the two different full duplex protocols have the same throughput performance when the IBFD STA and half duplex STA are not hidden to each other. This is because the full duplex transmission time of the proposed protocol is equal to that of the polite full duplex protocol. Figure 3.14b also shows that the total throughput when using the proposed protocol (i.e. 14.55 Mbps) is higher than that of when using the polite full duplex protocol (i.e. 15.37 Mbps). This is because the number of packet collisions caused by the hidden node effect has been reduced.

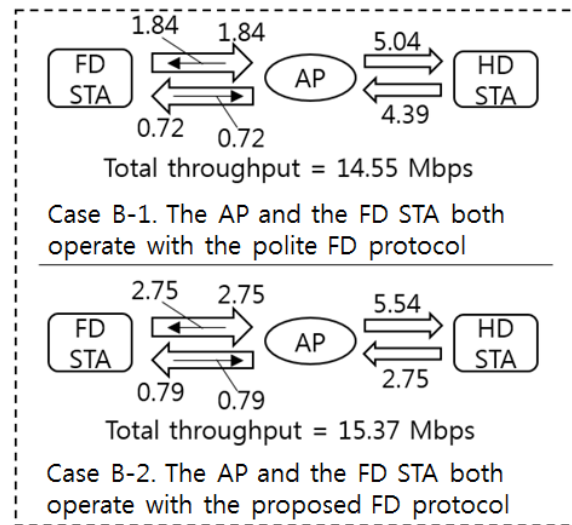
3.5.2 Evaluation of Centralized Random Backoff

Simulation Setup

In order to evaluate collision resolution performance of CRB, it is tested with the two different protocols: the basic MAC protocol in the legacy half duplex mode (as shown in Figure 3.8a) and the proposed full duplex MAC protocol (as



(a) $d=55$ [metre] (no hidden node).



(b) $d=65$ [metre] (the two stations are hidden to each other).

Figure 3.14: Comparison of throughput elements.

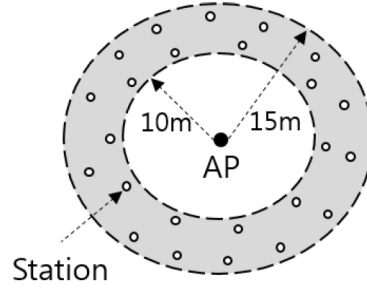


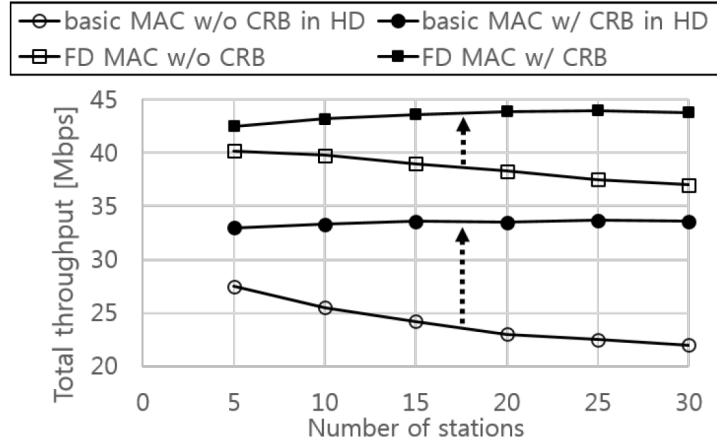
Figure 3.15: A two-dimensional simulation setup for testing CRB.

shown in Figure 3.8b). As shown in Figure 3.15 stations operating using CRB are randomly and uniformly placed at a range of 10 to 15 metres from the AP. There is no hidden node in the single BSS environment, and all the nodes use a constant data rate of 54 Mbps. Simulation parameters are summarized in Table 3.1.

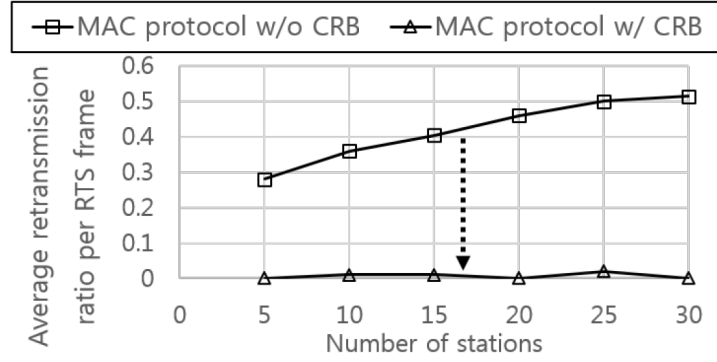
In this simulation, we assume that each of the distributed stations has a unique backoff count to each other in the initialisation phase. For example, the AP simply transmits a new unique backoff count to each station, which all the stations start to use at a specified time.

Simulation Results

Figure 3.16a shows that throughput of the two MAC protocols not using CRB decreases as the number of nodes increases. This is because the number of collisions caused by the random access algorithm increases with the number of stations. However, the total throughput of the two protocols operating using CRB does not decrease as the number of stations increase. The figure shows that the total throughput of full duplex nodes using CRB has been improved by 4% to 12% (depending on the number of stations) over the state of the art full duplex MAC protocol. Moreover, the total throughput of half duplex nodes using CRB has been improved by 10% to 38% compared to that of the legacy half duplex nodes following the IEEE 802.11 standard.



(a) Total throughput.



(b) Retransmission ratio.

Figure 3.16: Comparison of collision resolution performance.

In addition, Figure 3.16b shows average retransmission ratios, which are calculated in the simulation as the total number of retransmitted data frames (or the total number of retransmitted RTS frames in the proposed full duplex protocol) divided by the total number of transmitted data frames (or the total number of transmitted RTS frames). The retransmission ratio of the stations operating in CRB does not increase as the number of stations increases. This is shown to be more or less the same, and below 1%.

Lastly, in the simulation setup, RTS frames are shorter than data frames in terms of transmission time, which means that the wasted time caused by a collision of RTS frames is much less than that for a collision of data frames. This difference

can be seen in Figure 3.16a by the fact that the range of CRB gain of the proposed full duplex protocol is lower than that of the legacy half duplex protocol.

3.6 Conclusion

In this chapter, two solutions have been proposed, and evaluated through simulations. The first solution is the use of a busytone signal for a higher level of fairness in the presence of hidden nodes. The simulation results showed that the average Jain's fairness index (in terms of the number of channel accesses granted) between the legacy half duplex node and the full duplex node has been significantly improved (JFI= 1.00) compared to that of when using the polite full duplex MAC protocol (JFI= 0.92).

The second solution proposed in this chapter is the collision resolution method, called CRB. It was demonstrated through simulation that the total throughput of full duplex nodes using CRB has been improved by 4% to 12% (depending on the number of stations) over the state of the art full duplex MAC protocol. Moreover, the total throughput of half duplex nodes using CRB has been improved by 10% to 38% compared to that of the legacy half duplex nodes following the IEEE 802.11 standard.

In this chapter, we assumed in the evaluation of CRB that each of the distributed stations has a unique backoff count to each other in the initialisation phase. This assumption is relaxed in Chapter 4, and the performance of CRB is tested in a number of situations such as overlapping APs, mixed nodes, and hidden nodes. Moreover, Chapter 4 presents a tractable numerical analysis on the throughput performance of CRB.

Chapter 4

Performance Analysis of Centralized Random Backoff

This chapter presents a Markov chain model which can be used for analysing how a Wi-Fi network operating using CRB converges to a collision free state, and the throughput performance of CRB is obtained from the model. The time period required for the wireless network to move toward a collision free state is called the convergence time, during which the network automatically moves from the distributed mode to the collision free centralized mode. In Chapter 3, it was assumed that each of the CRB nodes can have a unique backoff count with respect to each other during an initialisation phase, and the convergence time was not considered in the evaluation. However, this assumption may not be realistic when the number of active nodes n changes over time.

The analysis results on the performance of CRB are compared to that of a deterministic backoff mechanism. Moreover, the performance of CRB is evaluated in a number of simulation configurations such as overlapping APs, mixed nodes, and hidden nodes. Evaluation results show that CRB significantly improves the

throughput performance by reducing the number of packet collisions, and it allows a larger number of nodes to operate in a collision free state (where the probability of a packet collision, p , is zero) without dynamic parameter adjustment.

Section 3.4.2 of this chapter will review benefits of the centralized random backoff method proposed in Chapter 3. Section 4.2 describes a system model, where the performance of CRB will be evaluated. Section 4.3 presents performance analysis of a WLAN operating using CRB. Section 4.4 shows simulation results to validate the analytic results obtained in the previous section, and compares its performance to those of the DCF protocol and a deterministic backoff technique. Section 4.5 summarizes this chapter.

4.1 Benefits of Centralized Random Backoff

The concept of CRB was initially proposed in Chapter 3, where backoff states are generated by the AP and allocated to the connected stations by means of ACK frames. The ACK frames from the AP are generally more reliable than the data frames from distributed stations for several reasons. For example, firstly, ACK frames are transmitted after a SIFS delay time without a contention process, while data frames are transmitted after a contention period through the random backoff procedure. This means that packet collisions are less likely for ACK frames. The second reason is that ACK frames are generally much shorter than data frames in length (i.e. shorter in transmission time). This implies that ACK frames are generally more robust to a bursty interference or to a rapid variation of the channel condition. Thirdly, according to the 802.11 standard, ACK frames are classified as control frames, and relatively robust modulation and coding schemes are used to transmit ACK frames. For example, although the 802.11a standard supports eight different rates in the range from 6 Mbps upto 54 Mbps, only three

rates (i.e. 6 Mbps, 12 Mbps, and 24 Mbps) are allowed to transmit control frames, including ACK frames. Lastly, to protect ACK frames in the presence of hidden nodes, stations use the EIFS wait time as specified in the 802.11 standard.

The numerical analysis results show that CRB is expected to be a more effective solution than deterministic backoff. This is because the value n_{max} in CRB is not limited to the value $\frac{W_0}{2}$, but increases with the convergence time. Theoretically, the value n_{max} in CRB is limited to the maximum contention window size ($=W_m$).¹ This means that given sufficient convergence time a larger number of nodes can automatically operate in a collision free state without dynamic parameter adjustment.

4.2 System Model

In this chapter, the Wi-Fi network described in Figure 4.1 is considered. It is assumed for simplicity that all nodes transmit in the basic half duplex mode where all nodes do not use RTS/CTS frames. It is also assumed that the AP and the connected STAs transmit signals with a constant transmission power ($=16$ dBm). All nodes support only the 802.11a physical layer standard, and they remain stationary (i.e. no mobility). The log distance propagation loss model (exponent=3) in [79], which predicts the received signal power as a deterministic function of distance, is assumed to apply to the transmitted signals.

In order to evaluate the throughput performance in saturated conditions, UDP data packets are used in this network model, and it is assumed that a real time streaming application is being used by each user. In addition, an initial assessment of CRB performance is conducted in unsaturated conditions through simulation.

¹According to the standard, the default values of W_0 and W_m are 16 and 1024 respectively.

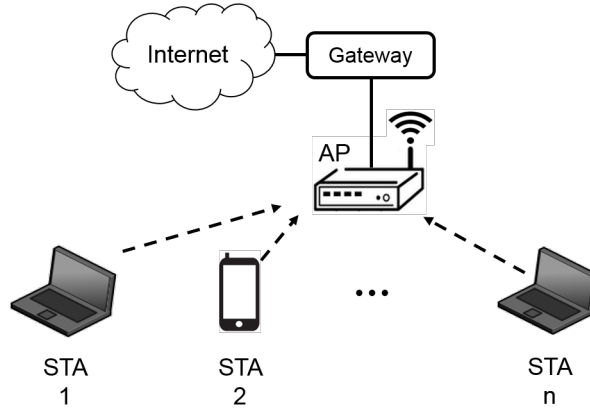


Figure 4.1: Wireless local area network configuration.

For numerical analysis in Section 4.3, it is assumed that interference from adjacent wireless networks is negligible, and we focus on a single BSS environment. This assumption enables a tractable numerical analysis. In Section 4.4, to demonstrate practicality of CRB, it is evaluated in a number of situations such as overlapping APs, mixed nodes, and hidden nodes.

4.3 Numerical Analysis of CRB

In this section, a single BSS Wi-Fi network consisting of n active (contending) nodes is considered. An ideal channel is assumed (i.e. the only reason of a transmission failure is assumed to be a packet collision), and there are no hidden nodes². These assumptions imply that no ACK frames are lost after successfully receiving a data frame.

Based on these conditions, the concept of CRB is firstly reviewed in subsection 4.3.1. Secondly, subsection 4.3.2 presents a numerical solution for the probability of a virtual collision in VBA. Thirdly, subsection 4.3.3 presents a

²A node is a hidden node if another node in the same BSS cannot carrier sense nor decode the first when it communicates with the AP.

simplified Markov chain model for analysing the probability of a backoff state of a node operating in CRB. Based on this, the transmission probability (τ) and the (real) collision probability (p) are obtained. After that, it is explained in subsection 4.3.4 how the number of SCNs changes over time. Lastly, in subsection 4.3.5, the throughput performance of CRB is analysed and compared to that of a deterministic backoff mechanism.

4.3.1 Review of CRB

As described in Chapter 3, the AP operating using CRB internally generates a unique backoff state and allocates it to each node. When the AP has received a successful data frame from a source node and discovered that the node has more data packets to send, the AP allocates a backoff state to the node using the ACK frame shown in Figure 3.8a in Chapter 3, where two octets are added to carry the backoff state. We assume that one bit of the *More Data* field in the MAC header of the data frame can be used to inform the AP that the source node has more data packets to send.

The backoff state includes two numbers: a backoff stage (BS) and a backoff count (BC). These are generated by the AP after successfully receiving the data frame from the source node and before transmitting the ACK frame. When the source node has successfully received the ACK frame with the backoff state and uses the backoff state for transmitting the next data frame, the source node is called a *synchronized CRB node (SCN)* and the allocated backoff count is called a *synchronized backoff count (SBC)*.

If the transmission of the data frame is unsuccessful and the source node fails to receive the ACK frame, then in order to start contention again for retransmission the source node generates a new backoff state by itself like a station operating

in the current IEEE 802.11 DCF. In this case, the source node is called an *unsynchronized CRB node (UCN)* and the independently generated backoff count is called an *unsynchronized backoff count (UBC)*.

The value of the backoff stage, i , is an integer in the range $[0, m]$, where m represents the maximum value of the backoff stage. The value of the backoff count, k , is an integer in the range $[0, W_i - 1]$, where W_i represents the contention window size at backoff stage i . The value of W_i is $2^i W_0$, where W_0 represents the minimum contention window. In this paper, it is assumed that $m = 6$ and $W_0 = 16$ by default. Therefore, the value of W_m is equal to 1024, and the maximum value of k is 1023.

After successfully receiving the data frame from the source node and before transmitting the ACK frame to the source node, the AP internally generates a backoff state (which is to be included in the ACK frame) as described with Figure 3.9 and Figure 3.10 in Section 3.4.4. In addition to Section 3.4.4, Figure 4.2 shows the flow of frames in CRB, where the backoff stage value x in step ⑤ is equal to the number of virtual collisions that have occurred during the VBA. In Figure 4.2, the j th slot time starts at time t_S^j (where $t_S^j < t_S^{j+1}$). The notation t_E^j represents the end of the j th slot time, i.e. $t_E^j = \lim_{\epsilon \rightarrow 0} (t_S^{j+1} - \epsilon)$. It is assumed that the backoff states of all nodes are updated between the time t_E^j and the time t_S^{j+1} .

Figure 4.3 presents pseudo-code for the operation of VBA, and Figure 4.4 presents the equivalent pseudo-code for operation of a station. Note that the *while* loop on line 4 in Figure 4.3 will not loop infinitely even when the schedule is full (i.e. when $n = W_m - 1$), because zero can be generated by the function $rand(0, 2^i W_0 - 1)$ on line 7. The value zero does not cause a virtual collision in VBA, but it would cause a monopolized channel access by the single node. However, in practice, the

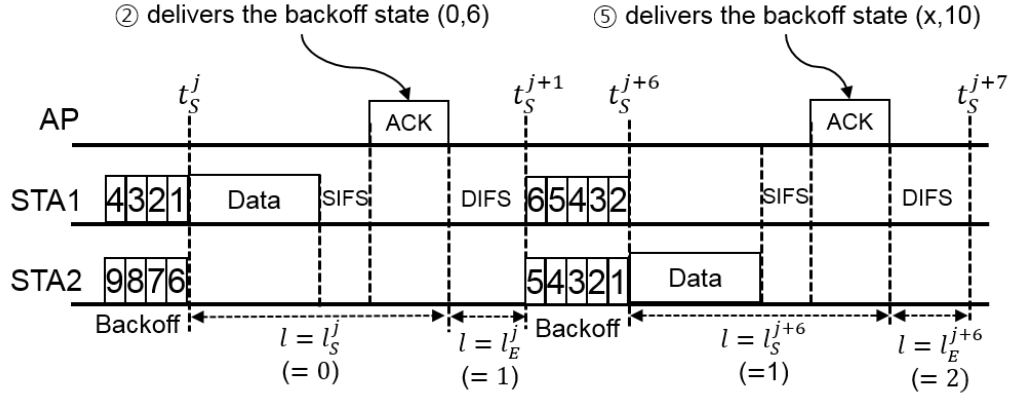


Figure 4.2: The flow of frames in CRB. The backoff stage value x in step ⑤ is equal to the number of virtual collisions that have occurred during the VBA.

```

1: if a successful reception of a data frame then
2:    $i = 0$ 
3:    $k = \text{rand}(0, 2^i W_0 - 1)$ 
4:   while  $k$  is not unique compared to the SBCs (i.e. a virtual collision occurs)
5:     if  $i < m$  then
6:        $i = i + 1$ 
7:        $k = \text{rand}(0, 2^i W_0 - 1)$ 
8:   Send the ACK frame with the backoff state  $(i, k)$ 
9: else
10:  Do not send an ACK frame

```

Figure 4.3: The pseudo-code of VBA.

value of $(W_m - 1)$ is sufficiently large so that the probability of the AP being full is very low.

4.3.2 Probability of a Virtual Collision

A node starts its backoff procedure by setting its backoff count by either uniformly choosing a random value from a contention window (after a transmission failure) or receiving a backoff state value from the AP (after a transmission success). The $(m + 1)$ backoff stages and the associated $(m + 1)$ contention windows can be

```

1: if Tx queue was empty, before a packet has arrived from upper layers then
2:   if channel is sensed idle then
3:     Start transmitting immediately
4:   else channel is sensed busy
5:      $i = 0$ 
6:      $k = \text{rand}(0, 2^i W_0 - 1)$ 
7:     Start backoff procedure with the state  $(i, k)$ 
8:   else (this node has been active, i.e. saturation condition)
9:     if a successful reception of a backoff state  $(i, k)$  from the AP then
10:      Start backoff procedure with the state  $(i, k)$ 
11:    else
12:      if  $i < m$  then
13:         $i = i + 1$ 
14:         $k = \text{rand}(0, 2^i W_0 - 1)$ 
15:      Start backoff procedure with the state  $(i, k)$ 

```

Figure 4.4: The pseudo-code of the operation of a station.

represented by Figure 4.5. In addition, for simplicity of the analysis, we define

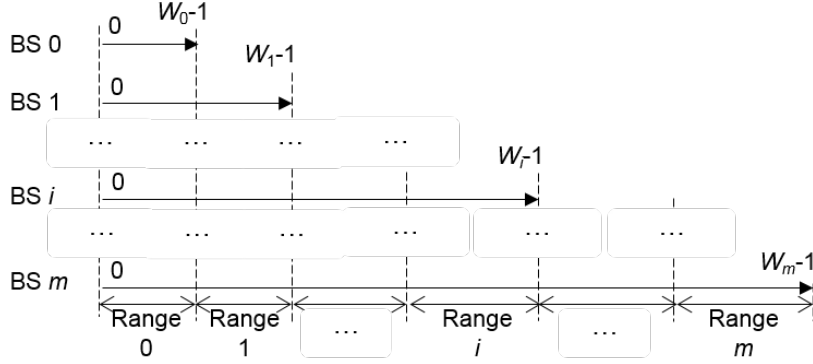


Figure 4.5: Backoff stages, contention windows, and ranges.

$(m + 1)$ Ranges as shown in the figure. Range 0 means the range of integers $[0, W_0 - 1]$, and Range i is the range $[W_{i-1}, W_i - 1]$ where $(1 \leq i \leq m)$.

The notation l is defined as the number of SCNs. (Since a SCN has only one SBC, the value l is equal to the number of SBCs.) In addition, the terms l_S^j and l_E^j are defined as the number of SCNs at time t_S^j and t_E^j , respectively. (For example, these two notations can be found in Figure 4.2.) This means the number of UCNs at time t_S^j and t_E^j are equal to $(n - l_S^j)$ and $(n - l_E^j)$, respectively.

Since each of the SCNs has a unique SBC with respect to each other, only one of the l_E^{j-1} SCNs can possibly start to transmit at time t_S^j . If one of the SCNs starts to transmit at time t_S^j (due to its SBC expiration), then $l_S^j = l_E^{j-1} - 1$. If the transmission is successful, then the source node receives a backoff state from the AP (i.e. $l_E^j = l_S^j + 1$); otherwise, the node independently generates a backoff state by itself and it becomes an UCN (i.e. $l_E^j = l_S^j$). In addition, if one of the UCNs starts to transmit at time t_S^j (due to its UBC expiration) and the transmission is successful, then the source node receives a backoff state from the AP (i.e. $l_E^j = l_E^{j-1} + 1$). In this way, the values l_S^j and l_E^j dynamically vary over time in the range of $[0, n]$.

Now, five variables are defined in order to analyse the distribution of SBCs in the range $[0, W_m - 1]$ when the AP internally generates a new backoff state to include in the ACK frame to be transmitted. First, the scalar N_i^l is defined as the number of SBCs in Range i when the total number of SCNs is l . For example, suppose that there are three SCNs, and the values of the SBCs are 3, 10, and 25. In this case, assuming $W_0 = 16$ and $m = 6$, we see the relations $l = 3$, $N_0^l = 2$, $N_1^l = 1$, and $N_i^l = 0$ given $(2 \leq i \leq m)$. We also have $\sum_{i=0}^m N_i^l = l$.

Second, the scalar Q_i^l is defined by equation (4.1) and is equal to the probability of a virtual collision at virtual backoff stage i when the number of SCNs is l .

$$Q_i^l = \frac{\sum_{k=0}^i N_k^l}{W_i} \quad 0 \leq i \leq m \quad (4.1)$$

For example, suppose that there are three SCNs, and the values of the SBCs are 3, 10, and 25. In this case, we see $Q_0^l = 2/16$ and $Q_i^l = 3/(16 \cdot 2^i)$ where $(1 \leq i \leq m)$. In addition, the notation Q_i^l can be found in Figure 3.10, where we see $l = 1$, $N_0^l = 1$, $N_i^l = 0$ given $(1 \leq i \leq m)$, and $Q_i^l = 1/W_i$ given $(0 \leq i \leq m)$.

Third, the notation P_i^l is defined by equation (4.2) which means the probability

of selecting a unique SBC in virtual backoff stage i when the number of SCNs is equal to l .

$$P_i^l = \begin{cases} (1 - Q_0^l) & i = 0 \\ (1 - Q_i^l) \prod_{k=0}^{i-1} Q_k^l & 1 \leq i < m \\ \prod_{k=0}^{m-1} Q_k^l & i = m \end{cases} \quad (4.2)$$

For example, suppose that there are three SCNs, and the values of the SBCs are 3, 10, and 25. In this case, assuming $W_0 = 16$ and $m = 6$, the value of P_0^l (i.e. the probability of selecting a unique SBC in the range of $[0, 15]$) is $14/16$, and the value of P_1^l (i.e. the probability of selecting a unique SBC in the range of $[0, 31]$) is $(29/32) \times (2/16) = 0.113$. It is assumed that the number n is less than the value of $(W_m - 1)$ to guarantee that the AP generates a unique SBC at any slot time with a successful data frame transmission. This implies the relation $\sum_{k=0}^m P_k^l = 1$.

Fourth, the notation Z^l is defined as the probability of selecting zero as a SBC when the number of SCNs is l . For example, suppose there are two SCNs, and the values of the SBCs are 3 and 10. In this case, we see the relations $l = 2$, $Q_i^l = 2/W_i$ given $(0 \leq i \leq m)$, and the value of Z^l is obtained by (4.3).

$$\begin{aligned} Z^l|_{SBCs=\{3,10\}} &= \sum_{i=0}^m (\text{Picking zero at the } i_{\text{th}} \text{ VBS}) \\ &= \frac{1}{16} + \frac{2}{16} \frac{1}{32} + \frac{2}{16} \frac{2}{32} \frac{1}{64} + \frac{2}{16} \frac{2}{32} \frac{2}{64} \frac{1}{128} + \frac{2}{16} \frac{2}{32} \frac{2}{64} \frac{2}{128} \frac{1}{256} + \frac{2}{16} \frac{2}{32} \frac{2}{64} \frac{2}{128} \frac{2}{256} \frac{1}{512} \\ &\quad + \frac{2}{16} \frac{2}{32} \frac{2}{64} \frac{2}{128} \frac{2}{256} \frac{2}{512} \frac{1}{1024} \left[1 + \frac{2}{1024} + \left(\frac{2}{1024} \right)^2 + \left(\frac{2}{1024} \right)^3 + \dots \right] \end{aligned} \quad (4.3)$$

Because zero can be allocated as a backoff count, it is possible for the source node to transmit multiple data frames consecutively without backoff. For example, as described in Figure 4.6, a zero backoff count can be allocated to the source node

in the j th slot time, and then a new non-zero SBC can be picked and allocated to the source node in step ⑥ in the $(j + 1)$ th slot time. In this case, the source node transmits two data frames without a backoff procedure between them.

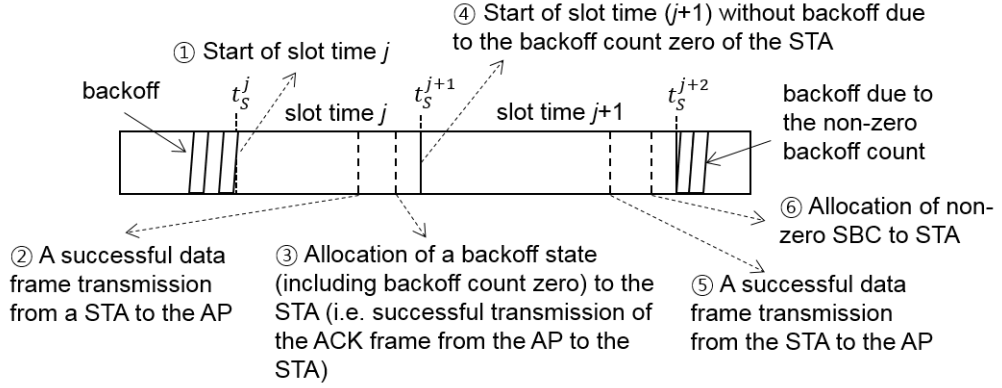


Figure 4.6: An example of two consecutive time slots granted to a node.

Lastly, the scalar D_i^l is defined as the probability of selecting a new non-zero SBC in Range i (i.e. the probability of selecting the $(l + 1)$ th SBC in Range i) when the number of SCNs is l . The value of D_i^l can be expressed by equation (4.4),

$$\begin{aligned}
 D_i^l &= D_i^l|_{(1^{\text{st}} \text{ slot})} + D_i^l|_{(2^{\text{nd}} \text{ slot})} + D_i^l|_{(3^{\text{rd}} \text{ slot})} + \cdots \\
 &= D_i^l|_{(1^{\text{st}} \text{ slot})} + Z^l D_i^l|_{(1^{\text{st}} \text{ slot})} + (Z^l)^2 D_i^l|_{(1^{\text{st}} \text{ slot})} + \cdots \\
 &= D_i^l|_{(1^{\text{st}} \text{ slot})} \sum_{j=0}^{\infty} (Z^l)^j = \frac{D_i^l|_{(1^{\text{st}} \text{ slot})}}{1 - Z^l} \quad 0 \leq i \leq m
 \end{aligned} \tag{4.4}$$

where $D_i^l|_{(k^{\text{th}} \text{ slot})}$ represents the probability of selecting a non-zero SBC in Range i in the k th slot time in the series of the consecutive successful slot times. We see the relation $Z^l = (1 - \sum_{i=0}^m D_i^l|_{(1^{\text{st}} \text{ slot})})$, where the term $(\sum_{i=0}^m D_i^l|_{(1^{\text{st}} \text{ slot})})$ represents the probability of selecting a non-zero SBC in the first successful slot time.

Using equation (4.4) and the result of Appendix B, the equations in (4.5) are obtained. Note that since the value n is assumed to be less than the value of $(W_m - 1)$ to guarantee that the AP can generate a unique non-zero SBC for any

$$D_i^l = \begin{cases} \frac{(W_0 - N_0^l - 1)}{1 - Z^l} \left(\frac{1}{W_0} + \sum_{j=0}^{m-2} \left(\frac{\prod_{k=0}^j Q_k^l}{W_{j+1}} \right) + \frac{\prod_{k=0}^{m-1} Q_k^l}{W_m(1 - Q_m^l)} \right) & i = 0 \\ \frac{(W_{i-1} - N_i^l)}{1 - Z^l} \left(\sum_{j=i-1}^{m-2} \left(\frac{\prod_{k=0}^j Q_k^l}{W_{j+1}} \right) + \frac{\prod_{k=0}^{m-1} Q_k^l}{W_m(1 - Q_m^l)} \right) & 1 \leq i < m \\ \frac{(W_{m-1} - N_m^l)}{1 - Z^l} \frac{\prod_{k=0}^{m-1} Q_k^l}{W_m(1 - Q_m^l)} & i = m \end{cases} \quad (4.5)$$

series of successful consecutive slot times, we see $\sum_{i=0}^m D_i^l = 1$. Although the value of D_i^l is expressed by the two variables N_i^l and Q_i^l in equation (4.5), considering equation (4.1) we see that the value of D_i^l in equation (4.5) can be expressed by only N_i^l .

From the definition of the variable D_i^l , relation (4.6) is obtained.

$$N_i^{l+1} = \sum_{k=0}^l D_i^k \quad (4.6)$$

Since the value of D_i^l is expressed by N_i^l (according to the equations (4.1) and (4.5)), equation (4.6) means that the value of N_i^{l+1} can be calculated iteratively. In order to solve equation (4.6), we assume an initial condition that there was a SBC in Range 0 (i.e. $N_i^{l=0} = 1$ when $i = 0$ and $N_i^{l=0} = 0$ when $i \in [1, m]$).

In order to see the distribution of SBCs in the range $[0, W_m - 1]$ for a given l , equation (4.6) was computed with different values of l . Figure 4.7 shows that at a given Range i , the value of N_i^l increases as l increases. In addition, when $l \leq 50$, the value of N_i^l tends to decrease as the Range i increases. This result shows how SBCs are distributed over the seven different ranges. Moreover, a simple program written in the C language has been developed to simulate the operation of VBA. Figure 4.7 shows that the values of N_i^l obtained by the simulation are almost identical to that of the analysis results. The values of the simulation results are average values obtained through one million Monte Carlo repetitions.

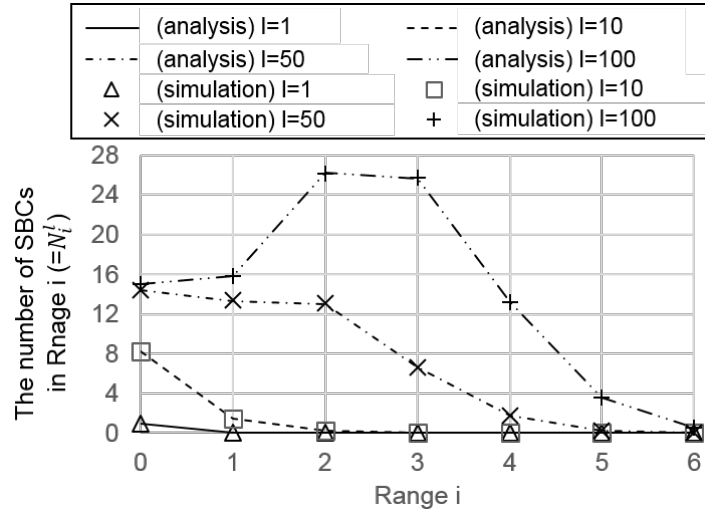
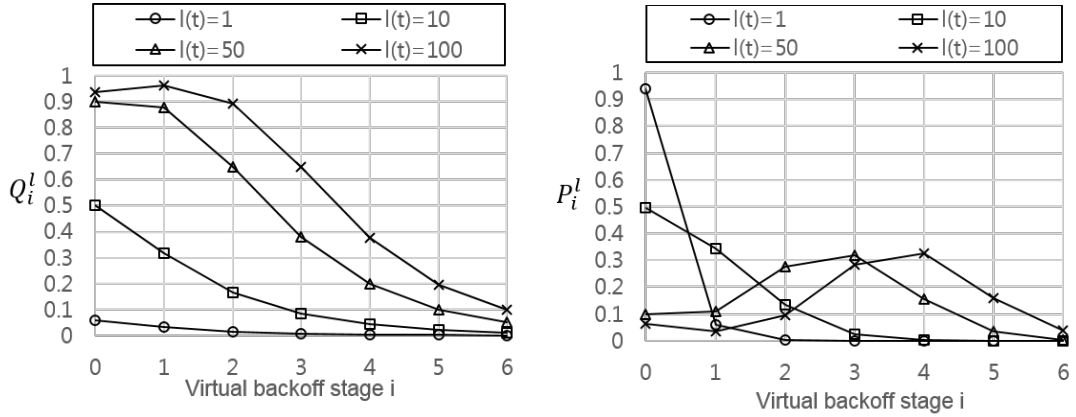


Figure 4.7: Analytical results and simulation results for N_i^l (i.e. the number of SBCs in Range i when the number of SCNs is l) given $W_0 = 16$ and $m = 6$.

The values Q_i^l and P_i^l also change, as the value l varies. Figure 4.8a shows that at a given VBS i , the value of Q_i^l increases as l increases. Using the calculated values of N_i^l with the initial condition, the values of P_i^l are obtained as shown in Figure 4.8b. The calculated value of P_i^l at a given l is used for Markov chain model analysis in Section 4.3.3 for calculating the transmission probability ($=\tau$) of a node operating in CRB.

4.3.3 Probability of a Collision

The network states during a convergence time period can be represented by Figure 4.9, where the notation $p(l)$ denotes the collision probability when the number of SCNs is l , and the notation $c(l)$ represents the probability of a node being synchronized when the number of SCNs is l . Since it is too complex to enable a closed form solution to be found, we propose the approximation in equation (4.7) and obtain a simplified chain model shown in Figure 4.10. In equation (4.7), the value l varies in the range $[1, n - 2]$, and the notation p in



(a) The probability of a virtual collision at VBS i (b) The probability of selecting a unique SBC in VBS i

Figure 4.8: Analysis results on Q_i^l and P_i^l ($W_0 = 16$ and $m = 6$).

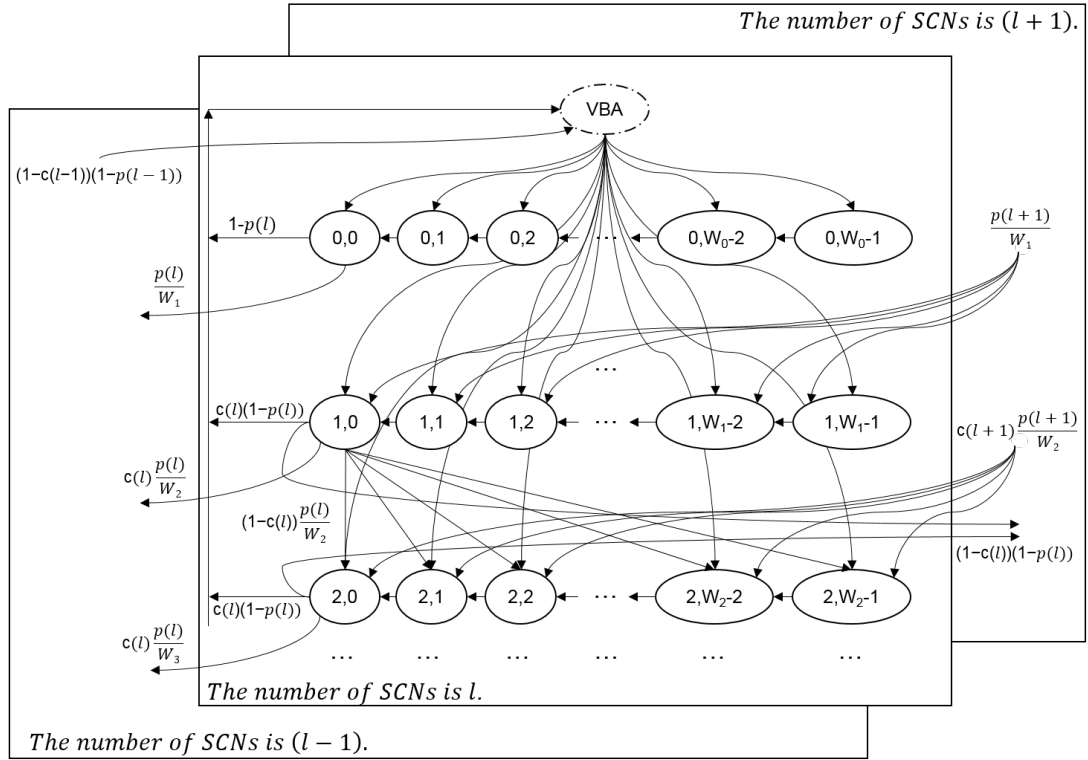


Figure 4.9: Markov chain representing the network states during a convergence time period.

Figure 4.10 (i.e. $p(l)$ in Figure 4.9) implicitly includes an approximation.

$$\begin{cases} p(l-1) \simeq p(l) \\ p(l+1) \simeq p(l) \end{cases} \quad (4.7)$$

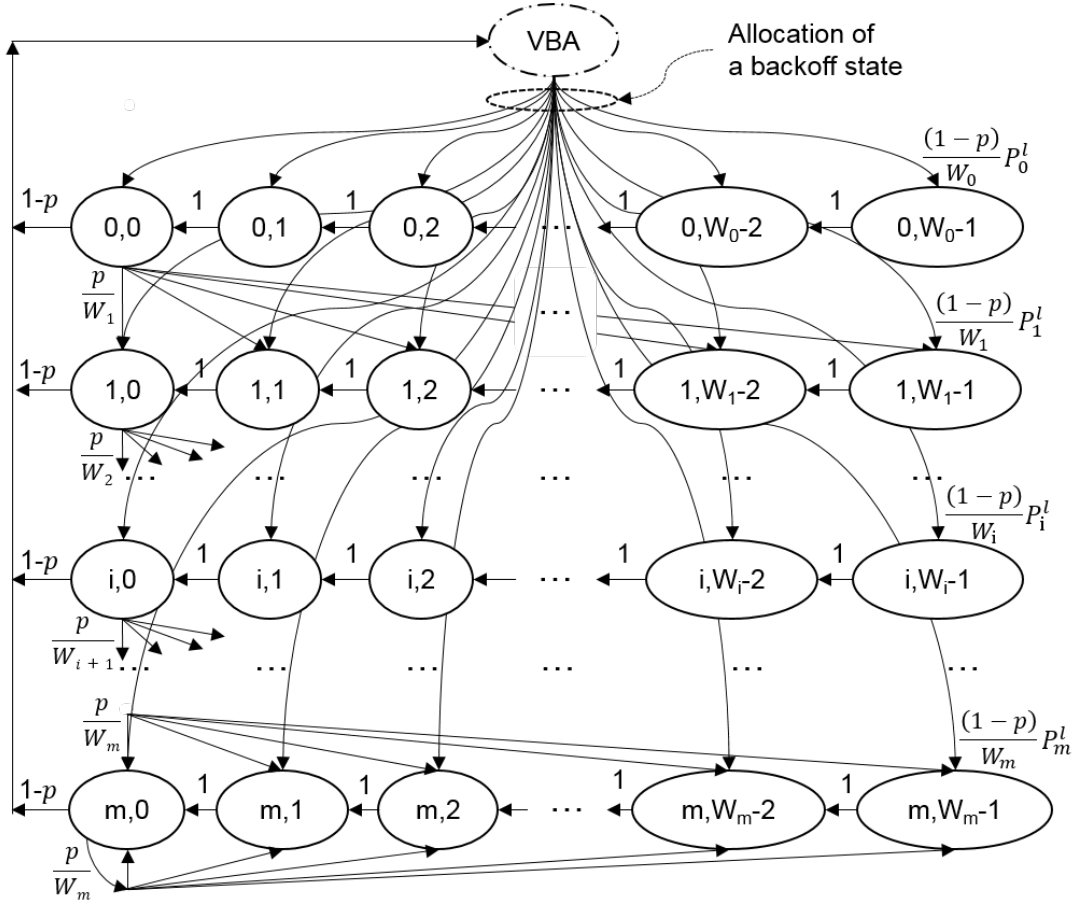


Figure 4.10: Markov chain model of a node operating in CRB. When $l \in [0, n - 1]$, the model represents a collision prone state where $(0 < p < 1)$. When $l = n$, the model represents a collision free state where $p = 0$.

In addition, when $l = n - 1$, we assume that $p(l - 1) \simeq p(l)$ and $p(l + 1) = 0$. These approximations are required to obtain a tractable numerical analysis in this thesis.

Chain model shown in Figure 4.10 illustrates an internal backoff state of a node. After a successful transmission, the node starts its backoff procedure with the allocated backoff state. The process of allocating the backoff state is illustrated by Figure 3.10 in Chapter 3 together with the curved lines in Figure 4.10.

The probability of a node being in backoff state $b_{i,k}$ (where $i \in [0, m]$ and

$$P\{i, k|i, k+1\} = 1 \quad k \in [0, W_i - 2], i \in [0, m] \quad (4.9a)$$

$$P\{j, k|i, 0\} = \frac{(1-p)}{W_j} P_j^l \quad k \in [0, W_j - 1], i \in [0, m], j \in [0, m] \quad (4.9b)$$

$$P\{i, k|i-1, 0\} = \frac{p}{W_i} \quad k \in [0, W_i - 1], i \in [1, m] \quad (4.9c)$$

$$P\{m, k|m, 0\} = \frac{p}{W_m} \quad k \in [0, W_m - 1] \quad (4.9d)$$

$k \in [0, W_i - 1]$) is defined as equation (4.8),

$$b_{i,k} = \lim_{N \rightarrow \infty} \frac{1}{N} \sum_{n=1}^N P\{s_n(t) = i, b_n(t) = k\} \quad (4.8)$$

where $s_n(t)$ and $b_n(t)$ denote the stochastic processes representing the backoff stage and the backoff counter respectively for the n -th independent realization at time t .

The transition probabilities in the Markov chain model shown in Figure 4.10 are given by equations from (4.9a) to (4.9d), where $P\{i_1, k_1|i_0, k_0\}$ denotes the probability of a backoff state transition from $\{i_0, k_0\}$ to $\{i_1, k_1\}$. Equation (4.9a) shows that the backoff count is decreased at the beginning of each slot time. The second equation (4.9b) represents the fact that a new packet following a *successful packet transmission* starts backoff with the allocated backoff state. Equations (4.9c) and (4.9d) model the state transition after an *unsuccessful transmission*. Equation (4.9c) shows that when an unsuccessful transmission occurs at backoff stage $(i-1)$, the backoff stage increases by one, and a new backoff count value is uniformly and independently chosen in the range $[0, W_i - 1]$. Equation (4.9d) models the fact that once the backoff stage value reaches the value m , a node stays in the backoff stage value m until a successful packet transmission.

From the Markov chain in Figure 4.10, the transmission probability can be

represented by (4.10):

$$\tau = \sum_{i=0}^m b_{i,0} = \frac{b_{0,0}}{(1-p)P_0^l} \quad (4.10)$$

If the value of l is zero, then $P_{i=0}^l = 1$ and $P_i^l = 0$ where $i \in [1, m]$. In this case, the Markov chain model in Figure 4.10 becomes identical to the Markov chain model presented in [22], and equations (4.9) and (4.10) also become identical to those of legacy DCF nodes presented in [22].

In Appendix C, we obtain $b_{0,0}$ as (4.11), where $f_i^j(l) = (p^{i-1-j})P_{j+1}^l/P_0^l$ for short.

$$b_{0,0} = \frac{1}{\frac{W_0+1}{2} + \sum_{i=1}^{m-1} \left[\frac{W_i+1}{2} (p^i + \sum_{j=0}^{i-1} f_i^j(l)) \right] + \frac{W_m+1}{2} \left(\frac{p^m}{1-p} + \sum_{j=0}^{m-1} \frac{f_m^j(l)}{(1-p)} \right)} \quad (4.11)$$

Equation (4.11) shows that the value $b_{0,0}$ is a function of p and P_i^l . This means that by substituting the value of $b_{0,0}$ in equation (4.10) with equation (4.11), the value of τ is given as a function of p and P_i^l . This is one relation between τ and p given both l and n . In order to find the values τ and p at given l and n , another equation relating τ and p is needed.

Let $P_{tr}(l)$ be the probability that there is at least one node starting to transmit in a considered slot time when the number of SCNs is l . The probability $P_{tr}(l)$ is obtained as (4.12),

$$P_{tr}(l) = 1 - (1 - P_{tr}^{un}(l))(1 - P_{tr}^{sn}(l)) \quad (4.12)$$

where the notation $P_{tr}^{un}(l)$ represents the probability that there is at least one UCN starting to transmit. The notation $P_{tr}^{sn}(l)$ represents the probability that there is at least one SCN starting to transmit. This probability depends on the number of SBCs in Range 0 (i.e. N_0^l). For example, as the value N_0^l becomes close to the value $(W_0 - 1)$, the SCNs will transmit in consecutive time slots. Since the values of SBCs decrease as time slots go on, the SBCs in Range 1 (i.e. N_1^l) will

move to Range 0 before the backoff counter reaches zero. The values of $P_{tr}^{un}(l)$ and $P_{tr}^{sn}(l)$ can be obtained by (4.13),

$$\begin{cases} P_{tr}^{un}(l) = 1 - (1 - \tau)^{n-l} \\ P_{tr}^{sn}(l) = 1 - \left(1 - \frac{N_0^l}{W_0 - 1}\right) (1 - P_{tr} P_s Z^l) \end{cases} \quad (4.13)$$

where the term $[N_0^l/(W_0 - 1)]$ in the second equation in (4.13) represents the density of SBCs in Range 0, and the term $[1 - N_0^l/(W_0 - 1)]$ means the density of non-allocated numbers in Range 0. The term $(1 - P_{tr} P_s Z^l)$ denotes the probability of allocating a non-zero backoff count.

The notation $P_s(l)$ is defined as the probability that a transmission occurring in a considered slot time is successful when the number of SCNs is l . This is equal to the probability that *exactly one station* transmits on the channel, conditioned on the fact that *at least one station* transmits. This yields equation (4.14),

$$P_s(l) = P_s^{un}(l) + P_s^{sn}(l) \quad (4.14)$$

where the notations $P_s^{un}(l)$ and $P_s^{sn}(l)$ represent the probability of a successful slot time with a packet sent by an UCN and a SCN, respectively. The values of $P_s^{un}(l)$ and $P_s^{sn}(l)$ are obtained by equations in (4.15).

$$\begin{cases} P_s^{un}(l) = \frac{(n-l)\tau(1-\tau)^{n-l-1}(1-P_{tr}^{sn}(l))}{P_{tr}(l)} \\ P_s^{sn}(l) = \frac{P_{tr}^{sn}(l)(1-P_{tr}^{un}(l))}{P_{tr}(l)} \end{cases} \quad (4.15)$$

Note that if the value l is zero, then $P_{tr}^{sn}(l) = 0$, $P_s^{sn}(l) = 0$, and the expression of $P_s(l)$ becomes identical to that for legacy DCF nodes presented in [22].

The probability p that a packet encounters a collision is equal to the probability that at least one of the $(n-1)$ remaining stations starts to transmit in the

considered slot time. If one UCN starts transmitting a packet in a considered slot time, then there will be no collision if neither the $(n - l - 1)$ UCNs nor the l SCNs start transmitting at the same time. In the case that a SCN starts transmitting a packet, since each of the SCNs has a unique backoff count to each other, there will be no collision provided that the $(n - l)$ UCNs do not start transmitting at the same time. This yields the two equations in (4.16),

$$\begin{cases} p^{un}(l) = 1 - (1 - \tau)^{n-l-1}(1 - P_{tr}^{sn}(l)) \\ p^{sn}(l) = 1 - (1 - \tau)^{n-l} \end{cases} \quad (4.16)$$

where the notation $p^{un}(l)$ and $p^{sn}(l)$ represents the probability of a collision seen by a packet transmitted by an UCN and a SCN, respectively.

By taking the average between $p^{un}(l)$ and $p^{sn}(l)$, the value p is obtained as (4.17),

$$p = \frac{(n - l)\tau}{(n - l)\tau + P_{tr}^{sn}(l)} p^{un}(l) + \frac{P_{tr}^{sn}(l)}{(n - l)\tau + P_{tr}^{sn}(l)} p^{sn}(l) \quad (4.17)$$

where the denominator $[(n - l)\tau + P_{tr}^{sn}(l)]$ represents the total number of packets transmitted in the considered slot time. This equation is the second relationship between τ and p , and now we can obtain τ and p given both l and n .

4.3.4 The Number of Synchronized CRB Nodes

All nodes are assumed to be using the CRB protocol, and the number of SCNs ($=l$) dynamically varies in the range $[0, n]$. The vector P^j is defined as the probability distribution of the value l at slot time j , which can be expressed by (4.18).

$$P^j = \begin{bmatrix} p_0^j & p_1^j & \cdots & p_{n-1}^j & p_n^j \end{bmatrix} \quad (4.18)$$

Table 4.1: The value of Δl between two consecutive slot times.

Tx node(s)	Tx result	Probability		Δl
		Symbol	Value	
None (empty slot)	-	$P_0(l)$	$1 - P_{tr}(l)$	0
Only one UCN	S	$P_1(l)$	$P_{tr}(l)P_s^{un}(l)$	+1
Only multiple UCNs (i.e. No SCN)	F	$P_2(l)$	$P_{tr}^{un}(l)(1 - P_{tr}^{sn}(l)) - P_{tr}(l)P_s^{un}(l)$	0
Only one SCN	S	$P_3(l)$	$P_{tr}(l)P_s^{sn}(l)$	0
UCN(s) and one SCN	F	$P_4(l)$	$P_{tr}^{un}(l)P_{tr}^{sn}(l)$	-1

* S for success, F for failure, and l for l_E^{j-1} .

Each element p_i^j (where $i \in [0, n]$) represents the probability that the value of l is equal to i at slot time j . This means $\sum_{i=0}^n p_i^j = 1$. This subsection finds the distribution vector P^j and investigates how the distribution vector P^j changes over slot times.

The notation Δl is defined as the gap between l_E^j and l_E^{j-1} , i.e. $\Delta l = l_E^j - l_E^{j-1}$. The possible values of Δl are now described. First, $\Delta l = 1$ if the j th slot time was successful with a transmission from one of UCNs (i.e. the UCN has been synchronized after the slot time). Second, $\Delta l = -1$ if a collision with a packet sent by a SCN occurred in the slot time (i.e. the SCN has become unsynchronized). Lastly, $\Delta l = 0$ in the three cases: an empty slot time, a collision among UCNs, and a successful transmission by a SCN. These five different cases are summarized in Table 4.1. The sum of the five different probabilities in the table is one for every slot time, i.e. $\sum_{k=0}^4 P_k(l) = 1$ where $(1 \leq j)$. Table 4.1 also shows the value of Δl for each of the five different cases.

The absorbing Markov chain model depicted in Figure 4.11 illustrates a state of the wireless network in terms of the number of SCNs. Note that the time scale of the chain model in Figure 4.10 is a considered time slot, while the time scale of the absorbing chain model in Figure 4.11 is the period during which the network moves from the initial state to a collision free state. The notation $P_{x,y}$

in Figure 4.11 presents the probability of a state transition from the state that $l = y$ to the state that $l = x$. The state that $l = 0$ (i.e. where all the nodes are unsynchronized) is identical to the state of wireless network operating in the legacy DCF protocol. As denoted in Figure 4.11, if the value of l is equal to n , then the state becomes a collision free state (which is an absorbing state). This means the value $P_{n,n}$ is always one. The absorbing Markov chain, which is

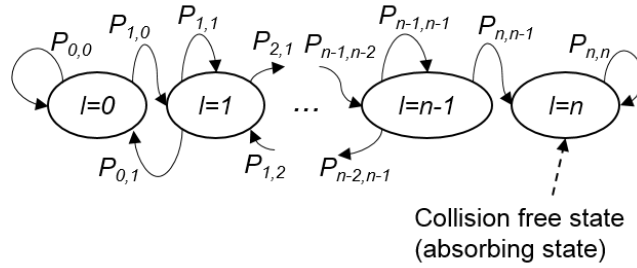


Figure 4.11: Markov chain model for analysis of the vector P^j .

denoted by the notation A , can be expressed by (4.19).

$$A = \begin{bmatrix} P_{0,0} & P_{1,0} & 0 & \cdots & 0 & 0 \\ P_{0,1} & P_{1,1} & P_{2,1} & \cdots & 0 & 0 \\ 0 & P_{1,2} & P_{2,2} & \cdots & 0 & 0 \\ 0 & 0 & P_{2,3} & \cdots & 0 & 0 \\ \cdots & & & \cdots & \cdots & \\ 0 & 0 & 0 & \cdots & P_{n-1,n-1} & P_{n,n-1} \\ 0 & 0 & 0 & \cdots & 0 & P_{n,n} \end{bmatrix} \quad (4.19)$$

From Table 4.1, relations in (4.20) are obtained.

$$P_{l,l} = P_0(l) + P_2(l) + P_3(l) \quad l \in [0, n-1] \quad (4.20a)$$

$$P_{n,n} = 1 \quad l = n \quad (4.20b)$$

$$P_{l+1,l} = P_1(l) \quad l \in [0, n-1] \quad (4.20c)$$

$$P_{l-1,l} = P_4(l) \quad l \in [1, n-1] \quad (4.20d)$$

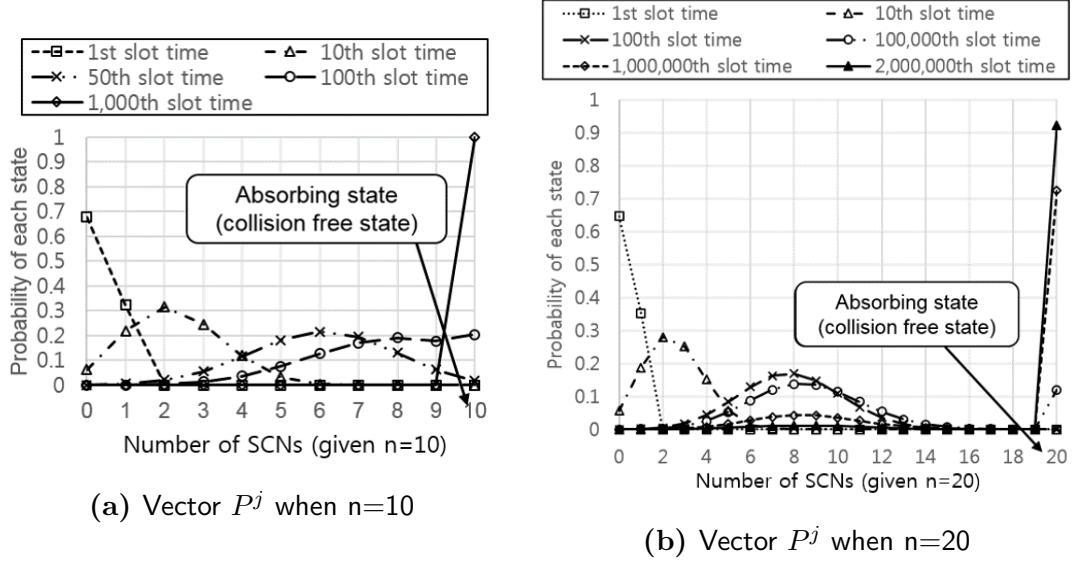


Figure 4.12: Analysis results of vector P^j ($W_0 = 16$ and $m = 6$).

Now, the vector P^j can be obtained by equation (4.21), where the vector I represents the initial state of the network. It is assumed that the value l is zero when $j = 0$ (i.e. all the nodes are assumed to be randomized/unsynchronized nodes at the beginning of the first time slot). This means the probability of the network state where $l = 0$ is one when $j = 0$.

$$P^j = IA^j \quad \text{where} \quad I = \begin{bmatrix} 1 & 0 & \dots & 0 & 0 \end{bmatrix} \quad (4.21)$$

Figure 4.12 shows the calculated results for the distribution vector P^j using equation (4.21) when $n = 10$ and $n = 20$. First of all, Figure 4.12a shows that the probability of the state $l = 10$ increases to 1, as the slot time increases up to 1000. Moreover, Figure 4.12b shows that the probability of the state $l = 20$ increases to 1, as the slot time increases to over 2,000,000. These results show that the wireless network operating in CRB moves toward a collision free state without adjusting/tuning the contention window size for the given number n . However, it is also seen that the number of slot times required to move toward a collision free state dramatically increases as the number of nodes n increases.

4.3.5 Throughput Performance

According to [22], the saturation throughput (S) is defined by equation (4.22).

$$S = E[\text{payload}] / E[\text{slot time}] \quad (4.22)$$

In this thesis, the throughput at slot time j (S^j) is given by (4.23), where $(P^j)^T$ represents the transpose of vector P^j . Each element S_i of the vector C denotes the saturation throughput when l is assumed to be i .

$$S^j = C \cdot (P^j)^T \text{ where } C = \begin{bmatrix} S_0 & S_1 & \cdots & S_{n-1} & S_n \end{bmatrix} \quad (4.23)$$

A successful transmission occurs in a slot time with probability $P_{tr}(l)P_s(l)$. The slot time is empty with probability $(1 - P_{tr}(l))$. The slot time contains a collision with probability $P_{tr}(l)(1 - P_s(l))$. Therefore, the value S_l can be obtained by (4.24),

$$S_l = \frac{P_{tr}(l)P_s(l)E[P]}{(1 - P_{tr}(l))\sigma + P_{tr}(l)P_s(l)T_s + P_{tr}(l)(1 - P_s(l))T_c} \quad (4.24)$$

where T_s denotes the average time the channel is sensed busy because of a successful transmission, and T_c represents the average time the channel is sensed busy due to a collision. The notation σ represents the duration of an empty slot time. The scalar $E[P]$ denotes the average packet payload size successfully transmitted.

The values T_s and T_c are given by (4.25),

$$\begin{aligned} T_s &= H + E[P] + SIFS + \delta + ACK + DIFS + \delta \\ T_c &= H + E[P^*] + DIFS + \delta \end{aligned} \quad (4.25)$$

where $H(= PHY_{hdr} + MAC_{hdr})$ denotes the packet header, δ represents the

Table 4.2: Parameters used to obtain numerical analysis results.

Parameters	Value
Bit rate for Data frames	54 Mbps
Bit rate for ACK frames	6 Mbps
UDP payload	1400 bytes
UDP header + IP header	28 bytes
empty time slot interval	$9 \mu s$
SIFS time interval	$16 \mu s$
DIFS time interval	$34 \mu s$
MAC header	34 bytes
Preamble signal duration	$16 \mu s$
PLCP header duration	$4 \mu s$
W_0	16
W_m	1024

propagation delay, and $E[P^*]$ is the average length of the longest packet payload involved in a collision. In the case all packets have the same fixed size, the value $E[P^*]$ becomes equal to the value $E[P]$. The term SIFS denotes the delay time required for a wireless interface to process a received frame and to respond with a response frame. The scalar ACK is the transmission time of an ACK frame. The term DIFS represents the standard wait time required before starting the random backoff procedure in the saturation condition.

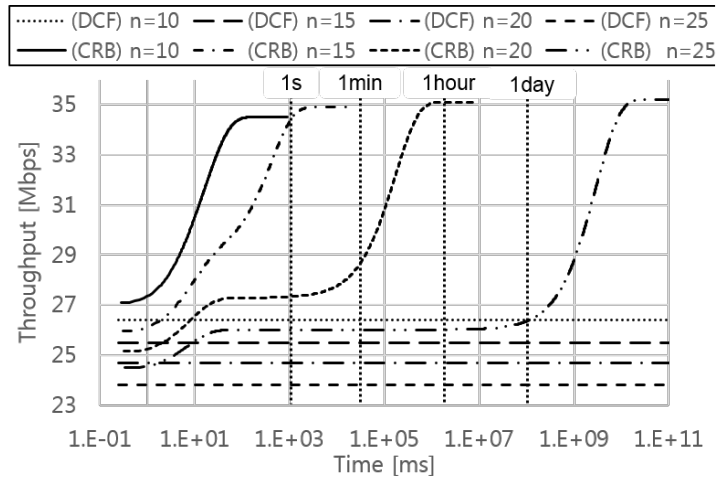
The parameters given in Table 4.2 are used to obtain analytical results shown in Figure 4.13. Figure 4.13a shows that the throughput converges to a maximum value as the time increases. The figure also shows that similar to Figure 4.12 the time period required for convergence dramatically increases, as the number of n increases. The maximum throughput value achieved in a collision free state is

slightly increased as the value n increases. This is because the probability of an empty slot time decreases, while the probability of a collision is zero.

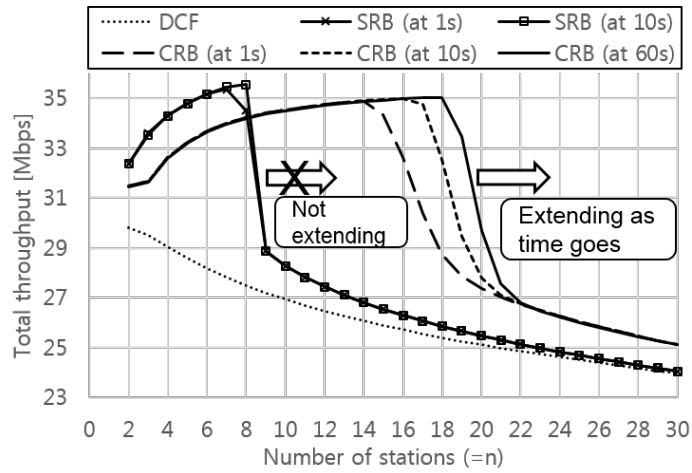
Figure 4.13b shows that the throughput performance changes over time (i.e. non-stationary state) when using CRB method. The figure also shows that given a sufficient time, the wireless network with a larger number of nodes does reach a collision free state. For example, 14 nodes can reach the collision free state within one second without tuning the contention window size (i.e. $W_0 = 16$ and $m = 6$). This is a significant advantage of CRB over SRB, because according to [50] the maximum number of SRB nodes that can converge to a collision free state (given $W_0 = 16$) is limited to 8. However, Figure 4.13 also shows that it takes an hour for 20 nodes to converge to the collision free state. In practice it is anticipated that the performance of a heavily loaded network will be between that of SRB and the optimum CRB.

Note that if the number of active nodes n becomes equal to the value W_m (i.e. if the schedule becomes full), then the VBA algorithm generates a backoff state with backoff count zero. This is because backoff count zero does not cause a virtual collision in the algorithm. This characteristic of VBA can cause a monopolized channel access by a single CRB node.

Figure 4.13b also shows that the total throughput performance when using SRB method in the range $[2, 8]$ is slightly larger than the total throughput when using CRB with VBA. This is because CRB method allows a larger number of idle timeslots compared to that of SRB method.



(a) Throughput versus time.



(b) Throughput versus the number of nodes.

Figure 4.13: Analysis results on the saturation throughput.

Table 4.3: Simulation parameters.

Parameters	Value
Wireless standard	IEEE 802.11a PHY
Frequency channel	5.0 GHz
Bandwidth	20 MHz
Propagation loss model	Log distance model (exponent=3)
Transport layer protocol	UDP
UDP payload length	1400 bytes
Modulation & coding for ACK frame	BPSK with a rate $\frac{1}{2}$ coding
Available data rates	6, 9, 12, 18, 24, 36, 48, and 54 Mbps
Transmission queue	Single queue
Traffic model	Full buffer
Tx power	16 dBm
Rx sensitivity	-91 dBm
W_0	16
W_m	1024
BER model	Reference [105]

4.4 Simulation and Numerical Results

In order to validate the numerical analysis, the NS-3 based simulator, described in Section 3.5, has been used to investigate the performance of CRB. The parameters used in simulation are summarized in Table 4.3. The OnOff application runs at each station and generates data packets to be transmitted through the MAC and PHY layers. During the ON state, constant bitrate traffic is generated, which is managed by parameters such as Data Rate and Packet Size. No traffic is generated during the OFF state.

4.4.1 Four Simulation Configurations

Figure 4.14 shows four different simulation scenarios. First, in a simulation setup shown in Figure 4.14a, there is no hidden node, and the channel condition is assumed to be perfect (i.e. no frame errors caused by channel fading or other effects). Random values selected from a triangular distribution in the range $[5, 10]$ are used for the distances from the AP to each of the stations, which is consistent with the circular coverage region shown in Figure 4.14a. The value 10 chosen for the range is small enough to guarantee a successful data frame transmission when a packet collision does not occur.

Second, Figure 4.14b shows a simulation setup for testing backward compatibility to the DCF protocol. It is assumed that there is an additional exchange of information between the AP and each station in the connection establishment procedure (e.g. exchange of *CRB support bit*). By doing so, the AP can use the legacy ACK frame format (i.e. not including CRB field) for legacy nodes, while it uses the proposed ACK frame format (including CRB field) for nodes supporting CRB. In this paper, backward compatibility means an improvement of total throughput performance of the wireless network where nodes operating using CRB coexist fairly with legacy nodes operating using DCF.

Third, using the simulation setup presented in Figure 4.14c, the effects of hidden nodes on the performance of CRB is investigated. Each of the stations in group 1 in Figure 4.14c can neither decode nor sense carrier signals from the stations in group 2, and vice versa. The distance between a node in group 1 and the AP is a uniformly selected random number in the range $[105, 115]$ meters. The distance between a node in group 2 and the AP is a uniformly selected random number in the range $[105, 115]$ meters, but the group 2 is placed on the opposite side of group 1. The values 105 and 115 for the range were chosen to implement the hidden node relation between group 1 and group 2.

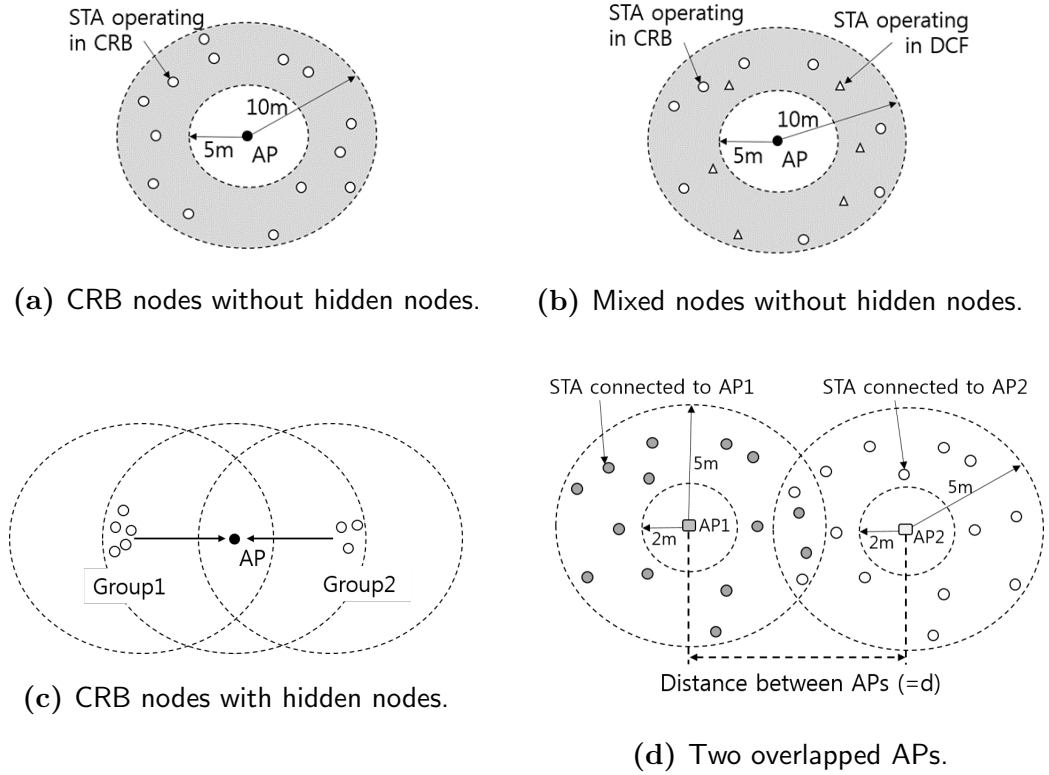


Figure 4.14: Two-dimensional simulation setups.

Lastly, Figure 4.14d shows the simulation configuration for testing CRB in two overlapped APs, where all nodes are assumed to be operating in the same frequency channel. Random values selected from a triangular distribution in the range $[2, 5]$ meters are used for the distances from the AP to each of the stations connected to the AP. The value 5 chosen for the range is small enough to guarantee a successful data frame transmission when a packet collision does not occur.

In this simulation, the performance of CRB method when using RTS/CTS frames is not considered. The performance gain from CRB method with RTS/CTS frames can be studied as a separate research.

4.4.2 Simulation Results

CRB Nodes without Hidden Nodes

Figure 4.15 shows simulation results for total throughput obtained for the setup shown in Figure 4.14a. In this case, a 54 Mbps constant rate was used for transmitting data frames, and a 6 Mbps constant rate was used for transmitting ACK frames. Because the network needs to settle into a collision free state, only statistics obtained for the last 0.2 seconds of each repeated simulation were used to draw simulation results.³ Figure 4.15a shows that the total throughput when using CRB outperforms that of using DCF, as the offered load⁴ per station increases above 2.7 Mbps. The values in the figure are average values obtained from 100 repetitions, and error bars in the figure denote standard deviation values.

Figure 4.15a also shows the simulation results for total throughput when using SRB method. As offered load at each station increase above 2.8 Mbps, the total throughput slightly and continuously increases. This is because the packet generation pattern by the OnOff application and queueing dynamics.

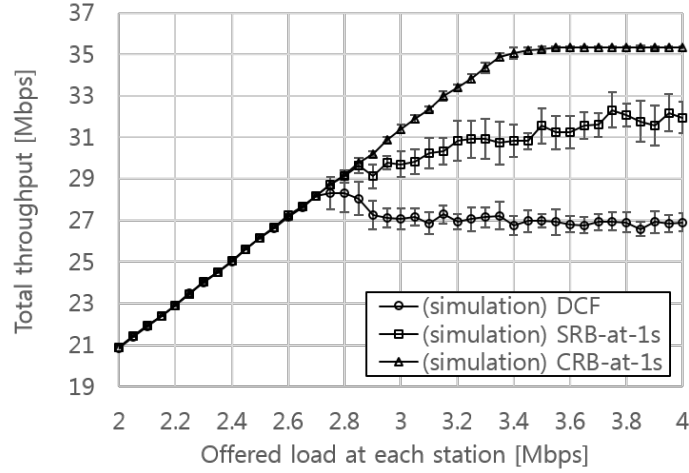
Figure 4.15a also shows that the maximum total throughput when using DCF protocol is achieved when offered load at each station is 2.8 Mbps. This pattern of total throughput performance when using DCF method was explained in the research in [23].

Figure 4.15b shows that when $n = 16$, the total throughput of CRB increases from 32.4 Mbps to 34.8 Mbps as the simulation time increases from 1 second

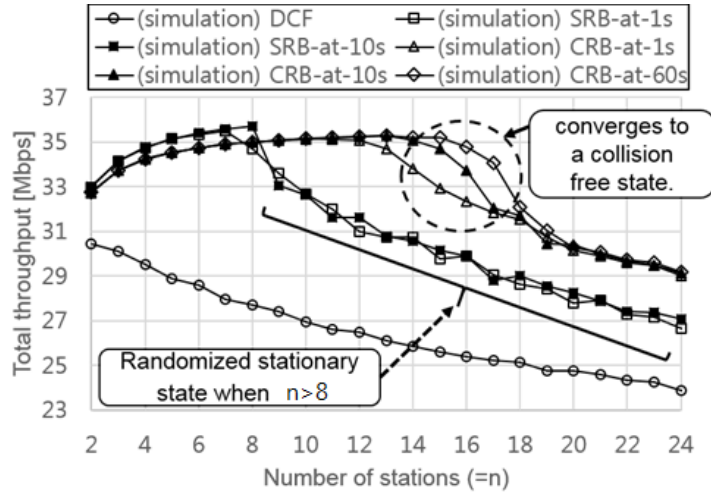
³The number of the data frames used to compute average values is larger than 500 when using the parameters in Table 4.3.

⁴In this thesis, *offered load* means UDP payloads generated by the on/off application per second, and *throughput* means successfully received MAC service data units (MSDUs) per second. The MSDUs include not only a UDP payload, but also a UDP header and an IP header.

to 60 seconds. In addition, when the value n is larger than 8, the throughput performance when using CRB outperforms that of using SRB.



(a) Offered load per station versus throughput ($n=10$)



(b) Number of stations versus total throughput

Figure 4.15: Simulation results on the throughput of CRB, SRB, and DCF in the single AP setup without hidden nodes ($W_0 = 16$ and $W_m = 1024$).

Mixed Nodes without Hidden Nodes

Figure 4.16 shows simulation results for the mixed node setup shown in Figure 4.14b. In this simulation, a 54 Mbps constant rate was used for

transmitting data frames, and a 6 Mbps constant rate was used for transmitting ACK frames. In Figure 4.16, the throughput ratio (which means the total throughput of the mixed network compared to that of the legacy DCF network) shows that as the proportion of CRB nodes increases, the total throughput increases. For example, when five nodes operating using CRB coexist with five nodes using DCF (i.e. the case 5(5) on the x-axis), the total throughput gain is about 3% compared to that of when all ten nodes use DCF (i.e. the case 0(10)). However, when eight nodes operating using CRB coexist with two nodes using DCF (i.e. 8(2)), the total throughput gain is about 12%.

In addition, Figure 4.16 shows the throughput per node operating in the mixed network. While the throughput per CRB node increases with the proportion of CRB nodes, the throughput per DCF node decreases. This is because as the proportion of CRB nodes increases, the DCF nodes tend to have a higher collision probability than the CRB nodes. Figure 4.16 also shows the Jain's Fairness Index (JFI) in terms of average throughput per node, which is calculated using equation (4.26) where the notation S_k represents the average throughput of node k for the last five seconds. Regardless of the proportion of CRB nodes, the Jain's fairness index of the mixed network is maintained above 0.95 in all the simulations.

$$\text{Jain's Fairness Index} = \frac{(\sum_{i=1}^n S_k)^2}{n \sum_{i=1}^n (S_k)^2} \quad (4.26)$$

In the Presence of Hidden Nodes

Simulations were performed in the hidden node setup shown in Figure 4.14c. In this simulation, an 18 Mbps constant rate was used for transmitting data frames, and a 6 Mbps constant rate was used for transmitting ACK frames. Five different combinations have been simulated, i.e. the total number of stations (the number of nodes in group 1, the number of nodes in group 2) was 2(1,1), 5(3,2), 10(7,3),

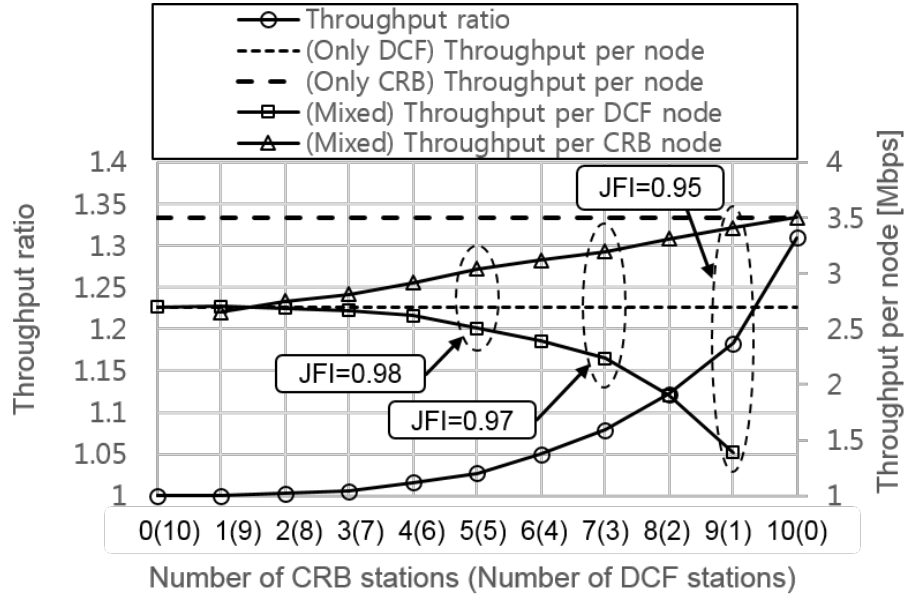


Figure 4.16: Simulation results in the mixed nodes scenario.

15(11,4), and 20(14,6). It was observed that the throughput when using DCF and that of when using CRB are significantly decreased in the presence of hidden nodes. In addition, the throughput when using CRB in the presence of hidden nodes is very close to that of using DCF in the presence of hidden nodes; however, the throughput when using CRB does not get worse than that of using DCF. It is also observed that the retransmission ratio per a data frame becomes very high (i.e. close to one) in the presence of hidden nodes.

Two Overlapped APs

The number of connected STAs to each of the two APs shown in Figure 4.14d is ten. A 54 Mbps constant rate was used for transmitting data frames, and a 6 Mbps constant rate was used for transmitting ACK frames. In order to obtain more practical simulation results, Nakagami fading model [79] was applied to the deterministic log distance propagation loss model. The values in the figure are average values obtained from 100 repetitions, and error bars in the figure denote standard deviation values.

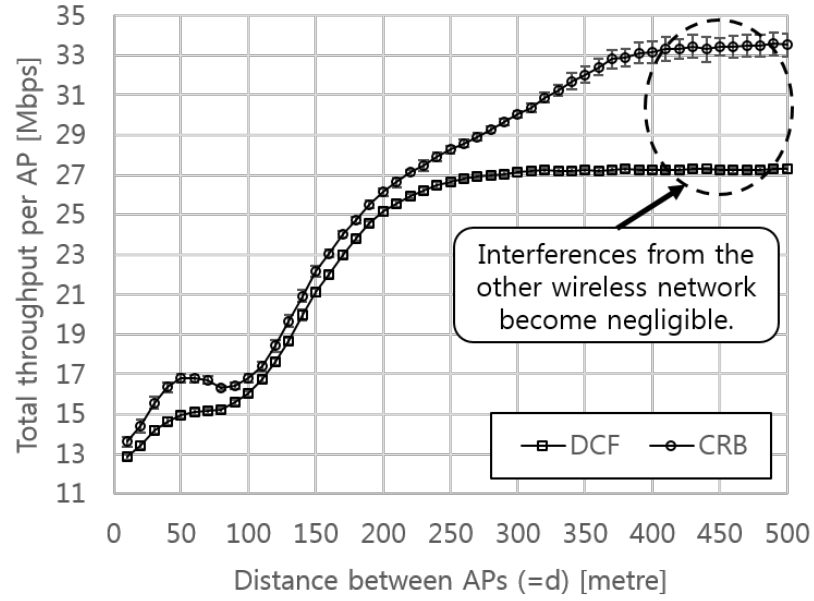


Figure 4.17: Simulation results in the two overlapped APs setup (n per each AP=10).

Figure 4.17 is obtained from the average values of the last 0.2 second of each repeated simulation. The figure shows that when the distance between the AP1 and AP2 (d) varies from 5 meters to 500 meters, the throughput when using CRB is always higher than that of using DCF. The figure shows that the total throughput per AP when using CRB method at around 50 meters reaches a local maximum value, i.e. 17 Mbps in the figure. This may be due to capture effect occurring between data packets sent by the stations connected to the AP1 and data packets sent by the stations connected to the AP2.

4.5 Summary

In this chapter, the performance of CRB with VBA was evaluated. The evaluation results showed that when a 1 second convergence time is allowed, 14 nodes using CRB can operate in a collision free state without changing the contention window size. Moreover, as time increases, the number of nodes that can operate in

a collision free state increases (up to the maximum contention window size). However, in the deterministic backoff scheme, the maximum number of nodes that can operate in a collision free state is limited to 8. Otherwise, it requires dynamic adjustment of the minimum contention window size when the number of nodes is varying. However, timely adjustment of the optimum ring size is a very complex issue, and it might be ineffective in practical wireless networks. Because of this CRB is more effective than SRB when the number of nodes varies with time.

In Chapter 5, an adaptive algorithm for CRB will be proposed to resolve the lengthy convergence time issue when the value n is large. In addition, Chapter 5 also presents numerical analysis on the fairness (in terms of channel access opportunity between devices) in the mixed network scenario.

Chapter 5

Centralized Random Backoff with Adaptive Algorithm

Maximizing network throughput while maintaining fairness between users in terms of channel access opportunity is a primary aim of wireless MAC protocols. Minimising packet collisions is one of approaches to achieve the aim. *Collision free* WLANs, where the collision probability is zero, have been reported in a number of studies [31, 33, 47–51, 102, 107–109]. These involve stations announcing their randomly chosen backoff count [47] to assist other nodes choosing non-conflicting backoff counts, adaptively choosing a backoff count based on historical use by other nodes [48], or using a deterministic, or semi-deterministic algorithm [49–51, 102, 107–109] that ensures an exclusive backoff count for each node. These approaches suffer from issues such as hidden nodes, or are constrained by a defined maximum number of nodes that can operate in a collision free state.

In CRB, after successful reception of a data frame from a station, the VBA algorithm operating in the AP generates a unique backoff state and the AP allocates it to the station by means of the ACK frame. In Chapter 4, the

performance of CRB with VBA was evaluated through both numerical analysis and practical simulations, and it was compared to that of a deterministic backoff mechanism. Evaluation results showed that CRB with VBA can significantly improve the throughput performance of Wi-Fi networks by reducing packet collisions, and it allows a larger number of nodes to operate in a collision free state without dynamic parameter adjustment in the absence of legacy DCF nodes. Moreover, although it does not achieve a collision free network in the presence of legacy DCF nodes, it provides a high level of fairness in terms of the number of channel accesses per node when nodes operating using CRB coexist with legacy nodes operating using DCF. However, as shown in Figure 4.13, evaluation results also showed that the convergence time dramatically increases as the number of active nodes n increases.

To achieve fast collision resolution regardless of the number of active nodes n , this chapter proposes a novel adaptive algorithm for CRB, which is called the *adaptive virtual backoff algorithm* (A-VBA). It can be observed in Chapter 4 that if the average number of virtual collisions is zero, then each CRB node is assigned a random backoff count by the AP, using the same algorithm as DCF nodes use to choose their own backoff count after a successful transmission. When virtual collisions occur in the VBA, it recomputes the backoff count to allocate a different backoff count to each CRB node, thus avoiding real collisions that DCF nodes typically experience.

The number of virtual collisions in the VBA tends to increase, as the number of stations contending to use the allocated backoff states (i.e. the number of SCNs) increases. In addition, as the number of virtual collisions increases, VBA tends to allocate a backoff state with a larger backoff count value. In CRB with A-VBA, the number of virtual collisions is monitored by the AP, and it is used to quickly converge to a collision free state while maintaining fairness. The proposed A-VBA automatically and dynamically adjusts the minimum virtual backoff stage (VBS)

value to the number of active nodes, without directly requiring an estimate of the number of active nodes n . Furthermore, this chapter presents numerical analysis on the throughput per node in a mixed network where CRB nodes coexist with legacy DCF nodes.

Section 5.1 of this chapter will explain the concept of CRB with A-VBA in detail. Section 5.2 presents numerical analysis of the performance of CRB with A-VBA. Section 5.3 shows simulation results to validate the analytical results obtained in Section 5.2, and compares its performance to those of the DCF, the deterministic backoff approach, and the CRB with VBA. Section 5.4 gives a summary of this chapter.

5.1 Concept of the Adaptive Virtual Backoff Algorithm (A-VBA)

The CRB method described in Chapter 3 and Chapter 4 uses the VBA algorithm running in the access point to choose a new backoff state for a given node upon successful packet reception. The point of this method is to allocate each node a unique backoff count in order to avoid collisions between nodes. Figure 4.3 defines the operation of the VBA, where W_0 denotes the minimum contention window size; the notation i represents the current backoff stage; the scalar k represents the currently chosen backoff count value. Using this algorithm, a wireless network takes less than 1 second to converge to a collision free condition when $n \leq 14$, while it takes more than 1000 seconds to converge to a collision free condition when $n = 20$.

In this chapter, the concept of A-VBA is proposed to achieve a collision free state within a much shorter convergence time. First, the notation N_{vc}^l is defined as the

average number of virtual collisions per allocated backoff state, where l denotes the average number of synchronized CRB nodes. The scalar l is known to the AP in the considered system model. Figure 5.1 explains the operation of A-VBA, where the minimum virtual backoff stage (VBS) value i in line 2 in Figure 5.1 is equal to the value N_{vc}^l , while the minimum VBS value i in the VBA (as seen in line 2 in Figure 4.3) is fixed at zero. The notation $\lfloor \cdot \rfloor$ in lines 3 and 7 in Figure 5.1 denotes the floor function which gives the greatest integer that is less than or equal to the input value.

```

1: if a successful reception of a data frame then
2:    $i = 0$ 
3:    $k = \text{rand}(0, 2^i W_0^a - 1)$  where  $W_0^a = \lfloor 2^{N_{vc}^{lba}(\tilde{l}(t))} \cdot W_0 \rfloor$ 
4:   while  $k$  is not unique compared to the SBCs (i.e. a virtual collision occurs)
5:     if  $i < m$  then
6:        $i = i + 1$ 
7:        $k = \text{rand}(0, \lfloor 2^i W_0 \rfloor - 1)$ 
8:   Send the ACK frame with the backoff state  $(i, k)$ 
9: else
10:  Do not send an ACK frame

```

Figure 5.1: The pseudo-code of A-VBA, where the minimum VBS value i in line 2 is equal to the value N_{vc}^l . The value N_{vc}^l increases with the number of CRB nodes.

The average number of virtual collisions, N_{vc}^l , increases with the number of SCNs l . Thus, as the value l increases, the A-VBA method tends to generate a larger backoff count value than that for VBA. By doing so, the A-VBA method adaptively allows a larger number of idle time slots compared to that of VBA. Because of this, the probability of a collision is reduced. This significantly reduces the convergence time, while the maximum total throughput in a collision free state with a given number of active nodes n slightly decreases because of the increased number of idle time slots. When the value n is large, the gain obtained from a reduced convergence time is much larger than the loss by the increased number of idle times.

Note that CRB with A-VBA does not require an estimate of the number of

active nodes n . Moreover, it does not need dynamic adjustment of the contention window size to the connected stations.

5.2 Numerical Analysis

In this section, the value N_{vc}^l given the number of SCNs l is obtained, and then the convergence time when using CRB with A-VBA is analysed.

5.2.1 Average Number of Virtual Collisions

The notation Q_i^l is defined in Chapter 4 as the probability of a virtual collision, where l is the number of SCNs, and i is the virtual backoff stage. This value is obtained from equations (1) to (6) in Chapter 4. Given the value Q_i^l , now the average number of virtual collisions N_{vc}^l can be obtained as:

$$\begin{aligned}
 N_{vc}^l &= Q_0^l + Q_0^l Q_1^l + Q_0^l Q_1^l Q_2^l + \cdots + \prod_{k=0}^{m-2} Q_k^l + \prod_{k=0}^{m-1} Q_k^l + \frac{\prod_{k=0}^m Q_k^l}{1 - Q_m^l} \\
 &= \sum_{j=0}^{m-1} \prod_{k=0}^j Q_k^l + \frac{\prod_{k=0}^m Q_k^l}{1 - Q_m^l}
 \end{aligned} \tag{5.1}$$

where m denotes the maximum number of backoff stages. Given $W_0 = 16$ and $m = 6$, the value N_{vc}^l is 0.70 when $l = 10$ and is 1.88 when $l = 30$. This means that while the range of the minimum virtual contention window (VCW) in VBA is fixed at $[0, 15]$, the range of the minimum VCW in A-VBA becomes $[0, 24]$ when $l = 10$ and it becomes $[0, 57]$ when $l = 30$.

The backoff stage value in CRB field when using A-VBA is a positive rational number, and the size of the backoff stage value becomes 14 bits as shown in Figure 5.2.

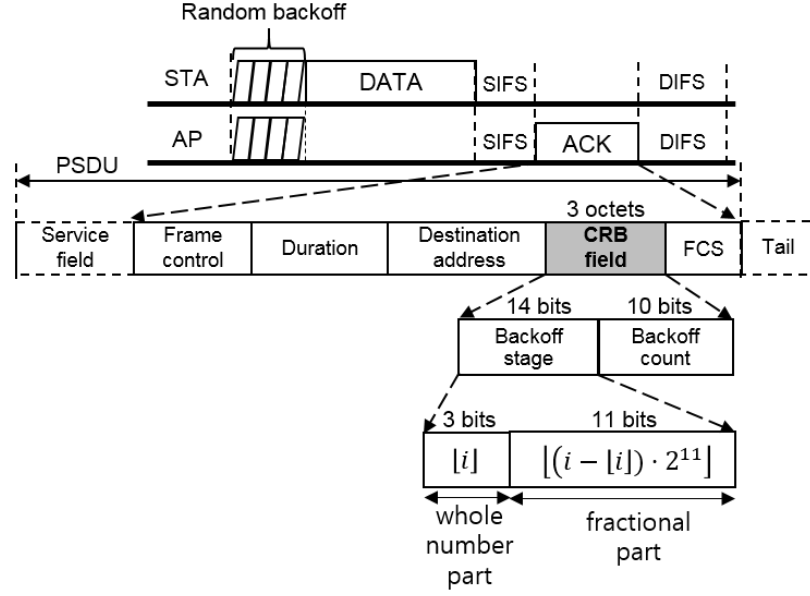


Figure 5.2: CRB field when using A-VBA.

5.2.2 Convergence Time for A-VBA

The convergence process when using VBA was analysed by the absorbing Markov chain model in Chapter 4, whereas the convergence process when using A-VBA can be depicted by Figure 5.3. The AP monitors the value N_{vc}^l , and it updates the minimum VBS value every Δt seconds. The notation L_0 represents the number of SCNs at the initial state, and the notation L_i (where $i \in [0, M]$) denotes the number of SCNs after $(i \cdot \Delta t)$ time period from the initial state. The notation L_M represents the number of SCNs in the collision free state (i.e. $L_M = n$). In the figure, the value l becomes equal to n after the $(M - 1)$ th adjustment, and the M -th adjustment is for robustness of the collision free state. Note that an AP operating using CRB with A-VBA does not directly estimate the number of active nodes n varying over time.¹

¹A WLAN operating using CRB is nonstationary during the convergence time, and run-time measurements (e.g. the collision probability and the ratio of busy time slots) change during the convergence time. This means that the estimation techniques [94, 95] do not work for a network using CRB.

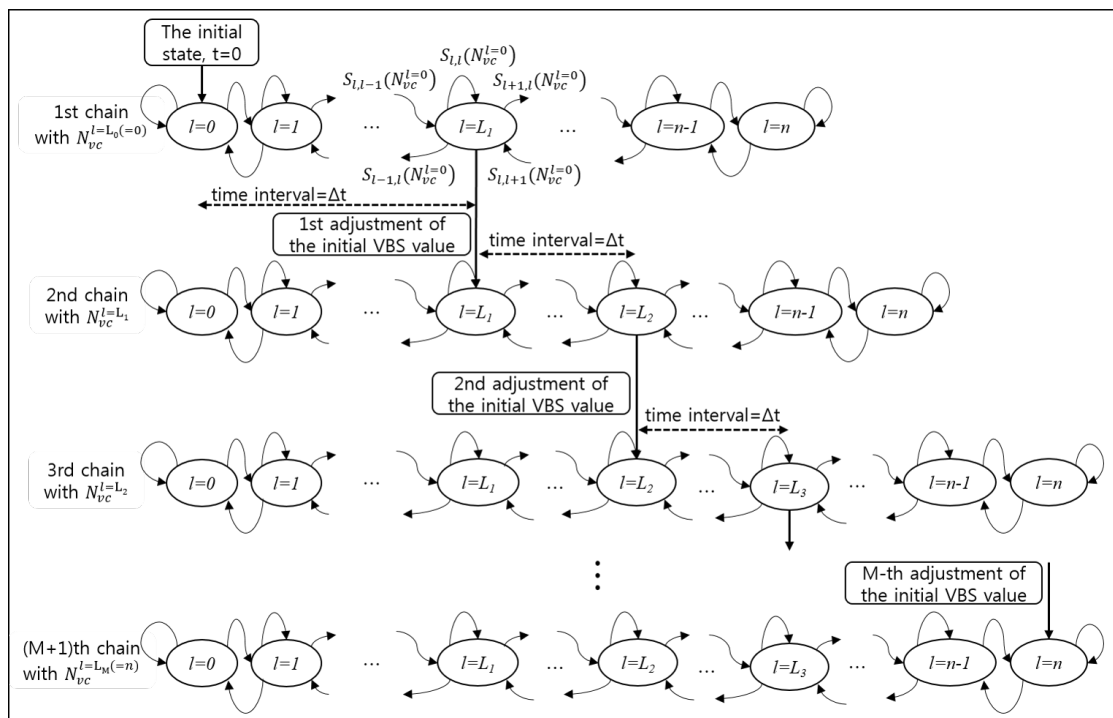


Figure 5.3: Absorbing Markov chain model of a network operating using CRB with A-VBA.

Following Chapter 4, the vector P^j is defined as the probability distribution of the number of SCNs, l , at time slot j :

$$P^j = \begin{bmatrix} p_0^j & p_1^j & \cdots & p_{n-1}^j & p_n^j \end{bmatrix} \quad (5.2)$$

where p_i^j denotes the probability that $l = i$ at time slot j . This distribution vector is obtained through Markov chain model analysis in Chapter 4.²

Now a new probability distribution vector $P_{N(l)}^j$ is defined as a function of the average number of virtual collisions, i.e. N_{vc}^l . The subscript $N(l)$ denotes the average number of virtual collisions N_{vc}^l for simplicity. The vector $P_{N(l)}^j$ can be expressed as:

$$P_{N(l)}^j = \begin{bmatrix} p_{0,N(l)}^j & p_{1,N(l)}^j & \cdots & p_{(n-1),N(l)}^j & p_{n,N(l)}^j \end{bmatrix} \quad (5.3)$$

where $p_{i,N(l)}^j$ ($i \in [0, n]$) denotes the probability that $l = i$ at time slot j when the minimum VBS value is equal to $N(l)$. Note that the vector P^j in the equation (5.2) is equal to the vector $P_{N(0)}^j$.

In this analysis, the convergence time is defined as the time taken by a wireless network operating using CRB to converge to the state where $l = n$. (Note that this equality is assumed when the probability that $l = n$, i.e. the value $p_{n,N(l)}^j$ in equation (5.3), exceeds 0.99.)

The vector $P_{N(L_i)}^j$ (where $i \in [0, M]$) can be obtained by equation (5.4),

$$P_{N(L_i)}^j = I_{N(L_i)} \cdot (A_{N(L_i)})^j \quad (5.4)$$

where the vector $I_{N(L_i)}$ represents the network state where $l = L_i$. For example, when $l = L_0 (= 0)$ the vector $I_{N(L_0)}$ is equal to $\begin{bmatrix} 1 & 0 & 0 & \cdots & 0 & 0 \end{bmatrix}$; in general

²i.e. the equations from equation (10) to equation (21) in Chapter 4.

when $l = L_i$ only the $(L_i + 1)$ th element of the vector $I_{N(L_i)}$ is equal to one while all the other elements are zero. The matrix $A_{N(L_i)}$ (where $i \in [0, M]$) represents each absorbing Markov chain shown in Figure 5.3. The matrix $A_{N(L_i)}$ can be obtained by (5.5),

$$A_{N(L_i)} = \begin{bmatrix} P_{0,0}^{N(L_i)} & P_{1,0}^{N(L_i)} & 0 & \cdots & 0 & 0 \\ P_{0,1}^{N(L_i)} & P_{1,1}^{N(L_i)} & P_{2,1}^{N(L_i)} & \cdots & 0 & 0 \\ 0 & P_{1,2}^{N(L_i)} & P_{2,2}^{N(L_i)} & \cdots & 0 & 0 \\ 0 & 0 & P_{2,3}^{N(L_i)} & \cdots & 0 & 0 \\ \cdots & & & \cdots & \cdots & \\ 0 & 0 & 0 & \cdots & P_{n-1,n-1}^{N(L_i)} & P_{n,n-1}^{N(L_i)} \\ 0 & 0 & 0 & \cdots & 0 & P_{n,n}^{N(L_i)} \end{bmatrix} \quad (5.5)$$

where each element $P_{x,y}^{N(L_i)}$ represents the probability that the number of SCNs changes from y to x when the minimum VBS value is equal to $N_{vc}^{L_i}$. The equations to obtain the values $P_{x,y}^{N(L_i)}$ are identical to those³ used to obtain the values $P_{x,y}$ (i.e. the probability that the number of SCNs changes from y to x when the minimum VBS value is zero) in Chapter 4 except for the minimum VBS value.

The value L_i (where $i \in [1, m]$) can be obtained from equation (5.6),

$$L_i = G \cdot (P_{N(i-1)}^j)^T \quad (5.6)$$

where the value j meets the condition $t_E^j \leq (i \cdot \Delta t) < t_E^{j+1}$. The notation $(P_{N(i-1)}^j)^T$ denotes the transpose of the distribution vector $P_{N(i-1)}^j$. The vector G is $\begin{bmatrix} 0 & 1 & 2 & \cdots & (n-1) & n \end{bmatrix}$.

Figure 5.4 shows analytical results on the value L_i when $\Delta t = 100$ ms and $n=20$. The parameters used to obtain the vector $P_{N(l)}^j$ can be found in Table 5.1. The

³i.e. the equations from equation (10) to (17) and the four equations in (20) in [33].

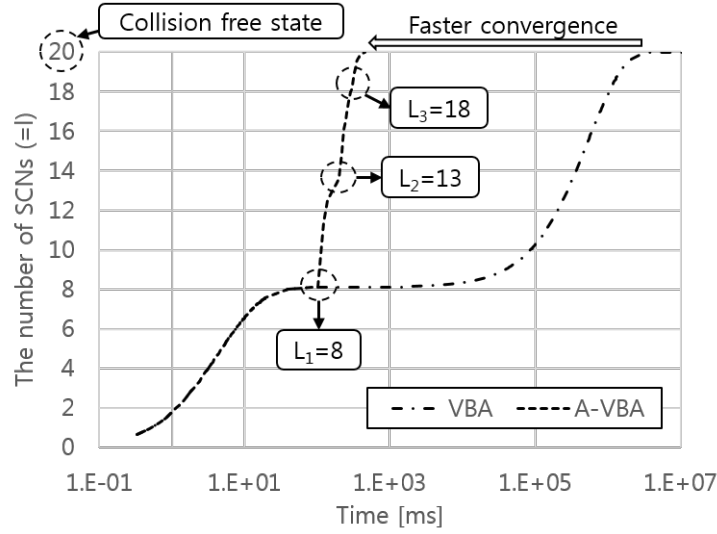


Figure 5.4: Analytical results for the number of SCNs over time when $n = 20$ and $\Delta t = 100$ ms. The number of SCNs at different time steps is shown for A-VBA.

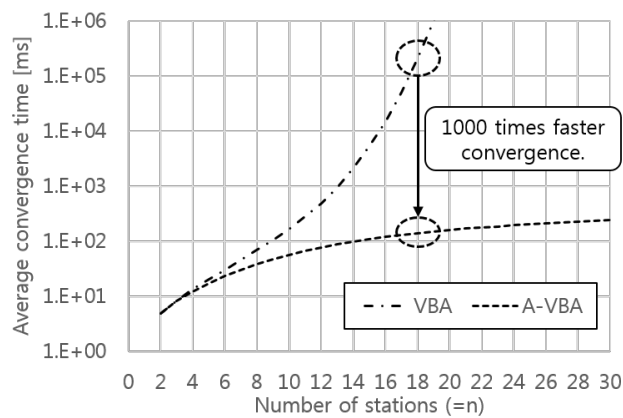
figure shows that when using VBA it takes about 3000 seconds for the network to converge to a collision free condition, whereas when using A-VBA it takes about 0.32 seconds with three adjustments of the minimum VBS value.

Figure 5.5 shows that the convergence time in CRB with VBA rapidly increases with the number of stations n , whereas the convergence time in CRB with A-VBA does not exceed 0.25 seconds in the range $[2, 30]$. For example, the convergence time when $n = 18$ is reduced from about 200 seconds to about 0.2 seconds. This means roughly 1000 times faster convergence to a collision free condition for the CRB network. Moreover, additional results show that the convergence time is 1.10 seconds when $n = 100$, and it is less than 10 seconds when $n \leq 200$. Note that the slope of the convergence time curve for CRB with VBA increases with the value n , while the slope of the curve for CRB with A-VBA decreases with the value n in the range $[2, 30]$. This is one of the key differences between VBA and A-VBA.

Figure 5.6 shows that as the value n increases above 14, the throughput gain of CRB with A-VBA outperforms that of CRB with VBA (because of faster

Table 5.1: Parameters used to obtain numerical analysis results.

Parameters	Value
Bit rate for Data frames	54 Mbps
Bit rate for ACK frames	6 Mbps
UDP payload	1400 bytes
UDP header + IP header	28 bytes
empty time slot interval	9 μs
SIFS time interval	16 μs
DIFS time interval	34 μs
MAC header	34 bytes
Preamble signal duration	16 μs
PLCP header duration	4 μs
W_0	16
W_m	1024

**Figure 5.5:** Analytic results for the convergence time when $\Delta t = 10$ ms.

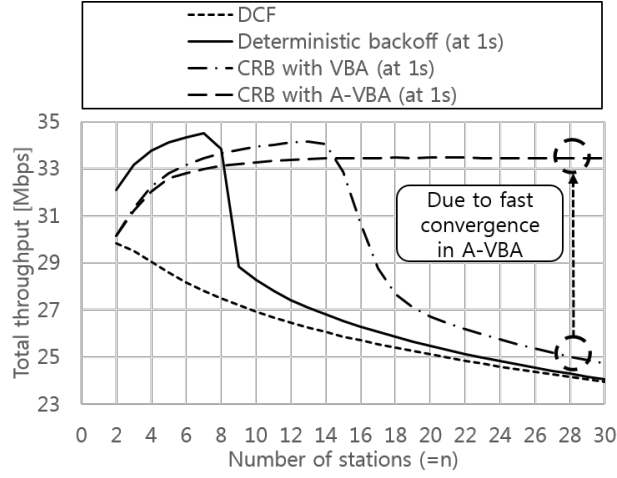


Figure 5.6: Analytical results for throughput performance when $\Delta t = 100$ ms.

collision resolution). In the range $[4, 14]$, the maximum throughput when using A-VBA is slightly lower than the maximum throughput when using VBA. This is because the minimum VBS value (i.e. N_{vc}^l) in A-VBA is larger than zero, while the minimum VBS value in VBA is zero (i.e. this small decrease of throughput is because of the larger number of idle time slots compared to that of VBA). However, because of the larger number of idle time slots, the A-VBA method is much more likely to operate in a collision free condition due to the fast collision resolution approach.

5.2.3 Fairness to Legacy Nodes

Now the average throughput per node when nodes using CRB exist with nodes using DCF is analysed. The notations n_d and n_c denote the number of DCF nodes and the number of CRB nodes respectively. The notation n represents the total number of active nodes in the mixed network, i.e. $n = n_d + n_c$. The number of synchronized CRB nodes l dynamically changes in the range $[0, n_c]$ over time. The number of unsynchronized CRB nodes is equal to $(n_c - l)$.

Probability of a Collision

The notation τ_d represents the probability that a DCF node transmits in a randomly chosen time slot. The notation p_d denotes the collision probability of a packet sent by a DCF node. According to [22], the value τ_d can be expressed as (5.7).

$$\tau_d = \frac{2(1 - 2p_d)}{(1 - 2p_d)(W_0 + 1) + p_d W_0 (1 - (2p_d)^m)} \quad (5.7)$$

The notation τ_c represents the probability that a CRB node (i.e. either a SCN or an UCN) transmits in a randomly chosen time slot. The notation p_c denotes the collision probability of a packet sent by a CRB node. According to Chapter 4, the value τ_c can be expressed as (5.8),

$$\tau_c = \frac{b_{0,0}}{(1 - p_c)P_0^l} \quad (5.8)$$

where the notation $b_{0,0}$ denotes the probability that a CRB node transmits at backoff stage zero. According to Chapter 4, the value $b_{0,0}$ is given as equation (5.9),

$$b_{0,0} = \frac{1}{\frac{W_0+1}{2} + \sum_{i=1}^{m-1} \left[\frac{W_i+1}{2} (p_c^i + \sum_{j=0}^{i-1} f_i^j(l)) \right] + \frac{W_m+1}{2} \left(\frac{p_c^m}{1-p_c} + \sum_{j=0}^{m-1} \frac{f_m^j(l)}{(1-p_c)} \right)} \quad (5.9)$$

where $f_i^j(l) = (p_c^{i-1-j})P_{j+1}^l/P_0^l$ for short. Note that the value $b_{0,0}$ is a function of the value p_c .

The probability p_d is the probability that at least one of the $(n - 1)$ nodes starts to send in the time slot. If a DCF node starts sending during a time slot, then there will be no collision if none of the other DCF nodes, nor any of the CRB nodes start sending in the same time slot. This yields equation (5.10),

$$p_d = 1 - (1 - \tau_d)^{n_d-1} (1 - \tau_c)^{n_c-l} (1 - P_{tr}^{sn}) \quad (5.10)$$

where the notation P_{tr}^{sn} represents the probability that a synchronized CRB node starts to send. The value P_{tr}^{sn} can be obtained from equation (5.11),

$$P_{tr}^{sn} = 1 - \left(1 - \frac{N_0^l}{W_0 - 1}\right) (1 - P_{tr}^{crb} P_s^{crb} Z^l) \quad (5.11)$$

where P_{tr}^{crb} denotes the probability that at least one CRB station starts to send during the time slot (i.e. $P_{tr}^{crb} = 1 - (1 - \tau_c)^{n_c - l} (1 - P_{tr}^{sn})$). The notation P_s^{crb} represents the probability that the transmission (occurring on the channel) from a CRB node is successful. The value P_s^{crb} can be obtained from equation (5.12).

$$P_s^{crb} = \frac{(n_c - l)\tau_c(1 - \tau_c)^{n_c - l - 1}(1 - \tau_d)^{n_d}(1 - P_{tr}^{sn})}{P_{tr}^{crb}} + \frac{(1 - \tau_c)^{n_c - l}(1 - \tau_d)^{n_d}P_{tr}^{sn}}{P_{tr}^{crb}} \quad (5.12)$$

The value P_{tr}^{crb} is a function of P_{tr}^{sn} and τ_c . The value P_s^{crb} is a function of P_{tr}^{sn} , τ_c , and τ_d . So, the value P_{tr}^{sn} in equation (5.11) becomes a function of τ_c and τ_d , and this means that the value p_d in equation (5.10) is also a function of τ_c and τ_d .

The collision probability p_c of CRB nodes is an average of the collision probability of synchronized CRB nodes (p_c^{sn}) and that of unsynchronized CRB nodes (p_c^{un}), which is obtained from equation (5.13).

$$p_c = \frac{(n_c - l)\tau_c p_c^{un} + P_{tr}^{sn} p_c^{sn}}{(n_c - l)\tau_c + P_{tr}^{sn}} \quad (5.13)$$

The denominator in the equation, i.e. $[(n_c - l)\tau_c + P_{tr}^{sn}]$, denotes the average number of packet transmission attempts by all of the CRB nodes (i.e. SCNs and UCNs) during the time slot.

The probability p_c^{un} is given by the probability that at least one of the $(n - 1)$ nodes starts to send. If a synchronized CRB node starts sending a data frame, then there will be no collision if none of the unsynchronized CRB nodes, nor any of the DCF nodes starts sending in the same time slot. This yields equation

(5.14).

$$\begin{cases} p_c^{un} = 1 - (1 - \tau_d)^{n_d}(1 - \tau_c)^{n_c-l-1}(1 - P_{tr}^{sn}) \\ p_c^{sn} = 1 - (1 - \tau_d)^{n_d}(1 - \tau_c)^{n_c-l} \end{cases} \quad (5.14)$$

This means that by substituting the values p_c^{un} and p_c^{sn} into equation (5.13) using the equations in (5.14), the value of p_c is given as a function of τ_c and τ_d . Now, given a set of the three variables n_c , n_d , and l , the four dependent variables (i.e. τ_c , τ_d , p_c , and p_d) are obtained from the four simultaneous equations, i.e. equations (5.7), (5.8), (5.10), and (5.13).

Let P_{tr} be the probability that at least one station starts to send in the mixed network in a considered time slot. The value P_{tr} is given as (5.15),

$$P_{tr} = 1 - (1 - P_{tr}^d)(1 - P_{tr}^{un})(1 - P_{tr}^{sn}) \quad (5.15)$$

where P_{tr}^d is the probability that at least one DCF node starts to send, i.e. $P_{tr}^d = 1 - (1 - \tau_d)^{n_d}$. The notation P_{tr}^{un} is the probability that at least one unsynchronized CRB node starts to send, i.e. $P_{tr}^{un} = 1 - (1 - \tau_c)^{n_c-l}$. Note that if $n_d = 0$, then P_{tr}^d is zero and equation (5.15) becomes identical to equation (4.12) in Chapter 4.

The notation P_s is defined as the probability that a transmission occurring on the channel is successful. This is equal to the probability that *exactly one station* transmits on the channel, conditioned on the fact that *at least one station* transmits. This yields equation (5.16),

$$P_s = P_s^d + P_s^{un} + P_s^{sn} \quad (5.16)$$

where P_s^d , P_s^{un} , and P_s^{sn} are the probability of a successful transmission by a DCF node, an unsynchronized CRB node, and a synchronized CRB node respectively.

The values of P_s^d , P_s^{un} , and P_s^{sn} are obtained by equations in (5.17).

$$\begin{cases} P_s^d = \frac{n_d \tau_d (1 - \tau_d)^{n_d-1} (1 - P_{tr}^{un}) (1 - P_{tr}^{sn})}{P_{tr}} \\ P_s^{un} = \frac{(n_c - l) \tau_c (1 - \tau_c)^{n_c-l-1} (1 - P_{tr}^d) (1 - P_{tr}^{sn})}{P_{tr}} \\ P_s^{sn} = \frac{P_{tr}^{sn} (1 - P_{tr}^d) (1 - P_{tr}^{un})}{P_{tr}} \end{cases} \quad (5.17)$$

The Number of Synchronized CRB Nodes

The number of SCNs l in the mixed network dynamically changes in the range $[0, n_c]$. The notation l^j is defined as the number of SCNs at time slot j . The notation Δl represents the difference between l^j and l^{j-1} , i.e. $\Delta l = l^j - l^{j-1}$. First, Δl is one if the j th time slot was successful with a transmission from an unsynchronized CRB node. Second, Δl is minus one if there was a collision with a data frame sent by a synchronized CRB node. Lastly, Δl is zero in six cases: (1) an idle time slot, (2) a collision between DCF nodes, (3) a collision between unsynchronized CRB nodes, (4) a collision between DCF nodes and unsynchronized CRB nodes, (5) a successful transmission by a synchronized CRB node⁴, and (6) a successful transmission by a DCF node. Table 5.2 shows these possible cases, where Δl for each case is shown.

The Markov chain model in Figure 5.7 shows the possible states of the mixed network with respect to the number of synchronized CRB nodes l . This chain model ($=A_{mix}$) can be expressed by (5.18).

⁴Following a successful transmission, the CRB node will be allocated a new time slot as the network is assumed saturated.

Table 5.2: The values of Δl

Tx node(s)	Tx result	Probability		Δl
		Symbol	Value	
None (idle slot)	-	P_0	$1 - P_{tr}$	0
Only one DCF	S	P_1	$P_{tr}P_s^d$	0
Only one UCN	S	P_2	$P_{tr}P_s^{un}$	+1
Only one SCN	S	P_3	$P_{tr}P_s^{sn}$	0
SCN and UCN(s)	F	P_4	$P_{tr}^{un}P_{tr}^{sn}$	-1
SCN and DCF(s)	F	P_5	$P_{tr}^dP_{tr}^{sn}$	-1
SCN, UCN(s), and DCF(s)	F	P_6	$P_{tr}^{un}P_{tr}^dP_{tr}^{sn}$	-1
Only multiple UCNs (i.e. Neither SCN nor DCF)	F	P_7	$P_{tr}^{un}(1 - P_{tr}^{sn})(1 - P_{tr}^d) - P_{tr}P_s^{un}$	0
Only multiple DCFs (i.e. Neither SCN nor UCN)	F	P_8	$P_{tr}^d(1 - P_{tr}^{sn})(1 - P_{tr}^{un}) - P_{tr}P_s^d$	0
UCN(s) and DCF(s)	F	P_9	$P_{tr}^{un}P_{tr}^d(1 - P_{tr}^{sn})$	0

* S for success and F for failure.

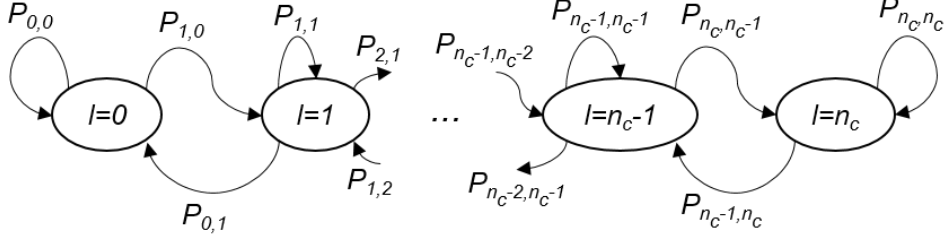


Figure 5.7: Markov chain model for the mixed network.

$$A_{mix} = \begin{bmatrix} P_{0,0} & P_{1,0} & 0 & \cdots & 0 & 0 & 0 \\ P_{0,1} & P_{1,1} & P_{2,1} & \cdots & 0 & 0 & 0 \\ 0 & P_{1,2} & P_{2,2} & \cdots & 0 & 0 & 0 \\ 0 & 0 & P_{2,3} & \cdots & 0 & 0 & 0 \\ \cdots & & & \cdots & \cdots & & \\ 0 & 0 & 0 & \cdots & P_{n_c-2,n_c-1} & P_{n_c-1,n_c-1} & P_{n_c,n_c-1} \\ 0 & 0 & 0 & \cdots & 0 & P_{n_c-1,n_c} & P_{n_c,n_c} \end{bmatrix} \quad (5.18)$$

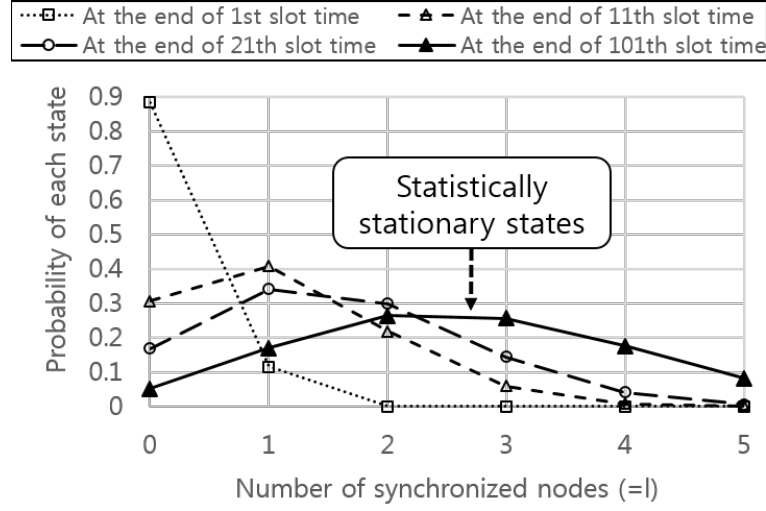
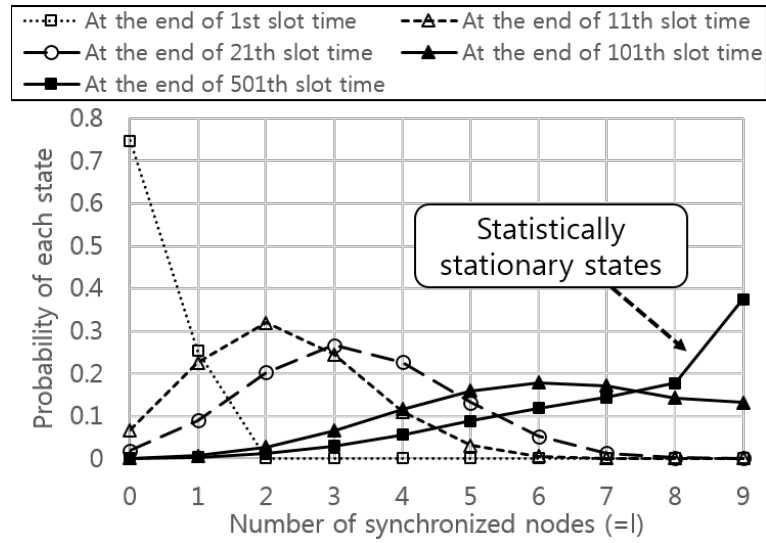
From Table 5.2, relations in (5.19) are obtained.

$$P_{l,l} = P_0 + P_1 + P_3 + P_7 + P_8 + P_9 \quad l \in [0, n_c] \quad (5.19a)$$

$$P_{l+1,l} = P_2 \quad l \in [0, n_c - 1] \quad (5.19b)$$

$$P_{l-1,l} = P_4 + P_5 + P_6 \quad l \in [1, n_c] \quad (5.19c)$$

Figure 5.8 shows the analysis results for the chain model when $n = 10$. As seen in Figure 5.8a, when $n_c = 5$ and $n_d = 5$, the network converges to a stationary state after about 100 time slots. The average number of synchronized CRB nodes in the stationary state is 2.65. Figure 5.8b shows the analysis results when $n_c = 9$ and $n_d = 1$. The figure shows that after about 500 time slots the network becomes statistically stationary, where the probability of the state that $l = 9$ is 0.38 and the average number of synchronized CRB nodes is 7.28.

(a) When $n = 10$, $n_c = 5$, and $n_d = 5$.(b) When $n = 10$, $n_c = 9$, and $n_d = 1$.Figure 5.8: Analytical results for the distribution vector $P_{N(l)}^j$ in the mixed network.

The Throughput per Node in The Mixed Network

Now we obtain the throughput per DCF node at time slot j ($=S_{dcf}^j$) and the throughput per CRB node at time slot j ($=S_{crb}^j$) from equations in (5.20),

$$\begin{cases} S_{dcf}^j = \frac{1}{n_d} \cdot C^{dcf} \cdot (P_{N(l)}^j)^T \\ S_{crb}^j = \frac{1}{n_c} \cdot C^{crb} \cdot (P_{N(l)}^j)^T \end{cases} \quad (5.20)$$

where the vectors C^{dcf} and C^{crb} are given by (5.21).

$$\begin{cases} C^{dcf} = [S_{l=0}^{dcf} & S_{l=1}^{dcf} & \cdots & S_{l=n_c-1}^{dcf} & S_{l=n_c}^{dcf}] \\ C^{crb} = [S_{l=0}^{crb} & S_{l=1}^{crb} & \cdots & S_{l=n_c-1}^{crb} & S_{l=n_c}^{crb}] \end{cases} \quad (5.21)$$

The elements $S_{l=i}^{dcf}$ and $S_{l=i}^{crb}$ (where $i \in [0, n_c]$) represent the total throughput of DCF nodes and the total throughput of CRB nodes when the value l is assumed to be i .

A successful transmission by a DCF node occurs in a time slot with probability $(P_{tr}P_s^d)$, and a successful transmission by a CRB node occurs in the time slot with probability $(P_{tr}P_s^{un} + P_{tr}P_s^{sn})$. The time slot is idle with probability $(1 - P_{tr})$; the time slot suffers from a collision with probability $(P_{tr}(1 - P_s))$. So, each element of the vectors C^{dcf} and C^{crb} can be obtained by the equations in (5.22),

$$\begin{cases} T_l^{dcf} = \frac{P_{tr}P_s^d E[P]}{(1 - P_{tr})\sigma + P_{tr}P_s T_s + P_{tr}(1 - P_s)T_c} \\ T_l^{crb} = \frac{P_{tr}(P_s^{un} + P_s^{sn}) E[P]}{(1 - P_{tr})\sigma + P_{tr}P_s T_s + P_{tr}(1 - P_s)T_c} \end{cases} \quad (5.22)$$

where the notations T_s , T_c , σ , and $E[P]$ were defined in Chapter 4.

Analytical results in Figure 5.9 show that the total throughput of the mixed network compared to the total throughput of the same size of purely DCF network increases with the ratio of nodes operating using A-VBA. In addition, the total

throughput when operating using A-VBA is very close to that of when operating using VBA. Figure 5.10 shows analytical results for the throughput values S_{dcf}^j and S_{crb}^j , where the value j is large enough to reach a stationary state. The figure shows that as the number of nodes using A-VBA increases above 7, the throughput gap between the DCF nodes and the nodes using A-VBA increases. The throughput gap is maximized when $n_c = 9$ and $n_d = 1$, but the Jain's fairness index (JFI) is maintained above 0.99 regardless of the proportion of CRB nodes. Moreover, it also shows that the throughput gap between the nodes using A-VBA and the nodes using DCF is smaller than the throughput gap between the nodes using VBA and the nodes using DCF. This is because the minimum VBS value (i.e. N_{vc}^l) in A-VBA increases with the proportion of nodes using A-VBA, whereas the minimum VBS value when operating using VBA is fixed at zero. The values of JFI were computed from equation (5.23),

$$\text{Jain's Fairness Index (JFI)} = \frac{(\sum_{k=1}^n S_k)^2}{n \sum_{k=1}^n (S_k)^2} \quad (5.23)$$

where the notation S_k represents the average throughput of node k in the mixed network.

5.3 Simulation Results

To validate the analytical results in this chapter, the network simulation used in Chapter 4 has been modified to dynamically adjust the minimum VBS value to the average number of virtual collisions per successful data frame reception.

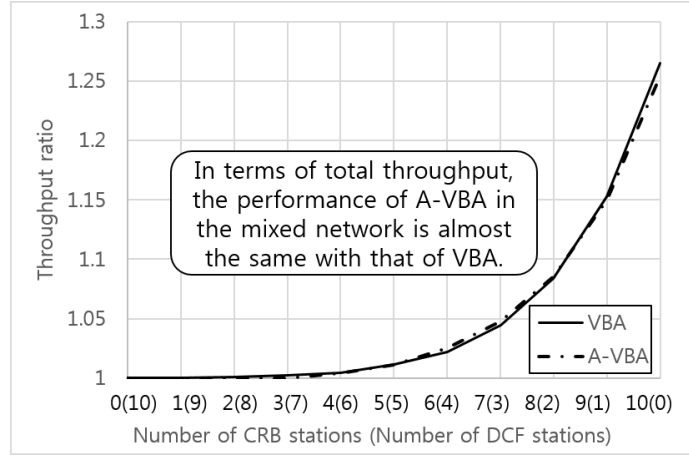


Figure 5.9: Analytical results for the total throughput compared to the total throughput of the DCF only network.

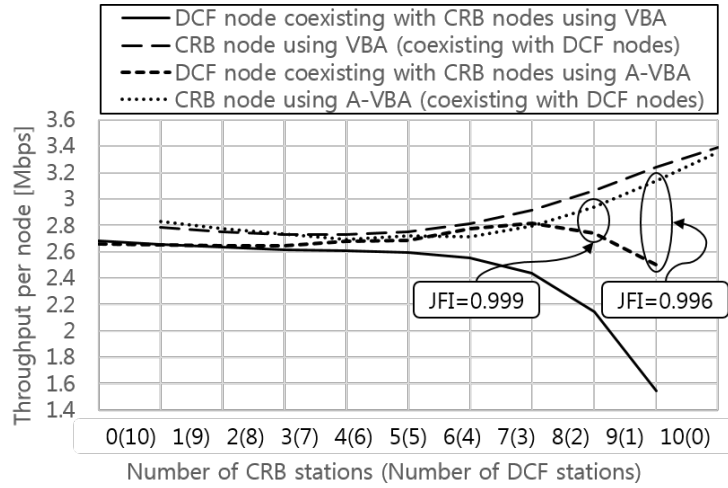


Figure 5.10: Analytical results for the throughput per station.

5.3.1 Simulation Setup

Figure 5.11 shows three different simulation configurations. The distances between the AP and stations are drawn from a triangular distribution in the range $[2, 5]$ meters. By doing so, stations are uniformly placed within the range in the two-dimensional setups. The value 5 meters chosen for the range is small enough to guarantee a successful data frame transmission when a packet collision

does not occur. A data rate of 54 Mbps is used for sending data packets, whilst ACK frames are transmitted at 6 Mbps.

All the nodes in the configurations of Figure 5.11a (i.e. setup-A) and Figure 5.11c (i.e. setup-C) support CRB, while in the configuration shown in Figure 5.11b (i.e. setup-B) nodes supporting CRB coexist with legacy DCF nodes. Details of the connection establishment for a mixed network (i.e. setup-B) are given in Chapter 4.

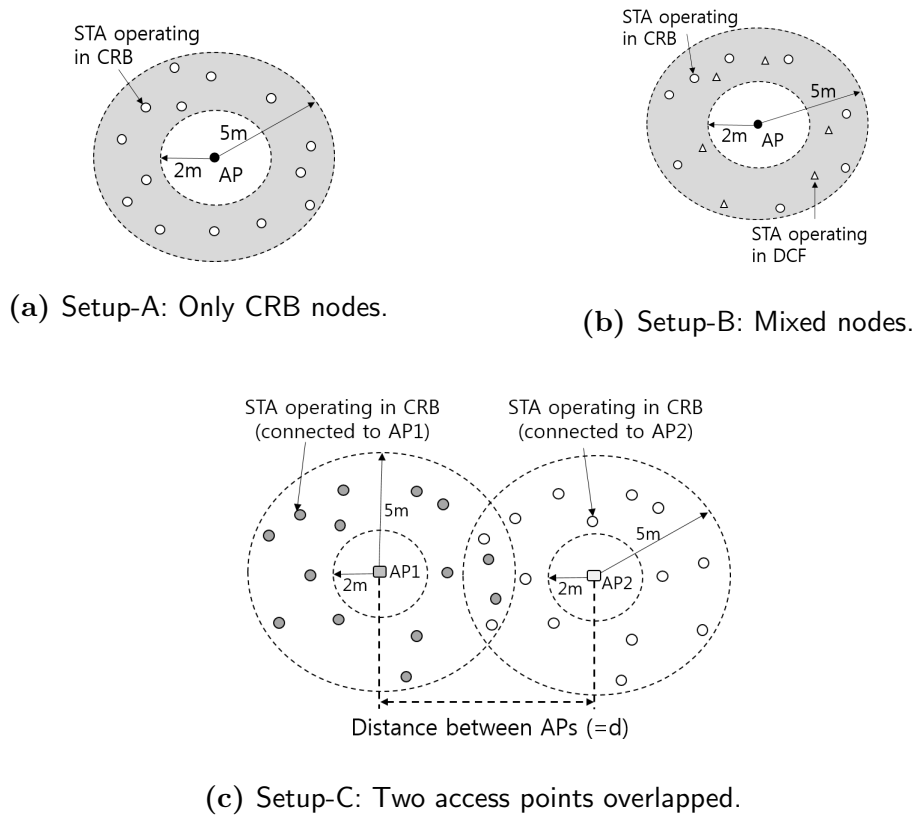


Figure 5.11: Two-dimensional setups.

In this simulation, the performance of CRB method when using RTS/CTS frames is not considered. The performance gain from CRB method with RTS/CTS frames can be studied as a separate research.

5.3.2 Results in Setup-A

Figure 5.12 shows simulation results for the total throughput when using A-VBA (with $\Delta t = 100$ ms) given one second of convergence time. The values in the figure are average values obtained from 100 repetitions, and error bars in the figure denote standard deviation values. The figure shows that the throughput performance of A-VBA outperforms that of VBA in the range $[14, 30]$ because of faster collision resolution. For example, the throughput of CRB with A-VBA outperformed that of CRB with VBA by 30% when the number of contending stations n is 30. The total throughput when using A-VBA in the range $[9, 30]$ outperforms that of the deterministic backoff algorithm. In addition, the throughput performance result of CRB with A-VBA is very close to the throughput performance result of CRB (in the case of using the basic MAC in half duplex communication) in Figure 3.16a in Chapter 3; however, CRB with A-VBA is more practical, since it does not require an initialisation phase for allocating unique backoff counts.

In the range $[4, 14]$, the maximum throughput when using A-VBA is slightly lower than the maximum throughput when using VBA. This is because the minimum VBS value in A-VBA is larger than zero, while the minimum VBS value in VBA is zero (i.e. this small decrease of throughput is because of the larger number of idle timeslots compared to that of VBA). However, because of the larger number of idle timeslots, the collision free condition when using A-VBA becomes much more robust through fast collision resolution.

Figure 5.13 shows simulation results when the number of nodes n increases by six every three seconds (shown by dashed vertical lines). Each point in the figure denotes an average throughput value obtained with a 0.2 second average window. Figure 5.13a shows that the network using CRB with A-VBA automatically

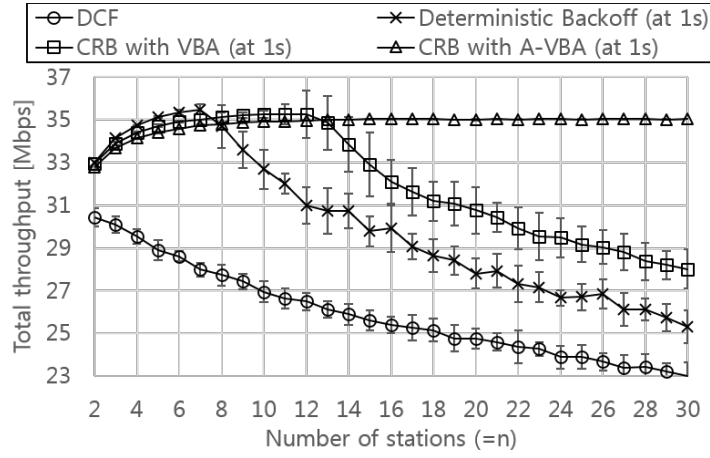
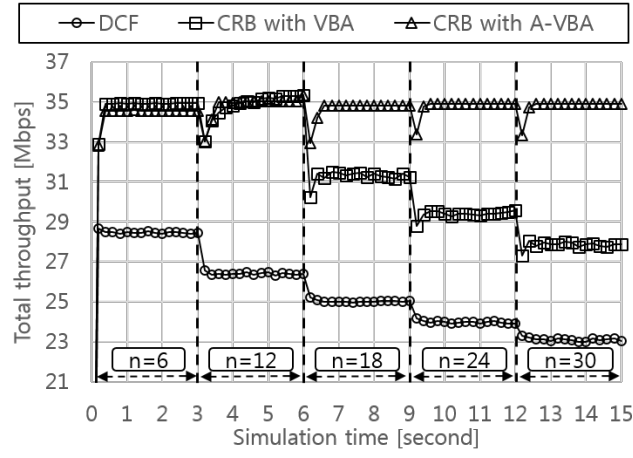


Figure 5.12: Results on total throughput performance.

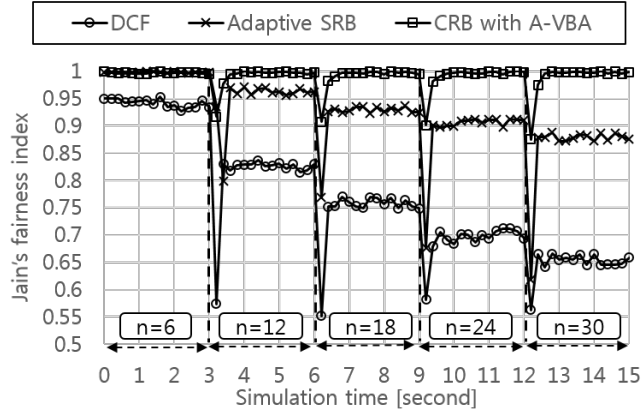
converges to a collision free state within one second regardless of the value n in the range $[2, 30]$. This results in a higher throughput performance than that for CRB with VBA.

Figure 5.13b shows that the JFI when using CRB with A-VBA is very close to one regardless of the number of active nodes, whereas the fairness index when using the adaptive SRB decreases as the number of active nodes increases above 6. This is due to the fact that each node using the adaptive SRB independently adjusts the deterministic backoff value in a distributed manner (as shown in Figure 3.6 in Chapter 4).

Full duplex nodes following the full duplex MAC protocol proposed in Section 3.3.1 in Chapter 3 transmit RTS/CTS frames before transmitting data frames. The length of RTS frames (i.e. 20 octets) is very short compared to the length of data frames used in the simulation (i.e. 1400 octets), and the wasted time due to RTS frame collisions is much smaller than that for data frame collisions when RTS/CTS frames are not used. This means that when RTS/CTS frames are used, the throughput gain from a collision resolution method becomes small.



(a) Throughput performance.



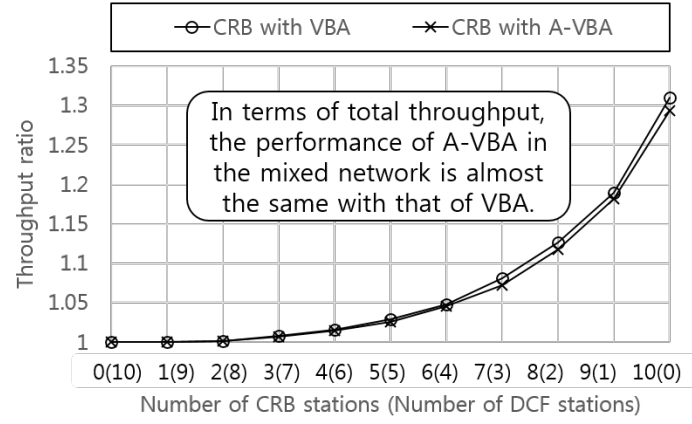
(b) Jain's fairness index.

Figure 5.13: Simulation results when the number of active nodes increases by 6 every 3 seconds (shown by dashed lines).

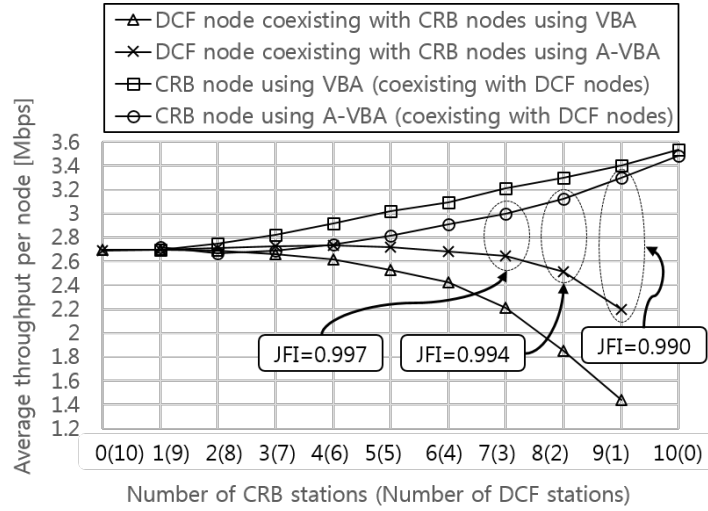
5.3.3 Results in Setup-B

Figure 5.14 shows that as the number of A-VBA nodes increases, improved performance for A-VBA is obtained compared to a DCF-only network, which is the 0(10) case. In addition, the total throughput when operating using A-VBA is very close to that of when operating using VBA.

Figure 5.14b shows that although the throughput for station using DCF in the



(a) Throughput ratio (i.e. throughput gain over the same size of purely DCF network).



(b) Average throughput per station in the mixed network.

Figure 5.14: Simulation results when $n = 10$ in setup-B.

mixed network decreases as the proportion of stations using A-VBA increases above 0.6, the throughput for node using A-VBA increases with this proportion. However, the JFI is maintained above 0.99. The figure also shows that the throughput gap between the nodes using A-VBA and the nodes using DCF is smaller than the throughput gap between the nodes using VBA and the nodes using DCF. This is because the nodes using A-VBA tend to use a larger backoff count value than that of the nodes using VBA.

5.3.4 Results in Setup-C

The two APs and all the stations shown in Figure 5.11c use the same channel. Each AP has 10 connected stations. The Nakagami fading [79] model is used along with a log distance propagation loss model.

Figure 5.15 shows that the total throughput per AP is consistently higher when A-VBA is used compared to using only DCF in the range $[10, 500]$. This is because although the network operating using A-VBA does not reach a collision free condition in the range $[10, 400]$ due to interference, some of the nodes (on average) use a unique backoff count to each other among them. In addition, Figure 5.15 shows that regardless of the value d the total throughput per AP when using A-VBA is very close to that achieved when using VBA. The figure also shows that the total throughput per AP when using CRB method at around 50 meters reaches a local maximum value, i.e. 17 Mbps in the figure. This may be due to capture effect occurring between data packets sent by the stations connected to the AP1 and data packets sent by the stations connected to the AP2.

5.4 Conclusion

This chapter proposed A-VBA for CRB, and evaluated its performance. A-VBA implements automatic adaptation of the minimum VBS value, when the number of active nodes n changes over time. By doing so, the wireless network converges to a collision free state within 1 second regardless of the value n in the range $[2, 30]$. The evaluation results showed that the throughput of CRB with A-VBA outperformed that of CRB with VBA by 30% when the value n is 30. Moreover, the simulation results showed that regardless of the proportion of nodes using

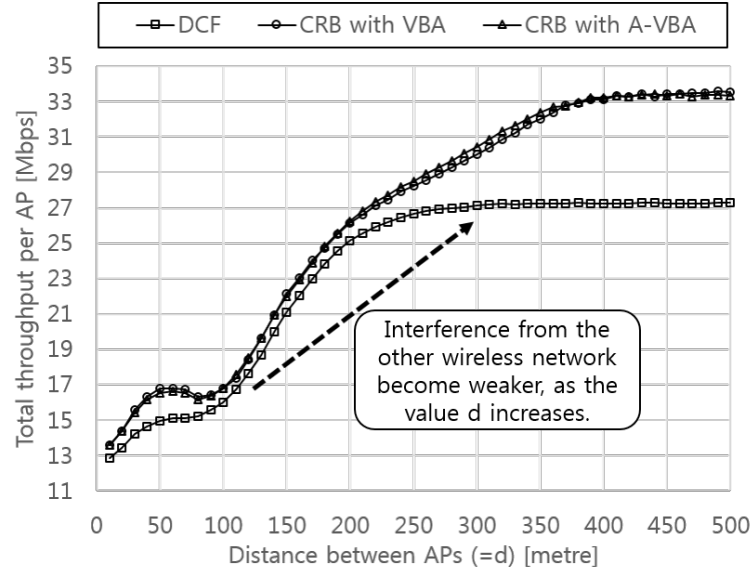


Figure 5.15: Total throughput in Setup-C, where the number of active stations connected to each AP is 10.

A-VBA in the mixed network configuration, the fairness index was maintained above 0.99. This means that A-VBA provides a higher level of fairness than that of the VBA in the mixed network (when using VBA, the Jain's fairness metric is maintained above 0.95). Because of this high level of fairness to the legacy DCF nodes in the mixed network, CRB with A-VBA could be easily adopted in the IEEE 802.11 standard. Since the adaptive CRB has some features of both decentralized and centralized scheduling methods, it could also be used for fair and efficient femtocell communications (or device to device communications) in unlicensed frequency bands where legacy Wi-Fi devices are expected to be operating.

Chapter 6

Conclusions

This thesis has been concerned with the MAC issues in order to improve the fairness and throughput performance in wireless local area networks. Evaluation results for the proposed methods demonstrate that the performance of wireless local area networks can be considerably improved while maintaining fairness. This chapter summarizes the key findings on the proposed methods, and explains how such findings can contribute to future wireless local area networks. In addition, it briefly describes limitations of the work presented in this thesis, and lastly it suggests possible research approaches to develop further the proposed methods.

6.1 Summary of the Thesis

Firstly, the busytone signal solution was proposed to maintain a high level of fairness between half duplex and full duplex nodes in the presence of the hidden node problem. The simulation results showed that the average Jain's fairness index (in terms of the number of channel accesses granted per node) between the legacy half duplex node and the full duplex node has been considerably improved

(JFI= 1.00) compared to that of when using the polite full duplex MAC protocol (JFI= 0.92).

Secondly, the collision resolution method, called CRB with VBA, was proposed. The simulation results showed that the total throughput of full duplex nodes using the CRB with VBA has been improved by 4% to 12% (depending on the number of stations) over the state of the art full duplex MAC protocol. Moreover, the total throughput of half duplex nodes using the CRB with VBA has been improved by 10% to 38% compared to that of the legacy half duplex nodes following the IEEE 802.11 standard.

Thirdly, the performance of CRB with VBA was more accurately analysed with the more practical initial condition that all the nodes are assumed to be randomized at first. The evaluation results showed that when a 1 second convergence time is allowed, 14 nodes using the CRB with VBA can operate in a collision free state without changing the contention window size. Moreover, as time increases, the number of nodes that can operate in a collision free state increases. This means that the CRB with VBA is more effective than the state of the art collision resolution technique (i.e. the deterministic backoff) when the number of active nodes varies with time.

Lastly, the A-VBA for CRB was proposed, and its performance was evaluated. The A-VBA implements automatic adaptation of the minimum VBS value, when the number of active nodes changes over time. The evaluation results showed that the wireless network converges to a collision free state within 1 second regardless of the number of active nodes in the range [2, 30]. The results also showed that the throughput of the CRB with A-VBA outperformed that of the CRB with VBA by 30% when the number of active nodes is 30. Moreover, the simulation results showed that regardless of the proportion of nodes using the A-VBA in the mixed network setup, the fairness index was maintained above 0.99. This means

that the A-VBA provides a higher level of fairness than that of the VBA in the mixed network (when using VBA, the Jain's fairness metric is maintained above 0.95). Because of this high level of fairness to the legacy DCF nodes in the mixed network, CRB with A-VBA could be easily adopted in the IEEE 802.11 standard.

Nowadays people use Wi-Fi devices (such as smart phones and laptops) almost everyday, and Wi-Fi networks have been widely deployed over the past few decades. Basic knowledge of Wi-Fi technologies was described in Chapter 2 of this thesis. The random access protocol that Wi-Fi devices follow to transmit signals is simple to implement, cost efficient, and effective to maintain fairness between users. However, the performance of Wi-Fi networks decreases due to the packet collision issue. In Chapter 3 of this thesis, a novel channel access protocol, called *centralized random backoff*, was proposed to achieve collision free Wi-Fi networks. The performance of the proposed protocol was analysed further in Chapter 4, and it was compared the deterministic backoff method. The evaluation results showed that the centralized random backoff technique is more effective than the deterministic backoff method. This is because when using centralized random backoff protocol, the maximum number of active nodes that can operate in a collision free state increases with time. However, it was observed that the convergence time required for the network (using centralized random backoff protocol) to move toward a collision free state rapidly increases when the number of active nodes is large. In order to resolve this issue, a novel adaptive algorithm, named *adaptive virtual backoff algorithm*, was proposed in Chapter 5. The evaluation results presented in Chapter 5 showed that the convergence time is dramatically reduced by the adaptive algorithm. This means that regardless of the number of users, the packet collision issue in Wi-Fi networks can be resolved. In addition, the evaluation results also showed that a high level of fairness is maintained when nodes using the centralized random backoff method coexist with nodes using the legacy channel access protocol. This means Wi-Fi devices

being used everyday can fairly coexist with Wi-Fi devices using the centralized random backoff method with adaptive virtual backoff algorithm. Because of this, the centralized random backoff method with adaptive virtual backoff algorithm studied in this thesis could be easily adopted as a standard technology. By doing so, the packet collision issue in Wi-Fi networks can be resolved, and the performance of Wi-Fi networks can be improved.

6.2 Limitations and Future Work

The work presented in this thesis has several limitations. In Chapter 3, it was assumed that each node performs ideal cancellation of the transmitted signal. However, this assumption may not be practical. In this thesis, little attention has been paid to how the performance of the proposed busytone signal solution will change when self interference cancellation methods do not achieve perfect self interference cancellation.

The Markov chain model used to analyse the performance of CRB in Chapter 4 can be developed to consider more practical conditions, such as a limited number of retransmissions, imperfect channel conditions, unsaturated traffic conditions, use of an adaptive rate control algorithm, decorrelation between consecutive time slots, and capture effects. In addition, the analytical model should be simplified while not losing its accuracy if possible.

In the evaluation parts of this thesis, Wi-Fi devices are assumed to follow the 802.11a standard. However, recently Wi-Fi devices following the 802.11n standard are widely used. The 802.11n employs a frame aggregation technique. The frame aggregation method means that a source station can transmit multiple Data frames consecutively, and then receive a Block ACK (BACK) frame from the receiver device. The BACK frame informs the source station of the successfully

received Data frames. This means the source station can transmit multiple Data frames after a random backoff procedure. In addition, the 802.11n standard supports higher data rates compared to the 802.11a standard. Because of these differences from the 802.11a standard, the performance gain from CRB method would change when Wi-Fi devices are assumed to follow the 802.11n standard. In this thesis, little attention has been paid to the expected performance gain from CRB method when Wi-Fi devices are assumed to follow the 802.11n standard.

As future work, the throughput gap between a DCF station and a CRB station in the mixed network configuration should be reduced to zero, even when the proportion of CRB nodes is high. Moreover, CRB could be further developed to support various techniques such as quality of service control, power saving mode, multi-hop relay, ad-hoc networks, and so on. CRB method may be further expanded to operate along with multi-user MIMO (Multi-Input and Multi-Output) technologies. In addition, the performance of CRB method with TCP protocol should be tested.

Since the adaptive CRB has some features of both decentralized and centralized scheduling methods, it could be used for fair and efficient femtocell communications (or device to device communications) in unlicensed frequency bands where legacy Wi-Fi devices are expected to be operating.

Bibliography

- [1] C. Shannon. A mathematical theory of communication. *Bell System Technical Journal*, pages 3–55, 1948.
- [2] N. Abramson. The ALOHA system: another alternative for computer communications. *ACM Joint Computer Conference*, pages 281–285, Nov 1970.
- [3] W. Crowther, R. Rettberg, D. Walden, S. Ornstein, and F. Heart. A system for broadcast communication: Reservation-ALOHA. *Hawaii International Conference on System Sciences (HICSS)*, pages 371–374, 1973.
- [4] L. Roberts. ALOHA packet system with and without slots and capture. *ACM SIGCOMM Computer Communication Review*, pages 28–42, 1975.
- [5] D. Goodman, R. Valenzuela, K. Gayliard, and B. Ramamurthi. Packet reservation multiple access for local wireless communications. *IEEE Transactions on Communications*, 37(8):885–890, Aug. 1989.
- [6] D. Goodman and S. Wei. Efficiency of packet reservation multiple access. *IEEE Transactions on Vehicular Technology*, 40(1):170–176, Feb. 1991.
- [7] S. Nanda, D. Goodman, and U. Timor. Performance of prma: A packet voice protocol for cellular systems. *IEEE Transactions on Vehicular Technology*,

- 40(3):584–598, Aug. 1991.
- [8] G. Bianchi, F. Borgonovo, L. Fratta, L. Musumeci, and M. Zorzi. C-PRMA: A centralized packet reservation multiple access for local wireless communications. *IEEE Transactions on Vehicular Technology*, 46(2):422–436, May 1997.
- [9] A. Gummalla and J. Limb. Wireless medium access control protocols. *IEEE Communications Surveys and Tutorials*, 3(2):2–15, Sept. 2000.
- [10] D. Tse and P. Viswanath. *Fundamentals of Wireless Communication*. Cambridge University Press, 2005.
- [11] W. Dargie and C. Poellabauer. *Fundamentals of wireless sensor networks: theory and practice*. John Wiley and Sons, 2010.
- [12] E. Perahia and R. Stacey. *Next generation wireless LANs: 802.11n and 802.11ac*. Cambridge University Press, 2013.
- [13] G. Miao, J. Zander, K. Sung, and S. Slimane. *Fundamentals of Mobile Data Networks*. Cambridge University Press, 2016.
- [14] X. Li, R. Lu, X. Liang, X. Shen, J. Chen, and X. Lin. Smart community: An internet of things application. *IEEE Communications Magazine*, 49(11):68–75, Nov. 2011.
- [15] C. Perera, A. Zaslavsky, P. Christen, and D. Georgakopoulos. Context aware computing for the internet of things: A survey. *IEEE Communications Surveys & Tutorials*, 16(1):414–454, Jan. 2013.
- [16] A. Al-Fuqaha, M. Guizani, M. Mohammadi, M. Aledhari, and M. Ayyash. Internet of things: A survey on enabling technologies,

- protocols, and applications. *IEEE Communications Surveys and Tutorials*, 17(4):2347–2376, Nov. 2015.
- [17] K. Bilstrup, E. Uhlemann, E. Strom, and U. Bilstrup. Evaluation of the IEEE 802.11p MAC method for vehicle-to-vehicle communication. *IEEE Vehicular Technology Conference (VTC)*, pages 1–5, 2008.
- [18] A. Boukerche, H. Oliveira, E. Nakamura, and A. Loureiro. Vehicular ad hoc networks: A new challenge for localization-based systems. *Computer communications*, pages 2838–2849, 2008.
- [19] K. Hafeez, L. Zhao, J. Mark, X. Shen, and Z. Niu. Distributed multichannel and mobility-aware cluster-based MAC protocol for vehicular Ad Hoc networks. *IEEE Transactions on Vehicular Technology*, 62(8):3886–3902, Oct. 2013.
- [20] R. Bruno, M. Conti, and E. Gregori. Mesh networks: commodity multihop ad hoc networks. *IEEE Communications Magazine*, 43(3):123–131, Mar. 2005.
- [21] L. Pelusi, A. Passarella, and M. Conti. Opportunistic networking: Data forwarding in disconnected mobile Ad Hoc networks. *IEEE Communications Magazine*, 44(11):134–141, Nov. 2006.
- [22] G. Bianchi. Performance analysis of the IEEE 802.11 distributed coordination function. *IEEE Journal on Selected Areas in Communications*, 18(3):535–547, Mar. 2000.
- [23] D. Malone, K. Duffy, and D. Leith. Modeling the 802.11 distributed coordination function in nonsaturated heterogeneous conditions. *IEEE/ACM Transactions on Networking*, 15(1):159–172, Feb. 2007.

- [24] E. Felemban and E. Ekici. Single hop IEEE 802.11 DCF analysis revisited: Accurate modeling of channel access delay and throughput for saturated and unsaturated traffic cases. *IEEE Transactions on Wireless Communications*, 10(10):3256–3266, May 2011.
- [25] L. Laughlin, M. Beach, K. Morris, and J. Haine. Optimum single antenna full duplex using hybrid junctions. *IEEE Journal on Selected Areas in Communications*, 32(9):1653–1661, Sep 2014.
- [26] A. Sabharwal, P. Schniter, D. Guo, D. Bliss, S. Rangarajan, and R. Wichman. In-band full-duplex wireless: Challenges and opportunities. *IEEE Journal on Selected Areas in Communications*, 32(9):1637–1652, Sep 2014.
- [27] D. Kim, H. Lee, and D. Hong. A survey of in-band full-duplex transmission: from the perspective of PHY and MAC layers. *IEEE Communications Surveys & Tutorials*, 17(4):2017–2046, Feb. 2015.
- [28] Z. Zhang, X. Chai, K. Long, A. Vasilakos, and L. Hanzo. Full duplex techniques for 5G networks: self-interference cancellation, protocol design, and relay selection. *IEEE Communications Magazine*, 53(5):128–137, May 2015.
- [29] K. Thilina, H. Tabassum, E. Hossain, and D. Kim. Medium access control design for full duplex wireless systems: Challenges and approaches. *IEEE Communications Magazine*, 53(5):112–120, May 2015.
- [30] X. Zhang, W. Cheng, and H. Zhang. Full-duplex transmission in phy and mac layers for 5g mobile wireless networks. *IEEE Wireless Communications*, 22(5):112–121, Oct. 2015.

- [31] J. Kim, D. Laurenson, and J. Thompson. Fair and efficient full duplex MAC protocol based on the IEEE 802.11 DCF. *IEEE International Symposium on Personal, Indoor, and Mobile Radio Communications (PIMRC)*, 90:538–548, March 2016.
- [32] M. Duarte, A. Sabharwal, V. Aggarwal, R. Jana, K. Ramakrishnan, C. Rice, and N. Shankaranarayanan. Design and characterization of a full-duplex multiantenna system for WiFi networks. *IEEE Transactions on Vehicular Technology*, 63(3):1160–1177, March 2014.
- [33] J. Kim, D. Laurenson, and J. Thompson. Centralized random backoff for collision resolution in Wi-Fi networks. *IEEE Transactions on Wireless Communications*, 16(9):5838–5852, September 2017.
- [34] J. Kim. Source codes of the network simulator for centralized random backoff in Wi-Fi networks. *University of Edinburgh*, June 2017. available at <http://dx.doi.org/10.7488/ds/2068>.
- [35] J. Kim, D. Laurenson, and J. Thompson. Collision free Wi-Fi networks through centralized random backoff with adaptive algorithm. *in preparation*, Aug 2017.
- [36] International Standard Information Processing Systems - Open Systems Interconnection - Basic Reference Model - Part 4: Management framework, Nov. 1989.
- [37] Ieee 802 part 11: Wireless lan medium access control (MAC) and physical layer (PHY) specifications, Feb 2012.
- [38] J. Kim, S. Kim, S. Choi, and D. Qiao. CARA: Collision-aware rate adaptation for IEEE 802.11 WLANs. *IEEE INFOCOM*, pages 1–11, 2006.

- [39] A. Kamerman and L. Monteban. WaveLAN-II: A high-performance wireless LAN for the unlicensed band. *Bell Labs Technical Journal*, pages 118–133, 1997.
- [40] G. Holland, N. Vaidya, and P. Bahl. A rate-adaptive MAC protocol for multi-hop wireless networks. *ACM Proceedings of the 7th annual international conference on Mobile computing and networking*, pages 236–251, 2001.
- [41] M. Lacage, M. Manshaei, and T. Turletti. IEEE 802.11 rate adaptation: A practical approach. *ACM Proceedings of the 7th international symposium on Modeling, analysis and simulation of wireless and mobile systems*, pages 126–134, 2004.
- [42] D. Xia, J. Hart, and Q. Fu. Evaluation of the minstrel rate adaptation algorithm in IEEE 802.11g WLANs. *IEEE International Conference on Communications (ICC)*, pages 2223–2228, 2013.
- [43] P. Chatzimisios, A. Boucouvalas, and V. Vitsas. IEEE 802.11 packet delay a finite retry limit analysis. *IEEE GLOBECOM*, pages 950–954, 2003.
- [44] Y. Zheng, K. Lu, D. Wu, and Y. Fang. Performance analysis of IEEE 802.11 DCF in imperfect channels. *IEEE Transactions on Vehicular Technology*, 55(5):1648–1656, Sept. 2006.
- [45] A. Kumar, E. Altman, D. Miorandi, and M. Goyal. New insights from a fixed-point analysis of single cell IEEE 802.11 WLANs. *IEEE/ACM Transactions on Networking*, 15(3):588–601, June 2007.
- [46] C. Wang, B. Li, and L. Li. A new collision resolution mechanism to enhance the performance of IEEE 802.11 DCF. *IEEE Transactions on Vehicular*

- Technology*, 53(4):1235–1246, July 2004.
- [47] J. Choi, J. Yoo, and S. Choi. EBA: An enhancement of the IEEE 802.11 DCF via distributed reservation. *IEEE Transactions on Mobile Computing*, 4(4):378–390, July 2005.
- [48] J. Lee and J. Walrand. Zero collision random backoff algorithm. *IEEE INFOCOM*, pages 1–9, 2007.
- [49] J. Barcelo, B. Bellata, C. Cano, A. Sfairopoulou, M. Oliver, and K. Verma. Towards a collision-free WLAN: Dynamic parameter adjustment in CSMA/E2CA. *EURASIP Journal of Wireless Communications and Networking*, 1:1–11, 2011.
- [50] Y. He, J. Sun, X. Ma, A. Vasilakos, R. Yuan, and W. Gong. Semi-random backoff: towards resource reservation for channel access in wireless LANs. *IEEE/ACM Transactions on Networking*, 21(1):204–217, Feb. 2013.
- [51] L. Sanabria-Russo, F. Gringoli, J. Barcelo, and B. Bellalta. Implementation and experimental evaluation of a collision-free MAC protocol for WLANs. *IEEE International Conference on Communications (ICC)*, pages 1036–1042, 2015.
- [52] D. Bharadia, E. McMillin, and S. Katti. Full duplex radios. *ACM SIGCOMM Computer Communication Review*, 43(4):375–386, Sept. 2013.
- [53] D. Korpi, J. Tamminen, M. Turunen, T. Huusari, Y.-S. Choi, L. Anttila, S. Talwar, and M. Valkama. Full-duplex mobile device: pushing the limits. *IEEE Communications Magazine*, 54(9):80–87, Sept. 2016.
- [54] W. Choi, H. Lim, and A. Sabharwal. Power-controlled medium access control protocol for full-duplex WiFi networks. *IEEE Transactions on*

- Wireless Communications*, 14(7):3601–3613, July 2015.
- [55] V. Chandrasekhar, J. Andrews, and A. Gatherer. Femtocell networks: A survey. *IEEE Communications Magazine*, 46(9):59–67, Sept. 2008.
- [56] J. Andrews, H. Claussen, M. Dohler, S. Rangan, and M. Reed. Femtocells: Past, present, and future. *IEEE Journal on Selected Areas in Communications*, 30(3):497–508, April 2012.
- [57] B. Radunovic, D. Gunawardena, P. Key, A. Proutiere, N. Singh, V. Balan, and G. Dejean. Rethinking indoor wireless mesh design: Low power, low frequency, full-duplex. *IEEE Wireless Mesh Networks (WIMESH)*, pages 1–6, 2010.
- [58] E. Everett, A. Sahai, and A. Sabharwal. Passive self-interference suppression for full-duplex infrastructure nodes. *IEEE Transactions on Wireless Communications*, 2014.
- [59] J. Choi, M. Jain, K. Srinivasan, P. Levis, and S. Katti. Achieving single channel, full duplex wireless communication. *ACM Proceedings of the 6th annual international conference on Mobile computing and networking*, pages 1–12, 2010.
- [60] A. Sahai. *Wireless Full-Duplex: From Practice to Theory*. PhD thesis, Rice University, 2014.
- [61] W. Cheng, X. Zhang, and H. Zhang. RTS/FCTS mechanism based full-duplex MAC protocol for wireless networks. *IEEE Globecom Workshops*, pages 5017–5022, 2013.
- [62] A. Tang and X. Wang. A-duplex: Medium access control for efficient coexistence between full-duplex and half-duplex communications. *IEEE*

- Transactions on Wireless Communications*, 14(10):5871–5885, Oct 2015.
- [63] S. Kim, C.-B., and S. Choi. MASTaR: MAC protocol for access points in simultaneous transmit and receive mode. *IEEE Globecom Workshops*, pages 1–6, 2016.
- [64] H. Zuo, Y. Sun, S. Li, Q. Cao, Y. Chen, W. Shi, and X. Wang. A distributed IBFD MAC mechanism and non-saturation throughput analysis for wireless networks. *IEEE 13th International Wireless Communications and Mobile Computing Conference*, pages 1851–1856, 2017.
- [65] Q. Qu, B. Li, M. Yang, Z. Yan, and X. Zuo. MU-FuPlex: a multiuser full-duplex MAC protocol for the next generation wireless networks. *IEEE Wireless Communications and Networking Conference*, pages 1–6, 2017.
- [66] S. Kim, M. Sim, C.-B. Chae, and S. Choi. Asymmetric simultaneous transmit and receive in WiFi networks. *IEEE Access*, 5:14079–14094, July 2017.
- [67] M. Alim, M. Kobayashi, S. Saruwatari, and T. Watanabe. In-band full-duplex medium access control design for heterogeneous wireless LAN. *EURASIP Journal on Wireless Communications and Networking*, 83:1–15, 2017.
- [68] F. Tobagi and L. Kleinrock. Packet switching in radio channels: Part 2-the hidden terminal problem in carrier sense multiple-access and the busy-tone solution. *IEEE Transactions on Communications*, 23(12):1417–1433, Dec. 1975.
- [69] C. Fullmer and J. Garcia-Luna-Aceves. Solutions to hidden terminal problems in wireless networks. *ACM SIGCOMM Computer Communication*

- Review*, 27(4):39–49, Oct 1997.
- [70] Z. Hass and J. Deng. Dual busy tone multiple access (DBTMA) - a multiple access control scheme for Ad Hoc networks. *IEEE Transactions on Communications*, 50(6):975–985, June 2002.
- [71] M. Jain, J. Choi, T. Kim, D. Bharadia, S. Seth, K. Srinivasan, P. Levis, S. Katti, and P. Sinha. Practical, real-time, full duplex wireless. *ACM Proceedings of the 17th annual international conference on Mobile computing and networking*, pages 301–312, 2011.
- [72] N. Singh, D. Gunawardena, A. Proutiere, B. Radunovic, H. Balan, and P. Key. Efficient and fair MAC for wireless networks with self-interference cancellation. *IEEE International Symposium on Modeling and Optimization in Mobile, Ad Hoc and Wireless Networks (WiOpt)*, pages 94–101, 2011.
- [73] S. Goyal, O. Gurbuz, E. Erkip, and S. Panwar. A distributed MAC protocol for full duplex radio. *IEEE Asilomar Conference on Signals, Systems and Computers*, pages 788–792, 2013.
- [74] W. Zhou, K. Srinivasan, and P. Sinha. RCTC: Rapid concurrent transmission coordination in full duplex wireless networks. *IEEE International Conference on Network Protocols (ICNP)*, pages 1–10, 2013.
- [75] X. Xie and X. Zhang. Semi-synchronous channel access for full-duplex wireless networks. *IEEE International Conference on Network Protocols (ICNP)*, pages 209–214, 2014.
- [76] J.-K. Kim, W.-K. Kim, and J.-H. Kim. A new full duplex mac protocol to solve the asymmetric transmission time. *IEEE Globecom Workshops*, pages 1–5, 2015.

- [77] K. Tamaki, A. Raptino, and Y. Sugiyama. Full duplex media access control for wireless multi-hop networks. *IEEE Vehicular Technology Conference (VTC)*, pages 1–5, 2013.
- [78] S.-Y. Chen, T.-F. Huang, K. Lin, Y.-W. Hong, and A. Sabharwal. Probabilistic medium access control for full-duplex networks with half-duplex clients. *IEEE Transactions on Wireless Communications*, 16(4):2627–2640, Apr 2017.
- [79] M. Stoffers and G. Riley. Comparing the ns-3 propagation models. *IEEE International Symposium on Modeling, Analysis and Simulation of Computer and Telecommunication Systems*, pages 61–67, 2012.
- [80] L.-C. Wang, A. Chen, and S.-Y. Huang. A cross-layer investigation for the throughput performance of CSMA/CA-based WLANs with directional antennas and capture effect. *IEEE Transactions on Vehicular Technology*, 56(5):2756–2766, Sept. 2007.
- [81] H. Chen. Revisit of the markov model of IEEE 802.11 DCF for an error-prone channel. *IEEE Communications Letters*, 15(12):1278–1280, Dec. 2011.
- [82] Z. You and I.-T. Lu. Distributed coordination function protocol with unequal frame error rates. *IEEE Communications Letters*, 18(10):1819–1822, Oct. 2014.
- [83] J. Choi, K. Park, and C.-K. Kim. Analysis of cross-layer interaction in multirate 802.11 WLANs. *IEEE Transactions on Mobile Computing*, 8(5):682–693, May 2009.
- [84] M. Laddomada, F. Mesiti, M. Mondin, and F. Daneshgaran. On

- the throughput performance of multirate IEEE 802.11 networks with variable-loaded stations: Analysis, modeling, and a novel proportional fairness criterion. *IEEE Transactions on Wireless Communications*, 9(5):1594–1607, May 2010.
- [85] C.-L. Huang and W. Liao. Throughput and delay performance of IEEE 802.11e enhanced distributed channel access (EDCA) under saturation condition. *IEEE Transactions on wireless communications*, 6(1):136–145, Jan. 2007.
- [86] G. Min, J. Hu, and M. Woodward. Performance modelling and analysis of the TXOP scheme in wireless multimedia networks with heterogeneous stations. *IEEE Transactions on Wireless Communications*, 10(12):4130–4139, Dec. 2011.
- [87] D. Li and J. Pan. Performance evaluation of video streaming over multi-hop wireless local area networks. *IEEE Transactions on Wireless Communications*, 9(1):338–347, Jan. 2010.
- [88] E. Ghadimi, A. Khonsari, A. Diyanat, M. Farmani, and N. Yazdani. An analytical model of delay in multi-hop wireless ad hoc networks. *Wireless Networks*, 17(7):1679–1697, Oct 2011.
- [89] A. El-Sherif and K. Liu. Cooperation in random access networks: Protocol design and performance analysis. *IEEE Journal on Selected Areas in Communications*, 30(9):1694–1702, Oct. 2012.
- [90] I. Tinnirello, G. Bianchi, and Y. Xiao. Refinements on IEEE 802.11 distributed coordination function modeling approaches. *IEEE Transactions on Vehicular Technology*, 59(3):1055–1067, March 2010.

- [91] P. Swain, S. Chakraborty, S. Nandi, and P. Bhaduri. Performance modeling and analysis of IEEE 802.11 IBSS PSM in different traffic conditions. *IEEE Transactions on Mobile Computing*, 14(8):1644–1658, Aug. 2015.
- [92] D. Jia, R. Zhang, K. Lu, J. Wang, Z. Bi, and J. Lei. Improving the uplink performance of drive-thru internet via platoon-based cooperative retransmission. *IEEE Transactions on Vehicular Technology*, 63(9):4536–4545, Nov. 2014.
- [93] H. Wang, R. Ping, W. Ni, W. Chen, and I. Collings. VANET modeling and clustering design under practical traffic, channel and mobility conditions. *IEEE Transactions on Communications*, 63(3):870–881, March 2015.
- [94] G. Bianchi and I. Tinnirello. Kalman filter estimation of the number of competing terminals in an IEEE 802.11 network. *IEEE INFOCOM*, pages 844–852, 2003.
- [95] A. Toledo, T. Vercauteren, and X. Wang. Adaptive optimization of IEEE 802.11 DCF based on Bayesian estimation of the number of competing terminals. *IEEE Transactions on Mobile Computing*, 5(9):1283–1296, Sept. 2006.
- [96] F. Cali, M. Conti, and E. Gregori. Dynamic tuning of the IEEE 802.11 protocol to achieve a theoretical throughput limit. *IEEE/ACM Transactions on Networking*, 8(6):785–799, December 2000.
- [97] Z. Haas and J. Deng. On optimizing the backoff interval for random access schemes. *IEEE Transactions on Communications*, 51(12):2081–2090, Dec. 2003.
- [98] M. Heusse, F. Rousseau, R. Guillier, and A. Duda. Idle sense: An optimal

- access method for high throughput and fairness in rate diverse wireless LANs. *ACM SIGCOMM Computer Communication Review*, 35(4):121–132, Aug 2005.
- [99] D. Deng, C. Ke, H. Chen, and Y. Huang. Contention window optimization for IEEE 802.11 DCF access control. *IEEE Transactions on Wireless Communications*, 7(12):5129–5135, Dec. 2008.
- [100] L. Chen, S. Low, and J. Doyle. Random access game and medium access control design. *IEEE/ACM Transactions on Networking*, 18(4):1303–1316, Aug. 2010.
- [101] IEEE 802.11ax task group. available at http://www.ieee802.org/11/Reports/tgax_update.htm, last accessed in Sep 2017.
- [102] J. Barcelo, A. Toledo, C. Cano, and M. Oliver. Fairness and convergence of CSMA with enhanced collision avoidance (ECA). *IEEE International Conference on Communications (ICC)*, 4:511–523, December 2010.
- [103] L. Sanabria-Russo, J. Barcelo, B. Bellalta, and F. Gringoli. A high efficiency MAC protocol for WLANs: Providing fairness in dense scenarios. *IEEE/ACM Transactions on Networking*, 25(1):492–505, Feb. 2017.
- [104] N. Facchi, F. Gringoli, D. Malone, and P. Patras. Imola: A decentralised learning-driven protocol for multi-hop White-Fi. *Computer Communications*, 105:157–168, 2017.
- [105] M. Lacage and T. Henderson. Yet another network simulator. *ACM Proceeding from the 2006 workshop on NS-2: the IP network simulator*, pages 321–325, 2006.

-
- [106] V. Aggarwal and N. Shankaranarayanan. Performance of a random-access wireless network with a mix of full- and half-duplex stations. *IEEE Communications Letters*, 17(11):2200–2203, Nov. 2013.
- [107] Y. He, J. Sun, R. Yuan, and W. Gong. A reservation based backoff method for video streaming in 802.11 home networks. *IEEE Journal on Selected Areas in Communications*, 28(3):332–343, April 2010.
- [108] S. Misra and M. Khatua. Semi-distributed backoff: Collision-aware migration from random to deterministic backoff. *IEEE Transactions on Mobile Computing*, 14(5):1071–1084, Jan. 2015.
- [109] M. Tuysuz and H. Mantar. Exploiting the channel using uninterrupted collision free MAC adaptation over IEEE 802.11 WLANs. *Wireless Communications and Mobile Computing*, 91:1227–1230, 2015.

Appendix A

List of Publications

The author of this thesis has the following publications:

- [†]J. Kim, D. Laurenson, and J. Thompson. "Fair and Efficient Full Duplex MAC Protocol based on the IEEE 802.11 DCF", *IEEE International Symposium on Personal, Indoor, and Mobile Radio Communications (PIMRC)*, Sept 2016.
- [†]J. Kim, D. Laurenson, and J. Thompson. "Centralized Random Backoff for Collision Resolution in Wi-Fi Networks", *IEEE Transactions on Wireless Communications*, 16(9):5838-5852, Sept. 2017.
- J. Kim. "Source Codes of the Network Simulator for Centralized Random Backoff in Wi-Fi Networks", University of Edinburgh, June 2017, available at <http://dx.doi.org/10.7488/ds/2068>.

In preparation:

- J. Kim, D. Laurenson, and J. Thompson. "Collision Free Wireless Local Area

[†]These papers are reprinted in this appendix.

Networks through Adaptive Centralized Random Backoff', submitted to IEEE Transactions on Communications in Oct 2017.

Fair and Efficient Full Duplex MAC Protocol based on the IEEE 802.11 DCF

J. D. Kim

School of Engineering
The University of Edinburgh
Mayfield Road, Edinburgh,
United Kingdom, EH9 3JL
Email: j.kim@ed.ac.uk

D. I. Laurenson

School of Engineering
The University of Edinburgh
Mayfield Road, Edinburgh,
United Kingdom, EH9 3JL
Email: dave.laurenson@ed.ac.uk

J. S. Thompson

School of Engineering
The University of Edinburgh
Mayfield Road, Edinburgh,
United Kingdom, EH9 3JL
Email: john.thompson@ed.ac.uk

Abstract—Recent research has shown the feasibility of in-band full duplex (FD) wireless operation allowing wireless nodes to send and receive in the same frequency band at the same time. In this paper, we propose a novel FD medium access control (MAC) protocol, and discuss two issues related to the FD MAC layer. These include fairness between half duplex (HD) and FD users, and a channel access mechanism called centralized random backoff (CRB) to resolve collisions caused by the random backoff algorithm adopted in the IEEE 802.11 MAC standard. Simulation results show that the protocol provides evenly distributed channel access opportunities to both FD and legacy HD users. Moreover, it is demonstrated by simulation that using CRB complements the random backoff algorithm and improves the performance of HD and FD MAC protocols for Wi-Fi networks.

I. INTRODUCTION

Wireless technologies such as Wi-Fi (Wireless Fidelity) and LTE (Long Term Evolution) currently operate in half duplex (HD) mode in a single channel. HD communication means that in one time-frequency block, a node can either transmit or receive but not both simultaneously. The counterpart of HD communication is full duplex (FD) communication, where a node can simultaneously transmit one signal and receive another signal in the same band at the same time. Compared to HD communication, FD communication has significant potential to improve spectral efficiency, which makes it an attractive feature for future wireless communication devices. However, simultaneous transmission and reception causes the transmitted signal to strongly interfere with the signal being received, which is called self interference [1-2]. Since the signal of interest being received is typically several orders of magnitude (50-100 dB) weaker than the self interference signal, successfully receiving a weak signal of interest in the presence of a strong self interference signal is one of the key requirements to enable FD radios. In this context, multiple authors [2-5] have reported different self interference cancellation methods.

In order to maximize the performance of FD radios and to share access to the medium fairly, several FD MAC (Medium Access Control) protocols have been proposed as summarized in [2, 6]. A practical FD MAC protocol operating with RTS (Request-to-Send) /CTS (Clear-to-Send) frames was presented in [4]. Based on the IEEE 802.11 DCF (Distributed

Coordination Function), the protocol was designed to support FD transmission between two nodes when both the access point (AP) and a station have a packet to send to each other. Moreover, new uses of a busytone signal in FD transmission have been introduced for resolution of the hidden node problem where FD nodes cannot hear each other when they communicate with a common node (i.e. the AP) [7-8]. However, little attention has been paid to a fairness issue between legacy HD and FD users in the presence of the hidden node problem.

The IEEE 802.11 DCF standard implements random backoff by exponentially increasing the contention window size for each transmission failure in order to avoid consecutive collisions. In both HD and FD MAC protocols based on the random backoff, a collision can occur when two or more stations contend to transmit. This is because each station independently selects a random number as its backoff count in the given contention window before transmitting. As a result, the throughput performance of the IEEE 802.11 DCF is significantly degraded as the number of nodes increases [9]; in addition, it was also reported in [8] that the throughput performance of the FD MAC protocol based on the IEEE 802.11 DCF is degraded as the number of FD nodes increases. Moreover, it has been found that random backoff is vulnerable to selfish backoff attacks consisting of non-standard implementations of the constituent backoff scheme [10-11].

In order to reduce the number of collisions, a large number of collision (or contention) resolution algorithms have been proposed [1, 12, 13]. According to [12], collisions can be resolved by each active node setting its backoff counter to a deterministic value upon a successful packet transmission, which is called a semi-random backoff or semi-distributed backoff. In case of a failed packet transmission, the station reverts to the standard random backoff procedure and probes for a new available time slot. However, as the number of active nodes increases, the convergence time (i.e. the time where nodes suffer from collisions as the system moves towards a collision free state) is dramatically increased. In [13], a station announces its future backoff count using the MAC header of its data frame being transmitted, which is called the Early Backoff Announcement (EBA). All the neighbouring stations receiving

the backoff information avoid collisions by excluding the same backoff count when selecting their future backoff value. However, the backoff information can also be overheard by a malicious user enabling a selfish backoff attack. On the other hand, a backoff count sharing scheme, called shared random backoff (SRB), was presented in [3] to perform efficient full duplex communication and to prevent neighbouring legacy HD nodes being starved by the full duplex communication. However, methods to reduce the collision probability were not considered in SRB.

In this regard, we propose a novel FD MAC protocol to fairly provide channel access opportunities to FD nodes coexisting with legacy HD nodes, and to improve the throughput performance of both HD and FD transmissions with a new collision resolution mechanism. The key contributions in the proposed protocol design can be divided into two parts. First, we identified a fairness problem between a legacy HD user and a FD user in the *polite full duplex* protocol presented in [4], and we suggest the use of a busytone signal in the FD MAC protocol to solve the issue. Second, we propose a novel collision resolution solution called centralized random backoff (CRB). Since CRB complements the random backoff algorithm, it is applicable to both HD and FD transmissions based on the 802.11 DCF standard. Stations operating with the CRB protocol do not suffer from collisions, because the AP dynamically allocates a unique backoff count to each station. CRB is also expected to be a more secure solution than EBA, because the backoff information in CRB can be encrypted to prevent it being overheard by a malicious neighbouring user.

Simulation results show that while not sacrificing performance, the proposed protocol provides fairness in terms of channel access opportunities between legacy HD and FD nodes in the presence of the hidden node problem; in addition, it is also shown that the average retransmission ratio has been lowered thanks to CRB. Therefore, the throughput performance of both HD and FD MAC protocols based on IEEE 802.11 DCF has been improved through the proposals.

The rest of the paper is organized as follows. In Section II, we review the system model discussed in this paper. In Section III, we describe the FD MAC protocol and explain the key contributions in detail. In Section IV, we explain the simulation results for validating the proposed MAC protocol. Section V concludes this paper.

II. SYSTEM MODEL

We consider a Wi-Fi network setup operating in the infrastructure mode in the IEEE 802.11 standard as shown in Fig. 1, where a single AP together with all connected stations (STAs) is called a BSS (Basic Service Set). We focus on a single BSS environment, where interference from adjacent wireless networks is assumed to be negligible. As shown in the figure, the network model includes a single AP, a gateway wired to the AP, wired nodes behind the gateway, and mixed Wi-Fi stations connected to the AP. In the network model, a legacy HD user can coexist with a FD user. In this evaluation scenario, we assume that the AP and the connected

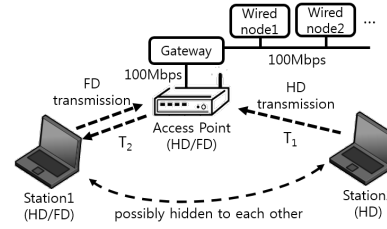


Fig. 1. Wi-Fi network configuration.

Wi-Fi stations transmit signals with a constant transmission power (≈ 16 dBm). They support only the 802.11a physical layer (PHY), and operate in the DCF mode. We assume that all nodes remain stationary (i.e. no mobility). The log distance propagation loss model (exponent=3) in [14], which predicts the received signal power as a deterministic function of distance, is assumed to apply to the transmitted signals.

In order to evaluate the throughput performance of CRB in the saturation conditions (i.e. where the transmission queue of each node is assumed to be always non-empty and each active node immediately attempts to transmit a packet after the completion of each transmission), we use the UDP (User Datagram Protocol) data packets in this simulation and assume that a real time streaming application is being used by each user. The wired nodes transmit UDP data packets of a constant size to Wi-Fi stations through the gateway and the AP. In a symmetric fashion, the Wi-Fi stations transmit UDP data packets of the same size to the wired nodes. The saturation assumption enables queueing dynamics to be negligible. CRB might be less effective for light traffic load conditions or for transmitting TCP (Transmission Control Protocol) packets, because the backoff counter of a node becomes unsynchronized with the AP when it has no data to send (or when it does not immediately attempt to transmit a packet after the completion of each transmission). The use of light traffic loads (or TCP packets) with CRB is not discussed in this paper due to space limitation.

III. FULL DUPLEX MAC PROTOCOL

In Section III-A, we first explain a fairness problem in the polite full duplex protocol, and a solution to the issue is proposed in Section III-B. After that, in Section III-C, we explain the second contribution of the paper, which is a novel collision resolution scheme called CRB.

A. State of the Art Protocol

In the IEEE 802.11 standard, all nodes use a longer wait time *EIFS* (Extended Inter Frame Space) rather than the standard wait time *DIFS* (DCF Inter Frame Space) if they receive an erroneous packet. The extended wait time is used to allow some other recipient for the packet who received the data correctly to be able to send an ACK frame without a collision occurring. As explained in [4], the neighbouring

legacy HD nodes that are not involved in a FD transmission would detect an erroneous data packet and thus wait for the *EIFS* wait time; however, the two FD nodes involved in the FD transmission can successfully decode the data packet and thus start their backoff timer after waiting for the *DIFS* wait time. Since the *DIFS* wait time is shorter than the *EIFS* wait time, there is higher likelihood for one of the two FD nodes to transmit on the channel again causing unfairness to legacy HD nodes.

In order to solve the imbalance of channel access opportunities between legacy HD and FD nodes, [4] proposed the *polite full duplex* protocol. This protocol means that the two FD nodes involved in a successful FD transmission wait for the *EIFS* time rather than the *DIFS* time in order to fairly share channel access opportunities with legacy HD nodes. This is shown in Fig. 2. However, this approach is still vulnerable to the hidden node problem. As shown in Fig. 1, the hidden node problem in a single BSS environment could still occur between a legacy HD node and a FD node. If Station2 in Fig. 1 is hidden from Station1, it will successfully overhear a signal transmitted by the AP while the AP performs a FD transmission with Station1. That means Station2 waits for the *DIFS* time period rather than the *EIFS* time period. In this case, there is again a higher likelihood for Station2 to then occupy the channel, since the *DIFS* waiting time is smaller than the *EIFS* waiting time.

B. Busytone Signal Solution

In order to solve the fairness problem caused in the presence of hidden nodes, we propose a FD MAC protocol as described in Fig. 2, which is designed to require minimal changes to the current Wi-Fi standard. We reuse the FD opportunity discovery process presented in [4], where FD nodes use RTS/CTS frames to detect a FD opportunity. After the discovery process, the AP and the FD station transmit a data frame to each other simultaneously. The AP then transmits the ACK1 frame to the station first, and lastly the FD station transmits the ACK2 frame to the AP.

The FD *initiator*, one of the two nodes involved in a FD transmission as shown in Fig. 2, initiates a FD transmission by transmitting the RTS frame. The other node becomes the FD *follower* when it performs a FD transmission with the initiator. When its backoff counter expires, a FD initiator transmits a packet at the head of the transmission queue, or transmits a packet that needs to be retransmitted. The FD initiator will conduct a retransmission if it fails to receive the CTS (or ACK frame) for the transmitted RTS (or data frame).

After transmitting the CTS frame, the FD follower waits for SIFS (Short Inter Frame Space) delay time (which is required for a wireless interface to process a received frame and to respond with a response frame), and transmits a data packet to the FD initiator in FD transmission when it has a packet for that node. Unlike the FD initiator, the FD follower does not retransmit after it fails to receive an ACK frame for the transmitted data frame, due to its follower status. Any

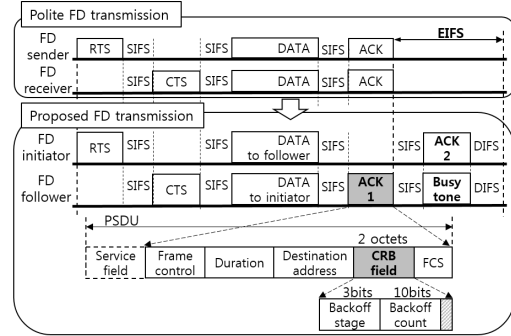


Fig. 2. The polite full duplex and the proposed full duplex transmissions.

data packet that is not delivered by a station while it is a FD follower can be transmitted again when it becomes a FD initiator.

If it is assumed that Station1 in Fig. 1 becomes a FD follower, it transmits a packet at the head of its transmission queue or a packet that needs to be retransmitted. However, if the AP becomes a FD follower while it is connected to multiple clients, the AP looks for a data packet to send to the FD initiator nearest to the head of the transmission queue. That is because the data packet at head of the transmission queue may not be addressed to that node. If the AP as a FD follower fails to receive an ACK frame for a transmitted data packet, it does not conduct a retransmission for that data packet but places it back into the original order in the transmission queue.

The two ACK frames presented in Fig. 2, ACK1 and ACK2 frames, are transmitted at different times. ACK1 is transmitted first in HD transmission by the AP, which is a modified ACK frame used to perform CRB for improving throughput gain. After that, ACK2 is transmitted by a FD station, which is a conventional half duplex ACK frame.

While receiving the ACK2 signal, the AP transmits a *busytone signal* in order to resolve the hidden node problem. The use of a busytone signal in FD transmission was also introduced in [7-8] for early detection of a collision of data frames and for alleviating the hidden node problem while transmitting data frames. It has not been used before for alleviating the hidden node problem while transmitting ACK frames. We assume that the busytone signal is a single subcarrier known by the AP to all stations in the wireless network.

After simultaneous transmission of the ACK2 and the busytone, the two FD nodes will wait for the *DIFS* delay time rather than the *EIFS* delay time. Because of the ACK1 frame transmitted in HD mode by the AP, all other nodes (hidden or not) will wait for the *DIFS* delay time as well. In this way, it is expected that channel access opportunities are evenly distributed between a legacy HD station and a FD station even though they are hidden from each other. Moreover, in the

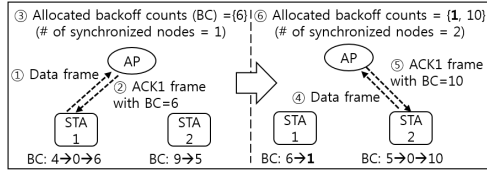


Fig. 3. Allocation of a backoff state to each node.

IEEE 802.11 standard, the *EIFS* time is specified as *SIFS* wait time plus *ACK* transmission time plus *DIFS* wait time. This means that the FD transmission time of the proposed FD protocol is almost equal to that of the polite FD protocol.

As represented in Fig. 2, the RTS/CTS frames and ACK1 frame are transmitted in a HD transmission format, which allows the 802.11 preamble signals, such as the STF (Short Training Field) and the LTF (Long Training Field), to be used for training the self interference cancellation mechanism.

C. Centralized Random Backoff (CRB) Solution

In the CRB mechanism, the AP allocates backoff information to each active node (either a source in HD mode or an initiator in FD mode) using an ACK frame, when the AP has received a successful data frame from the node and discovered that the node has more data packets to send. As seen in Fig. 2, two octets of CRB field are added in ACK1 frame to carry the backoff information. The backoff information is about a backoff state to be allocated to the node, which includes two numbers: a backoff stage (BS) and a backoff count (BC). This is generated by the AP just before transmitting the ACK1 frame, and then it is delivered to the node (Refer to steps ② and ⑤ in Fig. 3). If the data frame is unsuccessful, and the node fails to receive the ACK frame before starting contention again, then the node generates a new backoff state by itself following the current IEEE 802.11 DCF.

The AP generates a unique backoff state for each node as described below. After successfully receiving a data frame from STA2 (i.e., after step ④ and before step ⑤ in Fig. 3), the AP picks a random number from the range [0, 15] (*virtual backoff stage 0*) to send to STA2. However, if the selected number is the same as the backoff count of another station (*a virtual collision*), for example the backoff count of STA1 (=1) as shown in Fig. 3, the AP again picks another a random number in the doubled range [0, 31] (*virtual backoff stage 1*). If the newly selected number is unique compared to the backoff count of STA1, then the backoff state is allocated to STA2. However, if the number selected in [0, 31] is equal to the backoff count of STA1 again, then the AP picks again a random backoff count in the doubled range [0, 63] (*virtual backoff stage 2*). The process continues to the point where the range is [0, 1023] (*virtual backoff stage m* which is 6 by default in the 802.11 standard), whereupon random numbers (as backoff counts) are selected in this range until a unique value is obtained. We call this a virtual backoff algorithm

(VBA) in the AP. In addition, we allow the AP to allocate a unique backoff state to itself (by referring the allocated and synchronized backoff counts) just after receiving a successful ACK frame from a station. In this way, nodes contending at the same time for accessing the channel can be allocated a unique backoff count.

According to the IEEE 802.11a standard, although it supports eight different data rates in the range from 6 Mbps upto 54 Mbps, only three data rates (i.e. 6 Mbps, 12 Mbps, and 24 Mbps) of them are mandatory. This means in order to support backward compatibility to 802.11a devices, one of the three data rates must be used for transmitting control frames such as ACK frames. When 6 Mbps data rate (i.e. BPSK¹ modulation with rate 1/2 coding) is used for encoding ACK frames, an OFDM (Orthogonal Frequency-Division Multiplexing) symbol is encoded to carry three octets. A legacy ACK frame contains 16 octets in its PSDU (PLCP² Service Data Unit), which is followed by tail bits (6 bits). Therefore, 6 OFDM symbols are required to carry the PSDU and the tail bits. This means that adding two additional octets for including the CRB field in a legacy ACK frame will require an additional OFDM symbol. However, if 24 Mbps data rate (i.e. 16-QAM³ with rate 1/2 coding) is used for encoding ACK frames, an OFDM symbol is encoded to carry 12 octets. This means that adding two additional octets for including the CRB field in a legacy ACK frame will not require an additional symbol.

In the 802.11 DCF, backoff countdowns can be paused by carrier sense events called CCA (Clear Channel Assessment) in the 802.11 standard. Each station might see different channel busy patterns because of hidden nodes in a single BSS environment. In CRB scenario, if a station detects the presence of a hidden node by overhearing data frames and ACK frames, the station informs the AP of the fact by transmitting a unique and short busytone signal (a unique subcarrier for each station assigned by the AP in the connection establishment procedure) just after receiving a beacon signal. In this way, the AP can be made aware of the hidden node. The AP and the station perform CRB when no hidden node has been detected for a specific time period.

IV. SIMULATION AND NUMERICAL RESULTS

In order to evaluate the proposed protocol, we have developed a network simulator based on the Network Simulator-3 (NS-3)⁴. The *yans-wifi module* [15] has been modified to implement the proposed FD MAC protocol and the basic HD MAC protocol with CRB. Simulation parameters are presented in Table I. We run simulations for 30 s, where the first 10 s is omitted to remove the effect of traffics generated in connection establishment procedures. We assume that each node is able to support cancelling out its transmitted signal by 110 dB in its receiver, i.e. 110 dB self interference cancellation.

¹Binary Phase-Shift Keying

²PLCP: Physical Layer Convergence Protocol

³Quadrature Amplitude Modulation

⁴NS-3 version 3.22. This is an open source project available at <http://www.nsnam.org>.

Table I. Simulation parameters

Parameters	Value
Wireless standard	IEEE 802.11a PHY, DCF MAC
Frequency channel	5.0 GHz
Bandwidth	20 MHz
Simulation time	30 sec
Propagation loss model	Log distance model (exponent=3)
Transport layer	UDP (User Datagram Protocol)
UDP payload	1400 bytes
Modulation and coding for control/management frames	BPSK and 1/2 coding rate (6 Mbps constant rate)
Available data rates	6, 9, 12, 18, 24, 36, 48, and 54Mbps
Transmission queue	Single queue
Traffic model	Full buffer
Tx power	16 dBm
Rx sensitivity	-91 dBm
Noise floor	-94 dBm
Self interference	-94 dBm
CWmin	16
CWmax	1024
BER (Bit Error Rate) model	Reference [15]

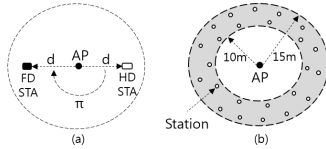


Fig. 4. A two-dimensional simulation setups. Setup (a) is for testing full duplex MAC protocols in the presence of hidden node problem, and setup (b) is for evaluating system throughput of CRB in each of the basic HD MAC and the proposed FD MAC protocols.

A. Fairness between HD and FD users

In order to evaluate the solution with respect to the fairness issue discussed in Section III-A, we set up a two-dimensional simulation configuration with three wireless nodes as shown in Fig. 4(a), and we investigate how many channel accesses are granted to each node. The AP and the HD STA use the RTS/CTS protocol to transmit packets to each other, and the AP and the FD STA use the proposed FD MAC protocol to each other. The HD STA and the FD STA in Fig. 4(a) are symmetrically located at a distance ($=d$) from the AP at opposite sides of the cell. So, it is expected that the HD STA and the FD STA will cause and suffer hidden node problems to each other if the value of d is large enough.

Fig. 5 shows that as the distance d increases, the number of accesses granted to each node to transmit the RTS frames (i.e. the number of backoff counter expirations per second) tends to decrease. That is because the simulation runs for 30 s (constant time), and the three nodes lower their data rate as the value of d increases. The figure also shows that as the distance d increases above 60 metres, the HD STA and the FD STA become hidden nodes to each other. This results in a dramatic increase in the number of accesses granted to the

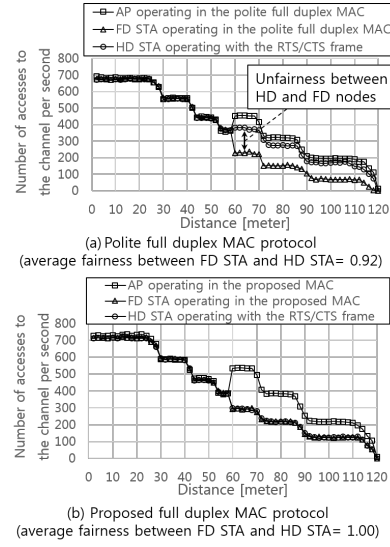


Fig. 5. Comparison of the number of accesses granted to each node.

AP (compared to those of the HD STA and the FD STA).

In the hidden node scenario, after a successful polite FD transmission between the FD STA and the AP, the FD STA waits for *EIFS* time while the HD STA waits for *DIFS* time. That explains the difference (unfairness) between the number of accesses granted to the HD STA and the FD STA as shown in Fig. 5(a). A fair MAC protocol should not penalize some users arbitrarily. Fairness in wireless MAC protocols has been defined in a number of different ways. Usually the proportional fairness metric, which can guarantee some portion of common resource to each node while maximizing resource utilization, has been applied to Wi-Fi networks. In this regard, we use Jain's fairness index as in (1),

$$\text{Jain's index} = \frac{(x_{HD} + x_{FD})^2}{2 \cdot (x_{HD}^2 + x_{FD}^2)} \quad (1)$$

where x_{HD} and x_{FD} represent the average number of accesses granted to the HD and FD nodes, respectively. When they are randomly placed in the range of 1 to 110 metres from the AP, the average value of the fairness is calculated as 0.92. However, when the AP and the FD STA operate in the proposed FD MAC protocol, the FD STA has more or less the same number of granted accesses to the channel compared to that of the HD STA even though they are placed in a hidden node configuration, which is shown in Fig. 5(b). When they are randomly placed in the range of 1 to 110 metres from the AP, the average value of the fairness is calculated as 1.00.

B. Performance of Centralized Random Backoff

In order to evaluate collision resolution performance of CRB, we have implemented it with the two different protocols

2016 IEEE 27th Annual IEEE International Symposium on Personal, Indoor and Mobile Radio Communications - (PIMRC): MAC & Cross-Layer Design

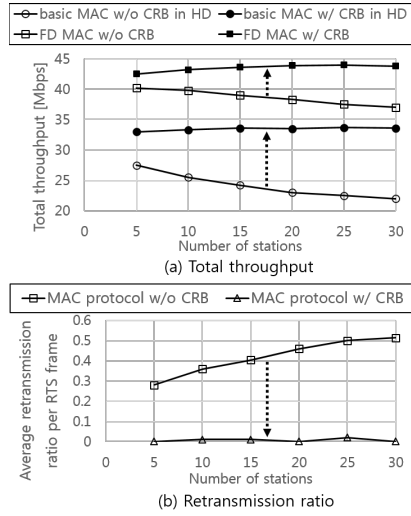


Fig. 6. Comparison of throughput performance.

(i.e., the basic MAC protocol in HD mode and the proposed FD MAC protocol). We configure stations randomly and uniformly placed in the range of 10 to 15 metres away from the AP as shown in Fig. 4(b), so that there is no hidden node in the single BSS environment we consider. All the nodes use a constant data rate of 54 Mbps.

Fig. 6(a) presents the simulation results where we see that throughput of the two MAC protocols not using CRB decrease as the number of nodes increases. This is because the collisions caused by the random access algorithm increases proportionally to the number of stations [9]. However, the total throughput of the two protocols operating with CRB do not decrease as the number of stations increase. Unlike current DCF, the protocols operating with CRB maintain the maximal throughput as the number of stations increases. This is explained by the simulation results in Fig. 6(b), which shows average retransmission ratios. The ratios are calculated in the simulation as the total number of retransmitted data frames (or retransmitted RTS frames in the FD mode) divided by the total number of transmitted data frames (or transmitted RTS frames). The retransmission ratio of the stations operating in CRB does not increase as the number of stations increases. This is shown to be more or less the same, and below 1%.

Lastly, in the simulation setup, the RTS frame is shorter than the data frame in terms of transmission time, which means that the wasted time caused by a collision of RTS frames is less than that for a collision of data frames. This difference is seen in Fig. 6(a) by the fact that the range of CRB gain of the proposed FD MAC is lower than that of the basic HD MAC.

V. CONCLUSIONS

Prior work documented the polite FD MAC protocol operating with RTS/CTS frames, but the unfair channel access

issue between HD and FD nodes in the presence of a hidden node problem was not investigated. In this paper, we have redesigned it for both a higher fairness and a higher throughput performance. The simulation results showed that the average fairness index between the legacy HD node and the FD node was improved significantly compared to that of the polite full duplex MAC protocol. The collision resolution performance of CRB was also demonstrated in the simulation. The total throughput of FD nodes using CRB was improved by 4% to 12% (depending on the number of stations) over the state of the art FD MAC protocol. Moreover, the total throughput of HD nodes using CRB was improved by 10% to 38% compared to that of the current basic MAC protocol in the IEEE 802.11 standard. Future research should focus on analysis of encryption techniques enabling secure transmission of the CRB field. In addition, the use of TCP on CRB protocol should be investigated.

ACKNOWLEDGMENT

Jinho D. Kim was supported by the Edinburgh Global Research Scholarship and the Principal's Career Development PhD Scholarship from the University of Edinburgh, Scotland.

REFERENCES

- [1] Gummalla, Ajay Chandra V., and John O. Limb. "Wireless medium access control protocols." IEEE Communications Surveys and Tutorials, 2000.
- [2] Kim, Dongkyu, Haesoon Lee, and Daesik Hong. "A survey of in-band full-duplex transmission: From the perspective of PHY and MAC layers." IEEE Communications Surveys and Tutorials, 17.4 (2015): 2017-2046.
- [3] Achaleshwar Sahai, "Wireless Full-Duplex: From Practice to Theory." PhD Thesis, Rice University, 2014.
- [4] Duarte, M., Sabharwal, A., Aggarwal, V., Jana, R., Ramakrishnan, K. K., Rice, C. W., and Shankaranarayanan, N. K., "Design and characterization of a full-duplex multi-antenna system for WiFi networks." IEEE Transactions on Vehicular Technology, 63(3), 1160-1177, 2014.
- [5] Laughlin, Leo, Mark A. Beach, Kevin A. Morris, and John L. Haine, "Optimum single antenna full duplex using hybrid junctions." IEEE Journal on Selected Areas in Communications, 32, no. 9, 2014.
- [6] K. M. Thilina, H. Tabassum, E. Hossain and D. I. Kim, "Medium access control design for full-duplex wireless systems: Challenges and approaches." IEEE Communication Magazine, 53(5), 112 - 120, 2015.
- [7] Jain, Mayank, et al. "Practical, real-time, full duplex wireless." Proceedings of the 17th annual international conference on Mobile computing and networking. ACM, 2011.
- [8] Goyal, Shri, et al. "A distributed MAC protocol for full duplex radio." IEEE Asilomar Conference on Signals, Systems and Computers, 2013.
- [9] Bianchi, Giuseppe. "Performance analysis of the IEEE 802.11 distributed coordination function." IEEE Journal on Selected Areas in Communications, 18.3 (2000): 535-547.
- [10] Konorski, Jerzy. "A game-theoretic study of CSMA/CA under a backoff attack." IEEE/ACM Transactions on Networking, 2006.
- [11] Konorski, Jerzy. "Solvability of a Markovian Model of an IEEE 802.11 LAN under a Backoff Attack." IEEE International Symposium on Modeling, Analysis, and Simulation of Computer and Telecommunication Systems, 2005.
- [12] He, Yong, et al. "Semi-random backoff: towards resource reservation for channel access in wireless LANs." IEEE/ACM Transactions on Networking 21.1 (2013): 204-217.
- [13] Choi, Jaehyuk, et al. "EBA: An enhancement of the IEEE 802.11 DCF via distributed reservation." IEEE Transactions on Mobile Computing, 4.4 (2005): 378-390.
- [14] Stoffers, Mirko, and George Riley. "Comparing the ns-3 propagation models." IEEE 20th International Symposium on Modeling, Analysis and Simulation of Computer and Telecommunication Systems, 2012.
- [15] Lacage, Mathieu, and T. R. Henderson. "Yet another network simulator." Proceeding from the 2006 workshop on NS-2: the IP network simulator. ACM, 2006.

Centralized Random Backoff for Collision Resolution in Wi-Fi Networks

Jinho D. Kim, David I. Laurenson, and John S. Thompson, *Fellow, IEEE*

Abstract—Wi-Fi devices operate following the 802.11 distributed coordination function in order to fairly use the channel that the devices share. However, the throughput performance of the Wi-Fi networks is known to be degraded due to packet collisions. So, we propose a novel multiple access protocol, called centralized random backoff (CRB) for collision-free Wi-Fi networks. In CRB, after a successful reception of a data frame from a station, the access point allocates a unique backoff state to the station by means of the ACK frame. We evaluate its performance by comparing to that of a deterministic backoff mechanism. Evaluation results show that CRB significantly improves the throughput performance by reducing collisions, and it allows a larger number of nodes to operate in a collision-free state without dynamic parameter adjustment.

Index Terms—Medium access control, MAC protocol, random access, distributed access, distributed coordination function, random backoff, collision resolution, and fairness.

I. INTRODUCTION

Wi-Fi technology following the IEEE 802.11 standard has become popular through operating with a simple decentralised MAC (Medium Access Control) protocol in unlicensed radio bands. Generally, Wi-Fi devices use the 802.11 DCF protocol to schedule their transmissions. The DCF implements random access by exponentially increasing the contention window size for each transmission failure in order to avoid consecutive collisions. Because each station independently selects a random number as its backoff count before transmitting, packet collisions can occur when two or more stations contend to transmit simultaneously.

Collision (or contention) resolution is one of the key goals of wireless MAC protocols [1]. In the 802.11 DCF, given a number of active nodes ($= n$) the collision probability ($= p$) tends to decrease as the minimum (or the initial) contention window size ($= W_0$) increases. However, the channel idle time (i.e. empty time slots) also increases with the value W_0 . The fact that an optimum value of W_0

exists for a given value n was explained with a Markov chain model in [2]. The chain model was further developed for more practical conditions (such as a finite retry limit, imperfect channels, and unsaturated traffic) [3]–[6], and several ideas were proposed to dynamically estimate the value n for timely adjustment of the optimum value of W_0 [7], [8]. Furthermore, in order to improve the throughput performance (while maintaining fairness) various mechanisms for tuning the contention window sizes were proposed in [9]–[13]. Recently the 802.11ax project [14] has been tackling the challenging goal of improving the throughput in dense user environments. However, the fact that collisions increase with n is still a feature of such systems, causing throughput degradation. In addition, when the value n varies over time, fast adaptation of the optimum value of W_0 is still a complex issue in practice.

A collision free Wi-Fi network, where the value p is zero, has been studied in [15]–[23]. In Early Backoff Announcement (EBA) [15], a station announces its future backoff count using the MAC header of its transmitted data frame. All the neighbouring stations that receive the backoff count avoid collisions by excluding the same backoff count when selecting their future backoff value. However, the performance of EBA is significantly limited in practice, because some of the neighbouring stations may not be able to overhear the announced backoff count in the data frame. This is because different data rates have a different transmission coverage to each other.¹

According to [17]–[20], a collision free Wi-Fi network can be achieved by each active node setting its backoff counter to a deterministic value upon a successful packet transmission. This deterministic backoff mechanism is called CSMA/ECA² in [19] and also called semi-random backoff (SRB) in [20]. In the case of a failed packet transmission, the station reverts to the standard random backoff procedure of DCF. However, the maximum value n that can operate in a collision free state ($= n_{max}$) is limited to the value $\frac{W_0}{2}$. So, to support a larger number of nodes in a collision free state, the value W_0 has to be increased. However, channel idle time also tends to increase with the value W_0 . Because of this, when the value n is assumed to change over time, the deterministic backoff requires dynamic adjustment of the optimum value of W_0 .

Manuscript received August 29, 2016; revised March 9, 2017 and June 6, 2017; accepted June 12, 2017. Date of publication June 21, 2017; date of current version September 8, 2017. The work of J. D. Kim was supported in part by the Edinburgh Global Research Scholarship and in part by the Principal's Career Development Ph.D. Scholarship from the University of Edinburgh, U.K. The associate editor coordinating the review of this paper and approving it for publication was A. Banchs. (*Corresponding author: Jinho D. Kim.*)

The authors are with the Institute for Digital Communications, School of Engineering, University of Edinburgh, Edinburgh EH9 3JL, U.K. (e-mail: j.kim@ed.ac.uk; dave.laurenson@ed.ac.uk; john.thompson@ed.ac.uk).

Digital Object Identifier 10.1109/TWC.2017.2716922

1536-1276 © 2017 IEEE. Personal use is permitted, but republication/redistribution requires IEEE permission. See http://www.ieee.org/publications_standards/publications/rights/index.html for more information.

¹e.g. the coverage of a station using a 54 Mbps data rate is much smaller than that of a station using a 6 Mbps data rate.

²Carrier Sense Multiple Access with Enhanced Collision Avoidance.

However, timely adjustment of the value W_0 is still a complex issue.³

We propose a novel collision resolution solution called *centralized random backoff (CRB)*, in which a backoff state is generated by the access point (AP) and allocated to the connected stations by means of ACK frames. The ACK frames from the AP are generally more reliable than the data frames from distributed stations. Like the deterministic backoff, CRB achieves a collision free state after a given convergence time⁴($= T_{cvg}$). However, it is expected to be a more effective solution than the deterministic backoff, because the value n_{max} in CRB is not limited to the value $\frac{W_0}{2}$, but increases with the convergence time.⁵ This means that a given sufficient convergence time a larger number of nodes can (automatically) operate in a collision free state without dynamic parameter adjustment.

CRB is different to the 802.11 PCF (Point Coordination Function). It is known that the PCF has several limitations. First, traffic to be sent under DCF during a CP (Contention Period) must wait until the end of the CFP (Contention Free Period) before channel access can be gained. This can severely impact delay sensitive traffic. Second, optimization of the ratio between CFP and CP may be too slow to cope with the variation of n in time. However, in CRB each time slot is randomly reserved by the virtual backoff algorithm (VBA) running in the AP. In order to select a time slot to be reserved, VBA imitates the standard DCF protocol.⁶ This results in randomly distributed empty time slots over time (like empty time slots when using the DCF), which is necessary to support new entrants using delay sensitive applications.

We present a Markov chain that models CRB, and analyse its performance. It is shown by analysis and simulation that CRB achieves a collision free state after a convergence time, and the throughput performance has been improved without a dynamic parameter adjustment. While the analysis results of collision free states closely match with the simulation results, there exists a small gap between the analysis results and simulation results in the collision prone states.⁷ This is because

³CSMA/ECA [19] proposed a centralized (and explicit) adjustment using beacon frames, and SRB [20] suggested a distributed (and implicit) adjustment. Due to the beacon interval, the first may not be fast for timely adjustment. The second may not be fair when the value n varies over time, because one of the stations may use a different parameter with that of the other stations.

⁴i.e. the time period required for the wireless network to move toward a collision free state, during which the network automatically moves from the distributed mode to the centralized mode.

⁵Theoretically, the value n_{max} in CRB is limited to the maximum contention window size ($= W_m$). According to the standard, the default values of W_0 and W_m are 16 and 1024 respectively.

⁶Legacy Wi-Fi devices perform random access following the CSMA/CA (Carrier Sense Multiple Access with Collision Avoidance) to transmit signals. This means that a deterministic TDMA (Time Division Multiple Access) scheduling would not be compatible with the Wi-Fi networks due to interferences with the signals transmitted by the legacy devices. Specifically, a deterministic TDMA scheduling would cause a fairness issue between the stations using a deterministic TDMA and the legacy stations; otherwise, it will require a dynamic parameter adjustment to the distributed stations to maintain fairness. However, the dynamic parameter adjustment is still a very complex issue when the number of users varies over time.

⁷Collision prone states means the network states during the convergence time period, where the value p is larger than zero.

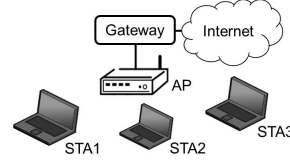


Fig. 1. Wi-Fi network configuration.

the Markov chain model implicitly includes simplifications when the network states varies during the convergence time period.⁸

The rest of the paper is organized as follows. In Section II, we review the system model to be discussed. In Section III, we explain how CRB operates in detail. In Section IV, we theoretically analyse the performance of CRB. In Section V, we present simulation results for validating the analysis model. Section VI concludes this paper.

II. SYSTEM MODEL

As shown in Fig. 1, we consider a Wi-Fi network model operating in the infrastructure mode in the IEEE 802.11 standard. A wireless network consisting of a single AP together with all the connected stations (STAs) is called a BSS (Basic Service Set). We assume that the AP and the connected STAs transmit signals with a constant transmission power ($= 16$ dBm). All the nodes support only the 802.11a physical layer (PHY), and they remain stationary (i.e. no mobility). The log distance propagation loss model (exponent $= 3$) in [24], which predicts the received signal power as a deterministic function of distance, is assumed to apply to the transmitted signals.

In order to evaluate the throughput performance when using CRB in saturation conditions,⁹ we use UDP (User Datagram Protocol) data packets in simulation and assume that a real time streaming application is being used by each user. In addition, we also perform an initial assessment of CRB performance in unsaturated conditions. For numerical analysis in Section IV we assume interference from adjacent wireless networks is negligible, and focus on a single BSS environment. This assumption enables a tractable numerical analysis in this paper. To demonstrate practicality, in Section V we evaluate the proposed protocol in a number of situations such as overlapping APs, mixed nodes, and hidden nodes.

III. CENTRALIZED RANDOM BACKOFF PROTOCOL

In the 802.11 DCF, each node independently selects a random number as its backoff count before transmitting. This means when two or more nodes contend to transmit simultaneously, some of the nodes can have the same backoff

⁸As seen in Section IV-B, we explain that a Markov chain modelling network states during the convergence time period is too complex to find a closed form solution.

⁹i.e. where the transmission queue of each node is assumed to be always non-empty and each active node immediately attempts to transmit a packet after the completion of each transmission. The saturation assumption means that the queueing dynamics are negligible.

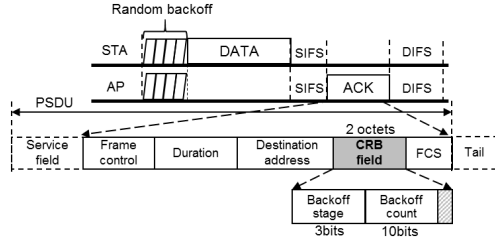


Fig. 2. CRB field.

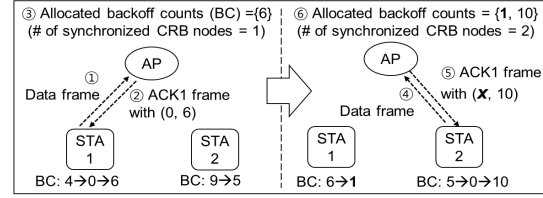
count, causing packet collisions. However, in CRB, the AP internally generates a unique backoff state and allocates it to each node. When the AP has received a successful data frame from a source node and discovered that the node has more data packets to send, the AP allocates a backoff state to the node using the ACK frame shown in Fig. 2, where two octets are added to carry the backoff state. (We assume that one bit of the *More Data* field in the MAC header of the data frame can be used to inform the AP that the source node has more data packets to send.)

The backoff state includes two numbers: a backoff stage (BS) and a backoff count (BC). These are generated by the AP after successfully receiving the data frame from the source node and before transmitting the ACK frame. When the source node has successfully received the ACK frame with the backoff state and uses the backoff state for transmitting the next data frame, we call it a *synchronized CRB node (SCN)* and the allocated backoff count is called a *synchronized backoff count (SBC)*.

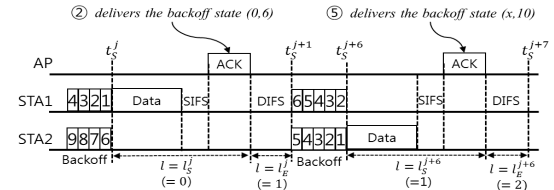
If the transmission of the data frame is unsuccessful and the source node fails to receive the ACK frame, then in order to start contention again for retransmission the source node generates a new backoff state by itself like a station operating in the current IEEE 802.11 DCF. In this case, we call the source node an *unsynchronized CRB node (UCN)* and the (independently) generated backoff count is called an *unsynchronized backoff count (UBC)*.

The value of BS ($= i$) is an integer in the range $[0, m]$, where m represents the maximum value of BS. The value of BC ($= k$) is an integer in the range $[0, W_i - 1]$, where W_i represents the contention window size at BS i . The value of W_i is $2^i W_0$, where W_0 represents the minimum contention window. In this paper, we assume that $m = 6$ and $W_0 = 16$ by default. Therefore, the value of W_m is 1024.

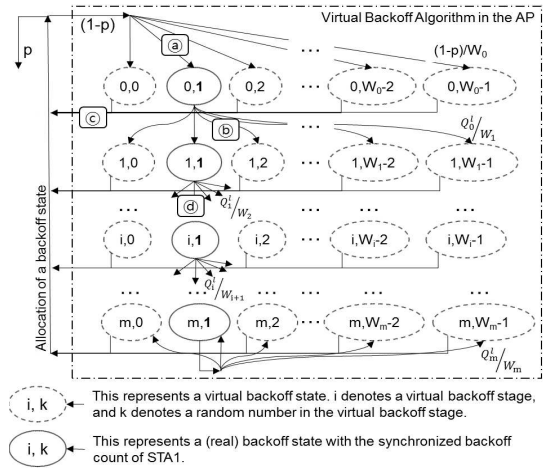
After successfully receiving the data frame from the source node and before transmitting the ACK frame to the source node, the AP internally generates a backoff state (which is to be included in the ACK frame) as described in Fig. 3. In Fig. 3a, after successfully receiving a data frame from STA1 (i.e. after step ① and before step ②), the AP uniformly selects a random number from the range $[0, 15]$ (*virtual backoff stage 0*) as a backoff count to be included in the ACK frame (e.g. number 6 as shown in Fig. 3a). In this case, the value of backoff stage to be included in the ACK frame is zero.



(a) Allocation of a unique backoff count



(b) The flow of frames in CRB. The backoff stage value x in step ⑤ is equal to the number of *virtual collisions* that have occurred during the VBA.



(c) Virtual backoff algorithm (VBA)

Fig. 3. Centralized random backoff (CRB) with virtual backoff algorithm (VBA).

At a later time, the AP then receives a data frame from STA2 (i.e. after step ④ and before step ⑤ in Fig. 3a), the AP uniformly selects a random number from the range $[0, 15]$ (*virtual backoff stage 0*) to generate a backoff state for STA2. At this point of time, the AP knows that STA1 has backoff count 1. This internal operation of the AP can be described by the state transitions denoted by ④ in Fig. 3c, where $W_0 = 16$. If the selected number is different to the backoff count of STA1, then the backoff state is allocated to STA2 (the state transitions denoted by ⑤ in Fig. 3c). In this case the value of backoff stage to be included in the ACK frame is zero. However, if the selected number is the same as the backoff count of another station (a *virtual collision*), for example the backoff count of STA1 ($= 1$) as shown in

```

1: if a successful reception of a data frame then
2:    $i = 0$ 
3:    $k = \text{rand}(0, 2^i W_0 - 1)$ 
4:   while  $k$  is not unique compared to the SBCs (i.e. a virtual collision occurs)
5:     if  $i < m$  then
6:        $i = i + 1$ 
7:        $k = \text{rand}(0, 2^i W_0 - 1)$ 
8:   Send the ACK frame with the backoff state  $(i, k)$ 
9: else
10:  Do not send an ACK frame

```

Fig. 4. The pseudo-code of VBA.

```

1: if Tx queue was empty, before a packet has arrived from upper layers then
2:   if channel is sensed idle then
3:     Start transmitting immediately
4:   else channel is sensed busy
5:      $i = 0$ 
6:      $k = \text{rand}(0, 2^i W_0 - 1)$ 
7:     Start backoff procedure with the state  $(i, k)$ 
8:   else (this node has been active, i.e. saturation condition)
9:     if a successful reception of a backoff state  $(i, k)$  from the AP then
10:      Start backoff procedure with the state  $(i, k)$ 
11:   else
12:     if  $i < m$  then
13:        $i = i + 1$ 
14:        $k = \text{rand}(0, 2^i W_0 - 1)$ 
15:       Start backoff procedure with the state  $(i, k)$ 

```

Fig. 5. The pseudo-code of the operation of a station.

Fig. 3a, the AP again picks another random number in the doubled range $[0, 31]$ (*virtual backoff stage 1*). This can be described by the state transitions denoted by ⑥ in Fig. 3c, where $W_1 = 32$. However, if the number selected in $[0, 31]$ is equal to the backoff count of STA1 again, then the AP selects again a random backoff count in the doubled range $[0, 63]$ (*virtual backoff stage 2*). This can be described by the state transitions denoted by ⑦ in Fig. 3c. The process continues to the point where the range is $[0, 1023]$ (*virtual backoff stage 6*), whereupon random numbers are selected in this range until a unique value (a backoff count to be included in the ACK frame) is obtained.¹⁰ We call this a virtual backoff algorithm (VBA) in the AP. In this way, nodes contending at the same time for accessing the channel can all be allocated a unique backoff count. (Fig. 4 presents pseudo-code for the operation of VBA, and Fig. 5 presents the equivalent pseudo-code for operation of a station.) We allow the AP to allocate a unique backoff state to itself (using the VBA based on the synchronized backoff counts) when it has a data frame to send.

According to the IEEE 802.11a standard, although it supports eight different rates in the range from 6 Mbps up to 54 Mbps, only three rates (i.e. 6 Mbps, 12 Mbps, and 24 Mbps) are mandatory. This means in order to support backward compatibility to 802.11a devices, one of the three

rates has to be used for transmitting control frames such as ACK frames. When the 6 Mbps rate (i.e. BPSK¹¹ modulation with rate 1/2 coding) is used for transmitting ACK frames, an OFDM (Orthogonal Frequency-Division Multiplexing) symbol is encoded to carry three octets. As seen in Fig. 2, a legacy ACK frame contains 16 octets in its PSDU (PLCP¹² Service Data Unit), and 6 bits in its tail. Therefore, 6 OFDM symbols are required to carry the PSDU and the tail bits. This means that adding two additional octets for including the CRB field in a legacy ACK frame will require an additional OFDM symbol. However, if the 24 Mbps rate (i.e. 16-QAM¹³ with rate 1/2 coding) is used for transmitting ACK frames, an OFDM symbol is encoded to carry 12 octets. This means that adding two additional octets for including the CRB field in a legacy ACK frame will not require an additional symbol.¹⁴

IV. NUMERICAL ANALYSIS

We consider a single BSS Wi-Fi network consisting of n active (contending) nodes. We assume ideal channel

¹¹Binary Phase-Shift Keying.

¹²Physical Layer Convergence Protocol.

¹³Quadrature Amplitude Modulation.

¹⁴We use 6 Mbps constant rate to transmit ACK frames in evaluation. Although use of the 6 Mbps (or the 12 Mbps) requires one additional OFDM symbol, the impact of the additional OFDM symbol is very small compared to the significant throughput gain from using CRB.

¹⁰This maximum value, $W_m - 1$, is chosen to match the operation of DCF in order to maintain fairness, but will limit the BSS to 1024 nodes.

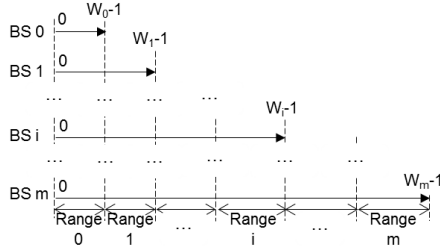


Fig. 6. Backoff stages, contention windows, and ranges.

conditions, and there is no hidden node.¹⁵ This assumption implies that no ACK frames are lost after successfully receiving a data frame.

Under these conditions, we first derive a numerical solution for the probability of a virtual collision in VBA. Second, we present a simplified Markov chain model for analysing the probability of a backoff state of a node operating in CRB. Based on this, we obtain the transmission probability ($= \tau$) and the (real) collision probability ($= p$). Third, using an absorbing Markov chain model, we explain how the number of SCNs changes over time. Lastly, the throughput performance of CRB is analysed and compared to that of a deterministic backoff mechanism.

A. Probability of a Virtual Collision

A node starts its backoff procedure by setting its backoff count by either uniformly choosing a random value from a contention window (after a transmission failure) or receiving a backoff state value from the AP (after a transmission success). The $(m + 1)$ backoff stages and the associated $(m + 1)$ contention windows can be represented by Fig. 6. In addition, for simplicity of the analysis, we define $(m + 1)$ Ranges as shown in the figure. Range 0 means the range of integers $[0, W_0 - 1]$, and Range i is the range $[W_{i-1}, W_i - 1]$ where $(1 \leq i \leq m)$.

We consider the j th slot time,¹⁶ which starts at time t_S^j (where $t_S^j < t_S^{j+1}$), and time t_E^j represents the end of the j th slot time, i.e. $t_E^j = \lim_{\epsilon \rightarrow 0} (t_S^{j+1} - \epsilon)$. We assume that the backoff states of all nodes are updated between the time t_E^j and the time t_S^{j+1} .

We define l as the number of SCNs. (Since a SCN has only one SBC, the value l is equal to the number of SBCs.) In addition, we define the terms l_S^j and l_E^j as the number of SCNs at time t_S^j and t_E^j , respectively. (For example, these two notations can be found in Fig. 3b.) This means the number of UCNs at time t_S^j and t_E^j are equal to $(n - l_S^j)$ and $(n - l_E^j)$, respectively.

Since each of the SCNs has a unique SBC with respect to each other, only one of l_E^{j-1} SCNs can possibly start to

transmit at time t_S^j . If one of the SCNs starts to transmit at time t_S^j (due to its SBC expiration), then $l_S^j = l_E^{j-1} - 1$. If the transmission is successful, then the source node receives a backoff state from the AP (i.e. $l_E^j = l_S^j + 1$); otherwise, the node (independently) generates a backoff state by itself and it becomes an UCN (i.e. $l_E^j = l_S^j$). In addition, if one of the UCNs starts to transmit at time t_S^j (due to its UBC expiration) and the transmission is successful, then the source node receives a backoff state from the AP (i.e. $l_E^j = l_E^{j-1} + 1$). In this way, the values l_S^j and l_E^j (dynamically) vary over time.

Now, we define five variables in order to analyse the distribution of SBCs in the range $[0, W_m - 1]$ when the AP internally generates a new backoff state to include in the ACK frame to be transmitted. First, the scalar N_i^l is defined as the number of SBCs in Range i when the total number of SCNs is l . For example, suppose that there are three SCNs, and the values of the SBCs are 3, 10, and 25. In this case, assuming $W_0 = 16$ and $m = 6$, we see the relations $l = 3$, $N_0^l = 2$, $N_1^l = 1$, and $N_i^l = 0$ given $(2 \leq i \leq m)$. We also see $\sum_{i=0}^m N_i^l = l$.

Second, the scalar Q_i^l is defined by equation (1) and is equal to the probability of a virtual collision at virtual backoff stage (VBS) i when the number of SCNs is l .

$$Q_i^l = \frac{\sum_{k=0}^i N_k^l}{W_i} \quad 0 \leq i \leq m \quad (1)$$

For example, suppose that there are three SCNs, and the values of the SBCs are 3, 10, and 25. In this case, we see $Q_0^l = 2/16$ and $Q_i^l = 3/(16 \cdot 2^i)$ where $(1 \leq i \leq m)$. In addition, the notation Q_i^l can be found in Fig. 3c, where we see $l = 1$, $N_0^l = 1$, $N_i^l = 0$ given $(1 \leq i \leq m)$, and $Q_i^l = 1/W_i$ given $(0 \leq i \leq m)$.

Third, we define the notation P_i^l by equation (2) which means the probability of selecting a unique SBC in VBS i when the number of SCNs is l .

$$P_i^l = \begin{cases} (1 - Q_0^l) & i = 0 \\ (1 - Q_i^l) \prod_{k=0}^{i-1} Q_k^l & 1 \leq i < m \\ \prod_{k=0}^{m-1} Q_k^l & i = m \end{cases} \quad (2)$$

For example, suppose that there are three SCNs, and the values of the SBCs are 3, 10, and 25. In this case, assuming $W_0 = 16$ and $m = 6$, the value of P_0^l (i.e. the probability of selecting a unique SBC in the range of $[0, 15]$) is $14/16$, and the value of P_1^l (i.e. the probability of selecting a unique SBC in the range of $[0, 31]$) is $(29/32) \times (2/16)$.

We assume that the number n is assumed to be less than the value of $(W_m - 1)$ to guarantee that the AP generates a unique SBC at any slot time with a successful data frame transmission. This implies the relation $\sum_{k=0}^m P_k^l = 1$.

Fourth, we define the notation Z^l as the probability of selecting zero as a SBC when the number of SCNs is l . For example, suppose there are two SCNs, and the values of the SBCs are 3 and 10. In this case, we see the relations $l = 2$,

¹⁵A node is a hidden node if another node in the same BSS cannot hear the first when it communicates with the AP.

¹⁶The term *slot time* in this paper is the time period of a time slot used in [2].

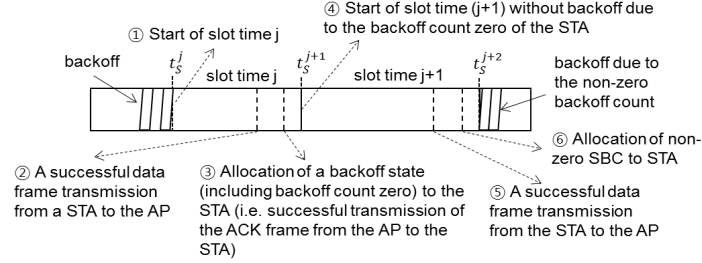


Fig. 7. An example of two consecutive slot times granted to a node.

$Q_i^l = 2/W_i$ given ($0 \leq i \leq m$), and the value of Z^l is obtained by (3).

$$\begin{aligned}
 Z^l|_{SBCs=\{3,10\}} &= \sum_{i=0}^m (\text{Picking zero at the } i\text{th VBS}) \\
 &= \frac{1}{16} + \frac{2}{2} \frac{1}{2} + \frac{2}{2} \frac{2}{2} \frac{1}{2} + \frac{2}{2} \frac{2}{2} \frac{2}{2} \frac{1}{2} \\
 &\quad + \frac{16}{2} \frac{32}{2} \frac{64}{2} \frac{128}{2} \frac{256}{2} + \frac{16}{2} \frac{32}{2} \frac{64}{2} \frac{128}{2} \frac{256}{2} \frac{512}{2} \\
 &\quad + \frac{16}{2} \frac{32}{2} \frac{64}{2} \frac{128}{2} \frac{256}{2} \frac{512}{2} \frac{1024}{2} \\
 &\quad \times \left[1 + \frac{2}{1024} + \left(\frac{2}{1024} \right)^2 + \left(\frac{2}{1024} \right)^3 + \dots \right] \quad (3)
 \end{aligned}$$

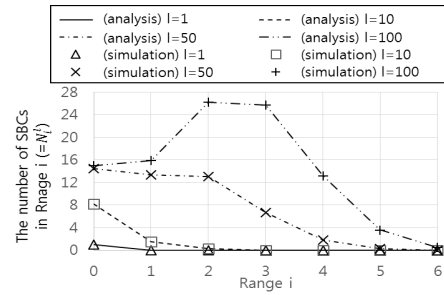
Because zero can be allocated as a backoff count, it is possible for the source node to transmit multiple data frames consecutively without backoff. For example, as described in Fig. 7, backoff count zero can be allocated to the source node in the j th slot time, and then a new non-zero SBC can be picked and allocated to the source node in step ⑥ in the $(j+1)$ th slot time. In this case, the source node transmits two data frames without backoff.

Lastly, we define the scalar D_i^l as the probability of selecting a new non-zero SBC in Range i (i.e. the probability of selecting the $(l+1)$ th SBC in Range i when the number of SCNs is l). The value of D_i^l can be expressed by equation (4),

$$\begin{aligned}
 D_i^l &= D_i^l|_{(1\text{st slot})} + D_i^l|_{(2\text{nd slot})} + D_i^l|_{(3\text{rd slot})} + \dots \\
 &= D_i^l|_{(1\text{st slot})} + Z^l D_i^l|_{(1\text{st slot})} + (Z^l)^2 D_i^l|_{(1\text{st slot})} + \dots \\
 &= D_i^l|_{(1\text{st slot})} \sum_{j=0}^{\infty} (Z^l)^j = \frac{D_i^l|_{(1\text{st slot})}}{1 - Z^l} \quad 0 \leq i \leq m \quad (4)
 \end{aligned}$$

where $D_i^l|_{(k\text{th slot})}$ represents the probability of selecting a non-zero SBC in Range i in the k th slot time in the series of the consecutive successful slot times. We now see the relation $Z^l = (1 - \sum_{i=0}^m D_i^l|_{(1\text{st slot})})$, where the term $(\sum_{i=0}^m D_i^l|_{(1\text{st slot})})$ represents the probability of selecting a non-zero SBC in the first successful slot time.

Using the equation (4) and the result of Appendix A, we obtain the equations in (5), as shown at the bottom of the next page. Note that since the value n is assumed to be less than the value of $(W_m - 1)$ to guarantee that the AP can generate a unique non-zero SBC for any series of successful consecutive slot times, we see $\sum_{i=0}^m D_i^l = 1$.

Fig. 8. Analysis and simulation results on N_i^l (i.e. the number of SBCs in Range i when the number of SCNs is l) given $W_0 = 16$ and $m = 6$.

Although the value of D_i^l is expressed by the two variables N_i^l and Q_i^l in (5), considering equation (1) we see that the value of D_i^l can be expressed by only N_i^l .

From the definition of the variable D_i^l , we obtain relation (6).

$$N_i^{l+1} = \sum_{k=0}^l D_i^k \quad (6)$$

Since the value of D_i^l is expressed by N_i^l (according to the equations (1) and (5)), equation (6) means that the value of N_i^{l+1} can be calculated iteratively. In order to solve equation (6), we assume an initial condition that there initially was a SBC in Range 0 (i.e. $N_i^{l=0} = 1$ when $i = 0$ and $N_i^{l=0} = 0$ when $i \in [1, m]$).

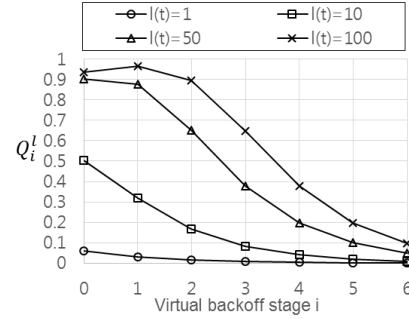
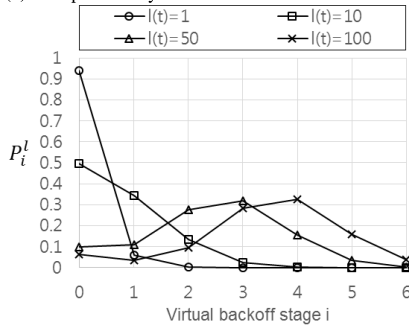
In order to see the distribution of SBCs in the range $[0, W_m - 1]$ for a given l , we computed equation (6) with different values of l . In Fig. 8, we see that at a given Range i , the value of N_i^l increases as l increases. In addition, when $l \leq 50$, the value of N_i^l tends to decrease as the Range i increases. This result shows that how SBCs are distributed over the seven different ranges. Moreover, in Fig. 8, we see that the values of N_i^l obtained by simulation¹⁷ are almost identical to that of the analysis results.

The values Q_i^l and P_i^l also change, as the value l varies. In Fig. 9a, we see that at a given VBS i , the value of Q_i^l increases as l increases. Using the calculated values of N_i^l with

¹⁷We have developed a simple program (written in C language) to simulate VBA. The values of the simulation result are average values obtained through one million repetitions.

5844

IEEE TRANSACTIONS ON WIRELESS COMMUNICATIONS, VOL. 16, NO. 9, SEPTEMBER 2017

(a) The probability of a virtual collision at VBS i (b) The probability of selecting a unique SBC in VBS i Fig. 9. Analysis results on Q_i^l and P_i^l ($W_0 = 16$ and $m = 6$).

the initial condition, we also obtain the value of P_i^l as shown in Fig. 9b. The calculated value of P_i^l at a given l is used for Markov chain model analysis for calculating the transmission probability ($= \tau$) of a node operating in CRB.

B. Probability of a Collision

The network states during a convergence time period can be represented by Fig. 10, where the notation $p(l)$ denotes the collision probability, and the notation $c(l)$ represents the probability of a node being synchronized. Since it is too complex to enable a closed form solution to be found, we propose a simplified chain model shown in Fig. 11.

Note that the value P_i^l is given at a value l . Now we find the values τ and p from Fig. 11. The chain model illustrates an internal backoff state of a node. After a successful

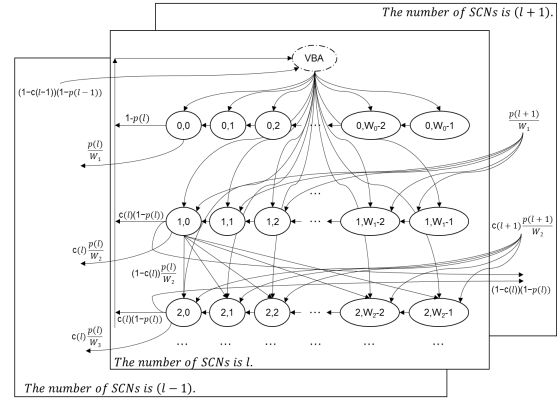
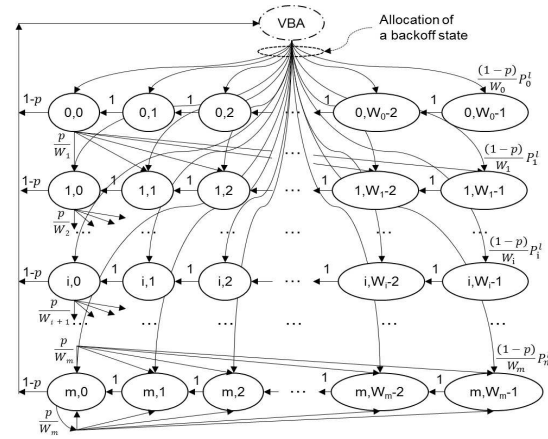


Fig. 10. Markov chain representing the network states during a convergence time period.

Fig. 11. Markov chain models of a node operating in CRB. When $l \in [0, n-1]$, the model represents a collision prone state where $(0 < p < 1)$. When $l = n$, the model represents a collision free state where $p = 0$.

transmission, the node starts its backoff procedure with the allocated backoff state. The process of allocating the backoff state is illustrated by the curved lines in Fig. 11. When the value l varies in the range $[1, n-2]$, the notation p (i.e. $p(l)$ in Fig. 10) implicitly includes an approximation.

$$D_i^l = \begin{cases} \frac{(W_0 - N_0^l - 1)}{1 - Z^l} \left(\frac{1}{W_0} + \sum_{j=0}^{m-2} \left(\frac{\prod_{k=0}^j Q_k^l}{W_{j+1}} \right) + \frac{\prod_{k=0}^{m-1} Q_k^l}{W_m(1 - Q_m^l)} \right) & i = 0 \\ \frac{(W_{i-1} - N_i^l)}{1 - Z^l} \left(\sum_{j=i-1}^{m-2} \left(\frac{\prod_{k=0}^j Q_k^l}{W_{j+1}} \right) + \frac{\prod_{k=0}^{m-1} Q_k^l}{W_m(1 - Q_m^l)} \right) & 1 \leq i < m \\ \frac{(W_{m-1} - N_m^l)}{1 - Z^l} \frac{\prod_{k=0}^{m-1} Q_k^l}{W_m(1 - Q_m^l)} & i = m \end{cases} \quad (5)$$

The approximation can be expressed by equation (7).

$$\begin{cases} p(l-1) \simeq p(l) \\ p(l+1) \simeq p(l) \end{cases} \quad (7)$$

In addition, when $l = n - 1$, we assume that $p(l-1) \simeq p(l)$ and $p(l+1) = 0$.

We define the probability of a backoff state $b_{i,k}$ (where $i \in [0, m]$ and $k \in [0, W_i - 1]$) as equation (8),

$$b_{i,k} = \lim_{N \rightarrow \infty} \frac{1}{N} \sum_{n=1}^N P\{s_n(t) = i, b_n(t) = k\} \quad (8)$$

where $s_n(t)$ and $b_n(t)$ denote the stochastic process representing the backoff stage and the backoff counter respectively for the n -th independent realization at time t .

The transition probabilities in the Markov Chain model shown in Fig. 11 are given by the equations from (9a) to (9d),

$$P\{i, k|i, k+1\} = 1 \quad k \in [0, W_i - 2], i \in [0, m] \quad (9a)$$

$$P\{j, k|i, 0\} = \frac{(1-p)}{W_j} P_j^l \quad k \in [0, W_j - 1], \\ i \in [0, m], j \in [0, m] \quad (9b)$$

$$P\{i, k|i-1, 0\} = \frac{p}{W_i} \quad k \in [0, W_i - 1], i \in [1, m] \quad (9c)$$

$$P\{m, k|m, 0\} = \frac{p}{W_m} \quad k \in [0, W_m - 1] \quad (9d)$$

where $P\{i_1, k_1|i_0, k_0\}$ denotes the probability of a backoff state transition from $\{i_0, k_0\}$ to $\{i_1, k_1\}$. Equation (9a) shows that the BC is decreased at the beginning of each slot time. The second equation (9b) represents the fact that a new packet following a *successful packet transmission* starts backoff with the allocated backoff state. Equations (9c) and (9d) model the state transition after an *unsuccessful transmission*. Equation (9c) shows that when an unsuccessful transmission occurs at BS $(i-1)$, the BS increases by one, and a new BC is uniformly and independently chosen in the range $[0, W_i - 1]$. Equation (9d) models the fact that once the BS reaches the value m , a node stays in the BS m until a successful packet transmission.

From the Markov chain in Fig. 11, the transmission probability can be represented by (10).

$$\tau = \sum_{i=0}^m b_{i,0} = \frac{b_{0,0}}{(1-p)P_0^l} \quad (10)$$

If the value of l is zero, then $P_{i=0}^l = 1$ and $P_i^l = 0$ where $i \in [1, m]$. In this case, the Markov Chain model in Fig. 11 becomes identical to the Markov chain model presented in [2], and the equations (9) and (10) also become identical to those of legacy nodes presented in [2].

In Appendix B, we obtain $b_{0,0}$ as (11), as shown at the bottom of the next page, where $f_i^j(l) = (p^{i-1-j})P_{j+1}^l/P_0^l$ for short. We see in equation (11) that $b_{0,0}$ is a function of p and P_i^l . This means that by substituting the value of $b_{0,0}$ in the equation (10) with the equation (11), the value of τ is given as a function of p and P_i^l . This is one relation between τ and p given both l and n . In order to find τ and p at given l and n , we need another equation relating τ and p .

Let $P_{tr}(l)$ be the probability that there is at least one node starting to transmit in a considered slot time when the number of SCNs is l . We obtain $P_{tr}(l)$ as (12),

$$P_{tr}(l) = 1 - (1 - P_{tr}^{un}(l))(1 - P_{tr}^{sn}(l)) \quad (12)$$

where the notation $P_{tr}^{un}(l)$ represents the probability that there is at least one UCN starting to transmit. The notation $P_{tr}^{sn}(l)$ represents the probability that there is at least one SCN starting to transmit. This probability depends on the number of SBCs in Range 0 (i.e. N_0^l). For example, as the value N_0^l becomes close to the value $(W_0 - 1)$, the SCNs will transmit in consecutive time slots. Since the values of SBCs decrease as time increases, the SBCs in Range 1 (i.e. N_1^l) will move to Range 0 before the backoff counter reaches zero. The values of $P_{tr}^{un}(l)$ and $P_{tr}^{sn}(l)$ can be obtained by (13),

$$\begin{cases} P_{tr}^{un}(l) = 1 - (1 - \tau)^{n-l} \\ P_{tr}^{sn}(l) = 1 - \left(1 - \frac{N_0^l}{W_0 - 1}\right)(1 - P_{tr}P_s Z^l) \end{cases} \quad (13)$$

where the term $[N_0^l/(W_0 - 1)]$ in the second equation in (13) represents the density of SBCs in Range 0, and the term $[1 - N_0^l/(W_0 - 1)]$ means the density of non-allocated numbers in Range 0. The term $(1 - P_{tr}P_s Z^l)$ denotes the probability of allocating a non-zero BC.

We define $P_s(l)$ as the probability that a transmission occurring on the channel is successful when the number of SCNs is l . This is equal to the probability that *exactly one station* transmits on the channel, conditioned on the fact that *at least one station* transmits. This yields equation (14),

$$P_s(l) = P_s^{un}(l) + P_s^{sn}(l) \quad (14)$$

where the notations $P_s^{un}(l)$ and $P_s^{sn}(l)$ represent the probability of a successful slot time with a packet sent by an UCN and a SCN, respectively. The values of $P_s^{un}(l)$ and $P_s^{sn}(l)$ are obtained by equations in (15).

$$\begin{cases} P_s^{un}(l) = \frac{(n-l)\tau(1-\tau)^{n-l-1}(1 - P_{tr}^{sn}(l))}{P_{tr}^{un}(l)} \\ P_s^{sn}(l) = \frac{P_{tr}^{sn}(l)(1 - P_{tr}^{un}(l))}{P_{tr}(l)} \end{cases} \quad (15)$$

Note that if the value of l is zero, then $P_{tr}^{sn}(l) = 0$, $P_s^{sn}(l) = 0$, and the expression of $P_s(l)$ becomes identical to that of legacy nodes presented in [2].

The probability p that a packet encounters a collision is equal to the probability that at least one of the $(n-1)$ remaining stations starts to transmit in the considered slot time. If one UCN starts transmitting a packet in a considered slot time, then there will be no collision if neither the $(n-l-1)$ UCNs nor the l SCNs start transmitting at the same time. In the case that a SCN starts transmitting a packet, since each of the SCNs has a unique backoff count to each other, there will be no collision provided that the $(n-l)$ UCNs do not start transmitting at the same time. This yields the two equations in (16),

$$\begin{cases} p^{un}(l) = 1 - (1 - \tau)^{n-l-1}(1 - P_{tr}^{sn}(l)) \\ p^{sn}(l) = 1 - (1 - \tau)^{n-l} \end{cases} \quad (16)$$

TABLE I
THE VALUE OF Δl BETWEEN TWO CONSECUTIVE SLOT TIMES

Tx node(s)	Tx result	Probability		Δl
		Symbol	Value	
None (empty slot)	-	$P_0(l)$	$1 - P_{tr}(l)$	0
Only one UCN	S	$P_1(l)$	$P_{tr}(l)P_s^{un}(l)$	+1
Only multiple UCNs (i.e. No SCN)	F	$P_2(l)$	$P_{tr}^{un}(l)(1 - P_{tr}^{sn}(l))$	0
Only one SCN	S	$P_3(l)$	$P_{tr}(l)P_s^{sn}(l)$	0
UCN(s) and one SCN	F	$P_4(l)$	$P_{tr}^{un}(l)P_{tr}^{sn}(l)$	-1

* S for success, F for failure, and l for l_E^{-1} .

where the notation $p^{un}(l)$ and $p^{sn}(l)$ represents the probability of a collision seen by a packet transmitted by an UCN and a SCN, respectively.

Taking the average between $p^{un}(l)$ and $p^{sn}(l)$, we obtain the value of p as (17),

$$p = \frac{(n-l)\tau}{(n-l)\tau + P_{tr}^{sn}(l)} p^{un}(l) + \frac{P_{tr}^{sn}(l)}{(n-l)\tau + P_{tr}^{sn}(l)} p^{sn}(l) \quad (17)$$

where the denominator $[(n-l)\tau + P_{tr}^{sn}(l)]$ represents the total number of packets transmitted in the considered slot time. This equation is the second relationship between τ and p , and now we can obtain τ and p given both l and n .

C. Number of Synchronized Nodes

All nodes are assumed to be using the CRB protocol, and the number of SCNs ($=l$) dynamically varies in the range $[0, n]$. We define a vector P^j as the probability distribution of the value l at slot time j , which can be expressed by (18).

$$P^j = [p_0^j \ p_1^j \ \cdots \ p_{n-1}^j \ p_n^j] \quad (18)$$

Each element p_i^j (where $i \in [0, n]$) represents the probability that the value of l is equal to i at slot time j . This means $\sum_{i=0}^n p_i^j = 1$. We find the distribution vector P^j and investigate how the distribution vector P^j changes over slot times.

Now, we define Δl as the gap between l_E^j and l_E^{j-1} , i.e. $\Delta l = l_E^j - l_E^{j-1}$. The possible values of Δl are now described. First, $\Delta l = 1$ if the j th slot time was successful with a transmission from one of UCNs (i.e. the UCN has been synchronized after the slot time). Second, $\Delta l = -1$ if a collision with a packet sent by a SCN occurred in the slot time (i.e. the SCN has been unsynchronized). Lastly, $\Delta l = 0$ in the three cases: an empty slot time, a collision among UCNs, and a successful transmission by a SCN. These five different cases are summarized in Table I. The sum of the five different probabilities in the table is one for every slot time,

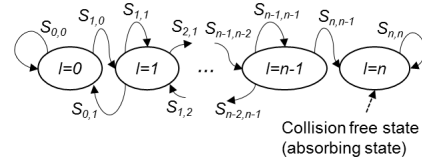


Fig. 12. Markov chain model for analysis of the vector P^j .

i.e. $\sum_{k=0}^4 P_k(l) = 1$ where $(1 \leq j)$. Table I shows the value of Δl for each of the five different cases.

The absorbing Markov chain model depicted in Fig. 12 illustrates a state of the wireless network in terms of the number of SCNs. Note that the time scale of the chain model in Fig. 11 is a considered time slot, while the time scale of the absorbing chain model in Fig. 12 is the period during which the network moves from the initial state to a collision free state. The notation $S_{x,y}$ in Fig. 12 presents the probability of a state transition from the state that $l = y$ to the state that $l = x$. The state that $l = 0$ (i.e. where all the nodes are UCNs) is identical to the state of wireless network operating in the legacy DCF protocol. As denoted in Fig. 12, if the value of l is equal to n , then the state becomes a collision free state (which is an absorbing state). This means $S_{n,n}$ is always one. The absorbing Markov chain can be expressed by (19).

$$A = \begin{bmatrix} S_{0,0} & S_{1,0} & 0 & \cdots & 0 & 0 \\ S_{0,1} & S_{1,1} & S_{2,1} & \cdots & 0 & 0 \\ 0 & S_{1,2} & S_{2,2} & \cdots & 0 & 0 \\ 0 & 0 & S_{2,3} & \cdots & 0 & 0 \\ \cdots & \cdots & \cdots & \cdots & \cdots & \cdots \\ 0 & 0 & 0 & \cdots & S_{n-1,n-1} & S_{n,n-1} \\ 0 & 0 & 0 & \cdots & 0 & S_{n,n} \end{bmatrix} \quad (19)$$

From Table I, we obtain relations in (20).

$$S_{l,l} = P_0(l) + P_2(l) + P_3(l) \quad l \in [0, n-1] \quad (20a)$$

$$S_{n,n} = 1 \quad l = n \quad (20b)$$

$$S_{l+1,l} = P_1(l) \quad l \in [0, n-1] \quad (20c)$$

$$S_{l-1,l} = P_4(l) \quad l \in [1, n-1] \quad (20d)$$

Now, the vector P^j can be obtained by equation (21), where the vector I represents the initial state of the network. We assume that the value l is zero when $j = 0$ (i.e. all the nodes are assumed to be randomized/synchronized nodes at the beginning of the first slot time). This means the probability of the network state where $l = 0$ is one when $j = 0$.

$$P^j = I A^j \quad \text{where } I = [1 \ 0 \ \cdots \ 0 \ 0] \quad (21)$$

$$b_{0,0} = \frac{1}{\frac{W_0+1}{2} + \sum_{i=1}^{m-1} \left[\frac{W_i+1}{2} (p^i + \sum_{j=0}^{i-1} f_i^j(l)) \right] + \frac{W_m+1}{2} \left(\frac{p^m}{1-p} + \sum_{j=0}^{m-1} \frac{f_m^j(l)}{(1-p)} \right)} \quad (11)$$

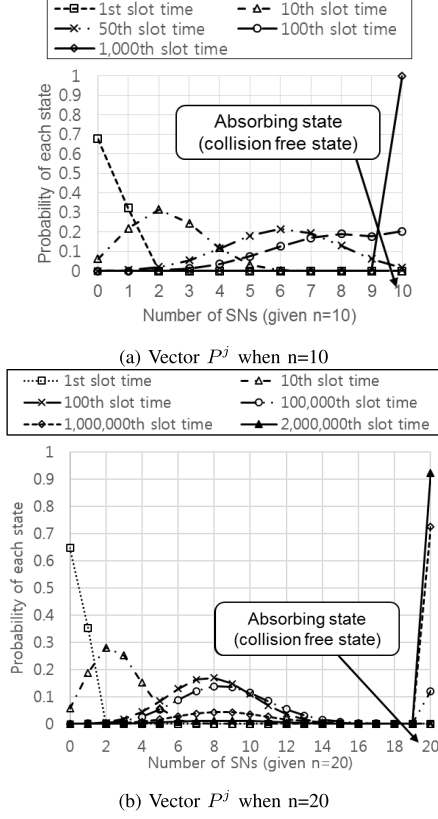
Fig. 13. Analysis results of vector P^j ($W_0 = 16$ and $m = 6$).

Fig. 13 shows the calculated results for the distribution vector P^j using equation (21) when $n = 10$ and $n = 20$. First of all, we see that the probability of the state $l = 10$ in Fig. 13a increases to 1, as the slot time increases up to 1000. Moreover, we see that the probability of the state $l = 20$ in Fig. 13b increases to 1, as the slot time increases over 2,000,000. In this result, we see an important result that the wireless network operating in CRB moves toward a collision free state without adjusting/tuning the contention window size for the given number n . However, we also see that the number of slot times required to move toward a collision free state dramatically increases as the number of nodes n increase.

D. Throughput Performance

We reuse the definition of saturation throughput ($= S$) in [2], which can be represented by equation (22).

$$S = E[\text{payload}] / E[\text{slot time}] \quad (22)$$

We compute the throughput at slot time j ($= S^j$) as in (23), where $(P^j)^T$ represents the transpose of vector P^j . Each element S_i of the vector C denotes the saturation throughput when l is assumed to be i .

$$S^j = C \cdot (P^j)^T \quad \text{where } C = [S_0 \ S_1 \ \cdots \ S_{n-1} \ S_n] \quad (23)$$

A successful transmission occurs in a slot time with probability $P_{tr}(l)P_s(l)$. The slot time is empty with probability $(1 - P_{tr}(l))$. The slot time contains a collision with probability $P_{tr}(l)(1 - P_s(l))$. Therefore, the value S_l can be obtained by (24),

$$S_l = \frac{P_{tr}(l)P_s(l)E[P]}{(1 - P_{tr}(l))\sigma + P_{tr}(l)P_s(l)T_s + P_{tr}(l)(1 - P_s(l))T_c} \quad (24)$$

where T_s denotes the average time the channel is sensed busy because of a successful transmission, and T_c represents the average time the channel is sensed busy due to a collision. The notation σ represents the duration of an empty slot time. The scalar $E[P]$ denotes the average packet payload size successfully transmitted.

The values T_s and T_c are given by (25),

$$\begin{aligned} T_s &= H + E[P] + SIFS + \delta + ACK + DIFS + \delta \\ T_c &= H + E[P^*] + DIFS + \delta \end{aligned} \quad (25)$$

where $H (= PHY_{hdr} + MAC_{hdr})$ denotes the packet header, δ represents the propagation delay, and $E[P^*]$ is the average length of the longest packet payload involved in a collision. In the case all packets have the same fixed size, the value $E[P^*]$ becomes equal to the value $E[P]$. The notation *SIFS* (Short Inter Frame Space) denotes the delay time required for a wireless interface to process a received frame and to respond with a response frame. The scalar *ACK* is the transmission time of an ACK frame. The notation *DIFS* (DCF Inter Frame Space) represents the standard wait time required before starting the random backoff procedure in the saturation condition.

The parameters given in Table II were used to obtain analysis results shown in Fig. 14. We see in Fig. 14a that the throughput converges to a maximum value as the time increases. The figure also shows that similar to Fig. 13 the time period required for convergence dramatically increases, as the number of n increases. The maximum throughput value achieved in a collision free state is slightly increased as the value n increases. This is because the probability of an empty slot time decreases, while the probability of a collision is zero.

We see in Fig. 14b that the throughput performance when using CRB changes over time (i.e. non-stationary state). The figure shows that given a sufficient time, the wireless network with a larger number of nodes does reach a collision free state. For example, the figure shows that 14 nodes can reach the collision free state within one second without tuning the contention window size (i.e. $W_0 = 16$ and $m = 6$). This is a significant advantage of CRB over SRB, because according to [20] the maximum number of SRB nodes that can converge to a collision free state (given $W_0 = 16$) is limited to 8. However, the figure also shows that it takes an hour for 20 nodes to converge to the collision free state. In practice we anticipate that the performance of a heavily loaded network will be between that of SRB and the optimum CRB.¹⁸

¹⁸To reduce the convergence time when the value n is large a re-synchronization process can be used. The AP simply transmits a new unique backoff count to each station, which all the stations start to use at a specified time.

TABLE II
PARAMETERS USED TO OBTAIN NUMERICAL ANALYSIS RESULTS

Parameters	Value	Parameters	Value	Parameters	Value
Bit rate for Data frames	54 Mbps	Empty slot time	9 μ s	Preamble signal duration	16 μ s
Bit rate for ACK frames	6 Mbps	SIFS time	16 μ s	PLCP header duration	4 μ s
UDP payload	1400 bytes	DIFS time	34 μ s	W_0	16
UDP header + IP header	28 bytes	MAC header	34 bytes	W_m	1024

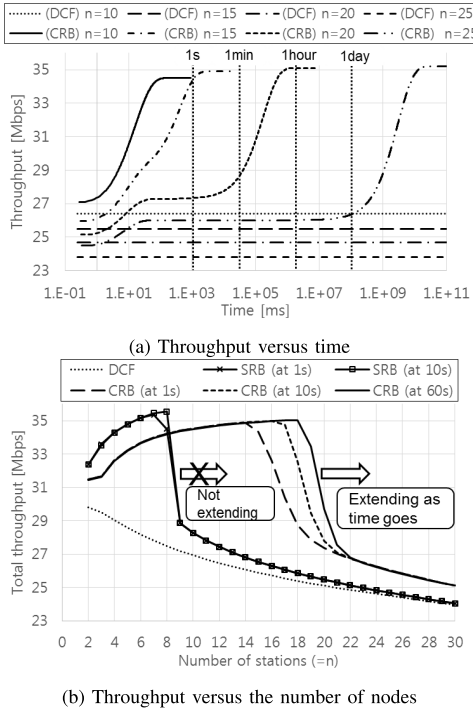


Fig. 14. Analysis results on total throughput.

V. SIMULATION AND NUMERICAL RESULTS

In order to validate the numerical analysis, we have developed a network simulator based on the Network Simulator-3 (NS-3).¹⁹ The NS-3 Wi-Fi module [25] has been modified to implement the CRB protocol. The parameters used in simulation are summarized in Table III.

Fig. 15 shows four different simulation scenarios. First, in a simulation setup shown in Fig. 15a, there is no hidden node, and the channel condition is assumed to be perfect (i.e. no frame errors caused by channel fading or other effects). Random values selected from a triangular distribution are used for the distances from the AP to each of the stations, which is consistent with a circular coverage region. Second, Fig. 15b shows a simulation setup for testing backward compatibility

to the DCF protocol.²⁰ In this paper, backward compatibility means an improvement of total throughput performance of the wireless network where the nodes operating in CRB coexist fairly with the nodes operating using DCF. Third, using the simulation setup presented in Fig. 15c, we observe the effects of hidden nodes on the performance of CRB. Each of the stations in group 1 in Fig. 15c can neither decode nor sense carrier signals from the stations in group 2, and vice versa. Lastly, Fig. 15(d) shows the simulation configuration for testing CRB in two overlapped APs.

A. CRB Nodes Without Hidden Nodes

Fig. 16 shows simulation results on total throughput obtained for the setup shown in Fig. 15a. In this case, a 54 Mbps constant rate was used for transmitting data frames, and a 6 Mbps constant rate was used for transmitting ACK frames. Because of the network needing to settle into a collision free state, only statistics obtained for the last 0.2 second of each repeated simulation were used to draw simulation results.²¹ Fig. 16a shows that the total throughput when using CRB outperforms that of using DCF, as the offered load²² per station increases above 2.7 Mbps. Fig. 16b shows that when $n = 16$, the total throughput of CRB increases from 32.4 Mbps to 34.8 Mbps as the simulation time increases from 1 second to 60 seconds. In addition, we see that when the value n is larger than 8, the throughput performance when using CRB outperforms that of using SRB.

B. Mixed Nodes Without Hidden Nodes

Fig. 17 shows simulation results for the mixed node setup shown in Fig. 15b. In this simulation, a 54 Mbps constant rate was used for transmitting data frames, and a 6 Mbps constant rate was used for transmitting ACK frames. In Fig. 17, throughput ratio (which means the total throughput of the mixed network compared to that of the legacy DCF network)

²⁰We assume that there is an additional exchange of information between the AP and each station in connection establishment procedure (e.g. exchange of CRB support bit). By doing so, the AP can use the legacy ACK frame format (i.e. not including CRB field) for legacy nodes, while it uses the proposed ACK frame format (including CRB field) for nodes supporting CRB.

²¹We calculate average values (e.g. average total throughput and average retransmission ratio per packet) by monitoring data frames transmitted for the last 0.2 s. The number of the data frames is larger than 500 in using the parameters in Table III.

²²In this paper, *offered load* means UDP payloads generated by the on/off application per second, and *throughput* means successfully received MAC service data units (MSDUs) per second. The MSDUs include a UDP header and an IP header.

¹⁹NS-3 version 3.25. This is an open source project available at <http://www.nsnam.org>.

TABLE III
SIMULATION PARAMETERS

Parameters	Value	Parameters	Value	Parameters	Value
Wireless standard	IEEE 802.11a PHY	Bandwidth	20 MHz	Frequency channel	5.0 GHz
Transmission queue	Single queue	Traffic model	Full buffer	UDP payload	1400 bytes
Propagation loss model	Log distance	W_0	16	Rx sensitivity	-91 dBm
Available data rates	6, 9, 12, 18, 24, 36, 48, and 54 Mbps	W_m	1024	Transport layer	UDP
		Tx power	16 dBm	BER model	Reference [25]

* BER: Bit Error Rate

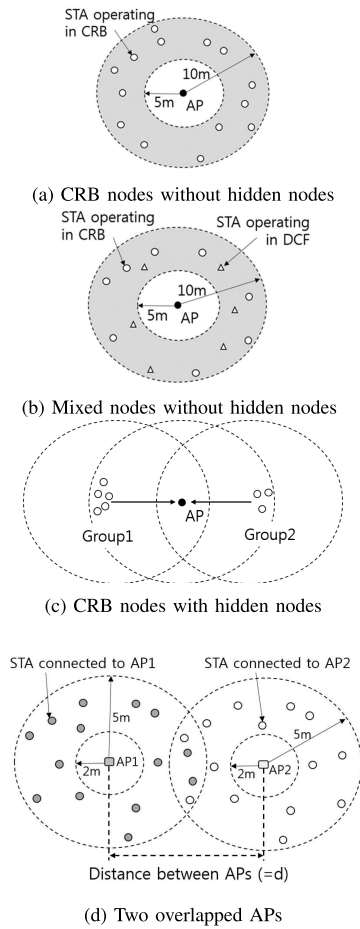
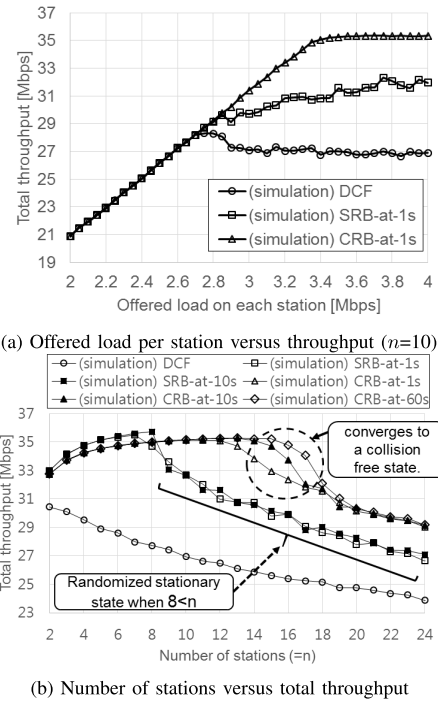


Fig. 15. Two-dimensional simulation setups.

shows that as the proportion of CRB nodes increases, the total throughput increases. For example, when five nodes operating in CRB coexist with five nodes using DCF (i.e. the case 5(5) on the x-axis), the total throughput gain is about 3% compared to that of when all ten nodes use DCF (i.e. the case 0(10)). However, when eight nodes operating in CRB coexist with two nodes using DCF (i.e. 8(2)), the total throughput gain is

Fig. 16. Simulation results on the throughput of CRB, SRB, and DCF in the single AP setup without hidden nodes ($W_0 = 16$ and $W_m = 1024$).

about 12%. In addition, Fig. 17 shows the throughput per each node operating in the mixed network. While the throughput per CRB node increases with the proportion of CRB nodes, the throughput per DCF node decreases. This is because as the proportion of CRB nodes increases, the DCF nodes tend to have a higher collision probability than the CRB nodes. However, regardless of the proportion of CRB nodes, the Jain's fairness index (in terms of average throughput per node) of the mixed network is maintained above 0.95.

C. In the Presence of Hidden Nodes

We performed simulations in the hidden node setup shown in Fig. 15c. In this simulation, an 18 Mbps constant rate was used for transmitting data frames, and a 6 Mbps constant rate was used for transmitting ACK frames. Five different

5850

IEEE TRANSACTIONS ON WIRELESS COMMUNICATIONS, VOL. 16, NO. 9, SEPTEMBER 2017

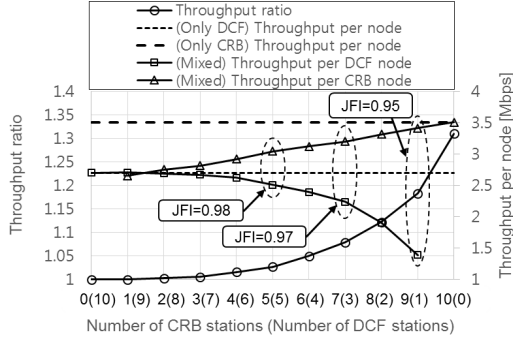
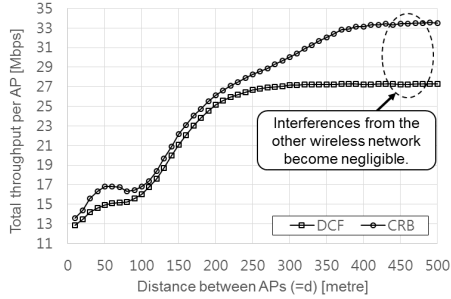


Fig. 17. Simulation results in the mixed nodes scenario.

Fig. 18. Simulation results in the two overlapped APs setup (n per each AP= 10).

combinations have been simulated, i.e. the total number of stations (the number of nodes in group 1, the number of nodes in group 2) was 2(1,1), 5(3,2), 10(7,3), 15(11,4), and 20(14,6). We observed that the throughput when using DCF and that of when using CRB are significantly decreased in the presence of hidden nodes.²³ In addition, the throughput when using CRB in the presence of hidden nodes is very close to that of using DCF in the presence of hidden nodes; however, the throughput when using CRB does not get worse than that of using DCF. We also observed that the retransmission ratio per a data frame becomes very high (i.e. close to one) in the presence of hidden nodes.

D. Two Overlapped APs

The two APs shown in Fig. 15(d) are assumed to be using the same frequency channel, and the number of connected STAs to each of the APs is ten. In this simulation, the log distance propagation loss model with Nakagami fading [24] was applied. A 54 Mbps constant rate was used for transmitting data frames, and a 6 Mbps constant rate was used for

²³A station can detect the presence of a hidden node by overhearing data frames and ACK frames, and it can inform the AP of the fact once in a while by transmitting a short and unique busytone signal just after receiving a specific beacon frame. We think that a unique subcarrier can be assigned to each station by the AP for this purpose in the connection establishment procedure. A similar use of unique subcarriers among stations (sharing a single AP) for notifying some information to the AP while not causing a collision can also be found in [26]. In this way, the AP can be made aware of the hidden node, and the AP can start to operate using CRB when no hidden node has been detected for a specific time period.

transmitting ACK frames. Fig. 18 is obtained from the average values of the last 0.2 second of each repeated simulation. We see that when the distance between the two APs ($= d$) varies from 5 meters to 500 meters, the throughput when using CRB is always higher than that of using DCF.

VI. DISCUSSION AND CONCLUSIONS

In this paper, we proposed the centralized random backoff protocol and evaluated its performance. The evaluation results showed that when 1 second convergence time is allowed, 14 nodes using CRB can operate in a collision free state without changing the contention window size. Moreover, as time increases, the number of nodes that can operate in a collision free state increases (up to the maximum contention window size). However, in the deterministic backoff, the maximum number of nodes that can operate in a collision free state is limited to 8. Otherwise, it requires dynamic adjustment of the ring size when the number of nodes is varying. However, timely adjustment of the optimum ring size is a very complex issue, and it might be ineffective in practical wireless networks. Because of this CRB is more effective than SRB when the number of nodes varies with time. As future work, an *adaptive* VBA will be studied that resolves the lengthy convergence time issue when the value n is large. In addition, the fairness in the mixed network scenario should be improved, and a finite retransmission limit should be considered. We think CRB could be considered to enable efficient device to device (D2D) communications in unlicensed channels.

APPENDIX A

PROOF OF $D_i^l|_{(1st\ slot)}$

Assuming $m = 6$, the scalar $D_0^l|_{(1st\ slot)}$ (i.e. the probability of selecting a new non-zero SBC in Range 0 in the first successful slot time when the number of SBC is l) is obtained by equation (26), as shown at the top of the next page, where the numerator $(W_0 - N_0^l - 1)$ represents available (i.e. non-allocated) non-zero numbers in Range 0. Equation (26) can be rewritten as relation (27), as shown at the top of the next page, when $i = 0$.

Note that although the value of $D_i^l|_{(1st\ slot)}$ is expressed by the two variables N_i^l and Q_i^l in equation (27), considering equation (1) we find that the value of $D_i^l|_{(1st\ slot)}$ can be expressed by only N_i^l . Now, equations (4) and (27) can be used to obtain equation (5).

APPENDIX B

PROOF OF $b_{0,0}$

The state transition probabilities of the Markov Chain model depicted in Fig. 11 are given by the equation (9). Based on this, we obtain (28), as shown at the top of the next page. If the value of l is zero in the equation (28), then $P_0^l = 1$ and $P_i^l = 0$ (given $i \in [1, m]$). In this case, the equation (28) becomes identical to that of legacy nodes presented in [2]. From the equations (10) and (28), we see equations in (29), as shown at the top of the next page. Using the equations in (29), we rewrite (28) as (30), as shown at the top of the next page.

$$\begin{aligned}
D_0^l | (1st \text{ slot}) &= \left(\frac{W_0 - N_0^l - 1}{W_0} \right) + Q_0^l \left(\frac{W_0 - N_0^l - 1}{W_1} \right) + Q_0^l Q_1^l \left(\frac{W_0 - N_0^l - 1}{W_2} \right) \\
&+ Q_0^l Q_1^l Q_2^l \left(\frac{W_0 - N_0^l - 1}{W_3} \right) + Q_0^l Q_1^l Q_2^l Q_3^l \left(\frac{W_0 - N_0^l - 1}{W_4} \right) \\
&+ Q_0^l Q_1^l Q_2^l Q_3^l Q_4^l \left(\frac{W_0 - N_0^l - 1}{W_5} \right) + Q_0^l Q_1^l Q_2^l Q_3^l Q_4^l Q_5^l \left(\frac{W_0 - N_0^l - 1}{W_6} \right) \frac{1}{1 - Q_6^l}
\end{aligned} \quad (26)$$

$$D_i^l | (1st \text{ slot}) = \begin{cases} (W_0 - N_0^l - 1) \left(\frac{1}{W_0} + \sum_{y=0}^{m-2} \left(\frac{\prod_{k=0}^y Q_k^l}{W_{y+1}} \right) + \frac{\prod_{k=0}^{m-1} Q_k^l}{W_m(1 - Q_m^l)} \right) & i = 0 \\ (W_{i-1} - N_i^l) \left(\sum_{y=i-1}^{m-2} \left(\frac{\prod_{k=0}^y Q_k^l}{W_{y+1}} \right) + \frac{\prod_{k=0}^{m-1} Q_k^l}{W_m(1 - Q_m^l)} \right) & 1 \leq i < m \\ (W_{m-1} - N_m^l) \frac{\prod_{k=0}^{m-1} Q_k^l}{W_m(1 - Q_m^l)} & i = m \end{cases} \quad (27)$$

$$b_{i,k} = \frac{W_i - k}{W_i} \begin{cases} (1-p)P_i^l \sum_{j=0}^m b_{j,0} & i = 0 \\ pb_{i-1,0} + (1-p)P_i^l \sum_{j=0}^m b_{j,0} & 0 < i < m \\ p(b_{m-1,0} + b_{m,0}) + (1-p)P_i^l \sum_{j=0}^m b_{j,0} & i = m \end{cases} \quad (28)$$

$$\begin{aligned}
b_{i,0} &= pb_{i-1,0} + b_{0,0} \frac{P_i^l}{P_0^l} \rightarrow b_{i,0} = b_{0,0} \left(p^i + \sum_{j=0}^{i-1} p^{i-j-1} \frac{P_{j+1}^l}{P_0^l} \right) \quad 0 < i < m \\
(1-p)b_{m,0} &= pb_{m-1,0} + b_{0,0} \frac{P_m^l}{P_0^l} \rightarrow b_{m,0} = \frac{b_{0,0}}{(1-p)} \left(p^m + \sum_{j=0}^{m-1} p^{m-j-1} \frac{P_{j+1}^l}{P_0^l} \right) \quad i = m
\end{aligned} \quad (29)$$

$$b_{i,k} = b_{0,0} \frac{W_i - k}{W_i} \begin{cases} 1 & i = 0 \\ p^i + \sum_{j=0}^{i-1} (p^{i-1-j}) \frac{P_{j+1}^l}{P_0^l} & 1 \leq i < m \\ \frac{p^m}{1-p} + \sum_{j=0}^{m-1} (p^{m-1-j}) \frac{P_{j+1}^l}{(1-p)P_0^l} & i = m \end{cases} \quad (30)$$

The equation (30) shows that all the values of $b_{i,k}$ can be expressed as a function of $b_{0,0}$, p , and P_i^l . Now, by imposing the normalization condition (31) we obtain $b_{0,0}$ as (11),

$$\begin{aligned}
1 &= \sum_{i=0}^m \sum_{k=0}^{W_i-1} b_{i,k} = \sum_{k=0}^{W_0-1} b_{0,k} + \sum_{i=1}^{m-1} \sum_{k=0}^{W_i-1} b_{i,k} + \sum_{k=0}^{W_m-1} b_{m,k} \\
&= b_{0,0} \sum_{k=0}^{W_0-1} \frac{W_0 - k}{W_0} \\
&+ b_{0,0} \sum_{i=1}^{m-1} \sum_{k=0}^{W_i-1} \left[\frac{W_i - k}{W_i} \left(p^i + \sum_{j=0}^{i-1} \frac{(p^{i-1-j}) P_{j+1}^l}{P_0^l} \right) \right] \\
&+ b_{0,0} \sum_{k=0}^{W_m-1} \frac{W_m - k}{W_m} \left(\frac{p^m}{1-p} + \sum_{j=0}^{m-1} \frac{(p^{m-1-j}) P_{j+1}^l}{(1-p)P_0^l} \right)
\end{aligned}$$

$$\begin{aligned}
&= b_{0,0} \frac{W_0 + 1}{2} + b_{0,0} \sum_{i=1}^{m-1} \left[\frac{W_i + 1}{2} \left(p^i + \sum_{j=0}^{i-1} f_i^j(l) \right) \right] \\
&+ b_{0,0} \frac{W_m + 1}{2} \left(\frac{p^m}{1-p} + \sum_{j=0}^{m-1} f_m^j(l) \right)
\end{aligned} \quad (31)$$

where $f_i^j(l) = (p^{i-1-j}) P_{j+1}^l / P_0^l$ for short.

ACKNOWLEDGMENT

The authors would like to thank the editors (Prof. A. Banchs and Prof. G. Bianchi) and four anonymous reviewers for helpful comments that have improved the quality of the paper. All data used within this publication can be accessed at: <http://dx.doi.org/10.7488/ds/2068>.

REFERENCES

- [1] A. Gummalla and J. Limb, "Wireless medium access control protocols," *IEEE Commun. Surveys Tuts.*, vol. 9, no. 2, pp. 1311–1321, 2nd Quart. 2000.
- [2] G. Bianchi, "Performance analysis of the IEEE 802.11 distributed coordination function," *IEEE J. Sel. Areas Commun.*, vol. 18, no. 3, pp. 535–547, Dec. 2000.
- [3] P. Chatzimisios, A. Boucouvalas, and V. Vitsas, "IEEE 802.11 packet delay-a finite retry limit analysis," in *Proc. IEEE GLOBECOM*, Dec. 2003, pp. 950–954.
- [4] Y. Zheng, K. Lu, D. Wu, and Y. Fang, "Performance analysis of IEEE 802.11 DCF in imperfect channels," *IEEE Trans. Veh. Technol.*, vol. 55, no. 5, pp. 1648–1656, Sep. 2006.
- [5] D. Malone, K. Duffy, and D. Leith, "Modeling the 802.11 distributed coordination function in nonsaturated heterogeneous conditions," *IEEE/ACM Trans. Netw.*, vol. 15, no. 1, pp. 159–172, Nov. 2007.
- [6] E. Felemban and E. Ekici, "Single hop IEEE 802.11 DCF analysis revisited: Accurate modeling of channel access delay and throughput for saturated and unsaturated traffic cases," *IEEE Trans. Wireless Commun.*, vol. 10, no. 10, pp. 3256–3266, May 2011.
- [7] G. Bianchi and I. Tinnirello, "Kalman filter estimation of the number of competing terminals in an IEEE 802.11 network," in *Proc. IEEE INFOCOM*, Apr. 2003, pp. 844–852.
- [8] A. Toledo, T. Vercouteren, and X. Wang, "Adaptive optimization of IEEE 802.11 DCF based on Bayesian estimation of the number of competing terminals," *IEEE Trans. Mobile Comput.*, vol. 5, no. 9, pp. 1283–1296, Sep. 2006.
- [9] F. Cali, M. Conti, and E. Gregori, "Dynamic tuning of the IEEE 802.11 protocol to achieve a theoretical throughput limit," *IEEE/ACM Trans. Netw.*, vol. 80, no. 6, pp. 166–188, Dec. 2000.
- [10] Z. Haas and J. Deng, "On optimizing the backoff interval for random access schemes," *IEEE Trans. Commun.*, vol. 51, no. 12, pp. 2081–2090, Feb. 2003.
- [11] C. Wang, B. Li, and L. Li, "A new collision resolution mechanism to enhance the performance of IEEE 802.11 DCF," *IEEE Trans. Veh. Technol.*, vol. 53, no. 4, pp. 1235–1246, Jul. 2004.
- [12] M. Heusse, F. Rousseau, R. Guillier, and A. Duda, "Idle sense: An optimal access method for high throughput and fairness in rate diverse wireless LANs," *ACM SIGCOMM Comput. Commun. Rev.*, vol. 35, no. 4, pp. 121–132, 2005.
- [13] D. Deng, C. Ke, H. Chen, and Y. Huang, "Contention window optimization for IEEE 802.11 DCF access control," *IEEE Trans. Wireless Commun.*, vol. 7, no. 12, pp. 5129–5135, Jul. 2008.
- [14] *The IEEE 802.11ax Task Group*, accessed on Jun. 2017. [Online]. Available: http://www.ieee802.org/11/Reports/tgax_update.htm
- [15] J. Choi, J. Yoo, and S. Choi, "EBA: An enhancement of the IEEE 802.11 DCF via distributed reservation," *IEEE Trans. Mobile Comput.*, vol. 4, no. 4, pp. 378–390, Jul. 2005.
- [16] J. Lee and J. Walrand, "Zero collision random backoff algorithm," in *Proc. IEEE INFOCOM*, 2007, pp. 120–128.
- [17] Y. He, J. Sun, R. Yuan, and W. Gong, "A reservation based backoff method for video streaming in 802.11 home networks," *IEEE J. Sel. Areas Commun.*, vol. 28, no. 3, pp. 332–343, Jan. 2010.
- [18] J. Barcelo, A. Toledo, C. Cano, and M. Oliver, "Fairness and convergence of CSMA with enhanced collision avoidance (ECA)," in *Proc. IEEE Int. Conf. Commun. (ICC)*, vol. 4, Dec. 2010, pp. 511–523.
- [19] J. Barcelo, B. Bellata, C. Cano, A. Sfairopoulou, M. Oliver, and K. Verma, "Towards a collision-free WLAN: Dynamic parameter adjustment in CSMA/E2CA," *EURASIP J. Wireless Commun. Netw.*, vol. 1, no. 1, p. 708617, 2011.
- [20] Y. He, J. Sun, X. Ma, A. Vasilakos, R. Yuan, and W. Gong, "Semi-random backoff: Towards resource reservation for channel access in wireless LANs," *IEEE/ACM Trans. Netw.*, vol. 128, no. 1, pp. 1610–1618, Feb. 2013.
- [21] S. Misra and M. Khatua, "Semi-distributed backoff: Collision-aware migration from random to deterministic backoff," *IEEE Trans. Mobile Comput.*, vol. 14, no. 5, pp. 1071–1084, Jan. 2015.
- [22] M. F. Tuysuz and H. A. Mantar, "Exploiting the channel using uninterrupted collision-free MAC adaptation over IEEE 802.11 WLANs," *Wireless Commun. Mobile Comput.*, vol. 91, no. 5, pp. 1227–1230, 2015.
- [23] J. Kim, D. Laurenson, and J. Thompson, "Fair and efficient full duplex MAC protocol based on the IEEE 802.11 DCF," *IEEE PIMRC*, vol. 90, no. 3, pp. 538–548, Mar. 2016.
- [24] M. Stoffers and G. Riley, "Comparing the ns-3 propagation models," in *Proc. IEEE Int. Symp. Modeling, Anal. Simulation Comput. Telecommun. Syst.*, Aug. 2012, pp. 61–67.
- [25] M. Lacage and T. Henderson, "Yet another network simulator," in *Proc. Workshop NS-2, IP Netw. Simulator, ACM*, 2006, p. 12.
- [26] S. Sen, R. Choudhury, and S. Nelakuditi, "No time to countdown: Migrating backoff to the frequency domain," in *Proc. 17th Annu. Int. Conf. Mobile Comput. Netw. ACM*, 2011, pp. 241–252.



Jinho D. Kim is currently pursuing the Ph.D. degree with the School of Engineering, University of Edinburgh. From 2008 to 2009, he was a Software Developer with Digital Stream Technology, where he implemented various network protocols, such as SNMP/MIBs and RTP/RTSP, and optimized micro Linux systems, such as digital cable box. From 2009 to 2014, he was a Research Engineer with LG Electronics, where he developed standard Wi-Fi applications, such as Miracast. His interests lie in fair and efficient network protocols.



David I. Laurenson is currently a Senior Lecturer with the University of Edinburgh, U.K. His interests lie in mobile communications at the link layer this includes measurements, analysis and modeling of channels and MAC protocols, whilst at the network layer this includes provision of mobility management and quality of service support. His research extends to practical implementation of wireless networks to other research fields, such as prediction of fire spread using wireless sensor networks, deployment of communication networks for distributed control of power distribution networks, and sensor networks for environmental monitoring and structural analysis. He is the U.K. Representative for the International Union of Radio Science Commission C, Radiocommunication Systems.



John S. Thompson (F'16) is currently a Professor in signal processing and communications with the School of Engineering, University of Edinburgh. He specializes in antenna array processing, cooperative communications systems, and energy efficient wireless communications. He has authored in excess of 300 papers on these topics, including 100 journal paper publications. He is currently the Project Coordinator for the EU Marie Curie International Training Network Project ADVANTAGE, which studies how communications and power engineering can provide future smart grid systems. He was an elected Member-at-Large for the Board of Governors of the IEEE Communications Society from 2012 to 2014, the second largest IEEE Society. He was a Distinguished Lecturer on the topic of energy efficient communications and smart grid for the IEEE Communications Society from 2014 to 2015. In 2016, he was elevated to fellow of the IEEE, for contributions to multiple antenna and multi-hop wireless communications. He is an Editor of the Green Communications and Computing Series that appears regularly in the *IEEE Communications Magazine*.

Appendix B

Proof of the Probability $D_i^l|_{(1^{st} \text{ slot})}$

Assuming $m = 6$, the scalar $D_0^l|_{(1^{st} \text{ slot})}$ (i.e. the probability of selecting a new non-zero SBC in Range 0 in the first successful slot time when the number of SBC is l) is obtained by equation (B.1), where the numerator $(W_0 - N_0^l - 1)$ represents available (i.e. non-allocated) non-zero numbers in Range 0. Equation (B.1) can be rewritten as relation (B.2) of when $i = 0$.

Note that although the value of $D_i^l|_{(1^{st} \text{ slot})}$ is expressed by the two variables N_i^l and Q_i^l in equation (B.2), considering equation (4.1) we find that the value of $D_i^l|_{(1^{st} \text{ slot})}$ can be expressed by only N_i^l . Now, equations (4.4) and (B.2) can be used to obtain equation (4.5).

$$\begin{aligned}
 D_0^l|_{(1^{st} \text{ slot})} = & \left(\frac{W_0 - N_0^l - 1}{W_0} \right) + Q_0^l \left(\frac{W_0 - N_0^l - 1}{W_1} \right) + Q_0^l Q_1^l \left(\frac{W_0 - N_0^l - 1}{W_2} \right) \\
 & + Q_0^l Q_1^l Q_2^l \left(\frac{W_0 - N_0^l - 1}{W_3} \right) + Q_0^l Q_1^l Q_2^l Q_3^l \left(\frac{W_0 - N_0^l - 1}{W_4} \right) \\
 & + Q_0^l Q_1^l Q_2^l Q_3^l Q_4^l \left(\frac{W_0 - N_0^l - 1}{W_5} \right) + Q_0^l Q_1^l Q_2^l Q_3^l Q_4^l Q_5^l \left(\frac{W_0 - N_0^l - 1}{W_6} \right) \frac{1}{1 - Q_6^l}
 \end{aligned}
 \tag{B.1}$$

$$D_i^l|_{(1^{\text{st}} \text{ slot})} = \begin{cases} (W_0 - N_0^l - 1) \left(\frac{1}{W_0} + \sum_{y=0}^{m-2} \left(\frac{\prod_{k=0}^y Q_k^l}{W_{y+1}} \right) + \frac{\prod_{k=0}^{m-1} Q_k^l}{W_m(1 - Q_m^l)} \right) & i = 0 \\ (W_{i-1} - N_i^l) \left(\sum_{y=i-1}^{m-2} \left(\frac{\prod_{k=0}^y Q_k^l}{W_{y+1}} \right) + \frac{\prod_{k=0}^{m-1} Q_k^l}{W_m(1 - Q_m^l)} \right) & 1 \leq i < m \\ (W_{m-1} - N_m^l) \frac{\prod_{k=0}^{m-1} Q_k^l}{W_m(1 - Q_m^l)} & i = m \end{cases} \quad (\text{B.2})$$

Appendix C

Proof of the Probability $b_{0,0}$

The state transition probabilities of the Markov chain model depicted in Fig. 4.10 are given by the equation (4.9). Based on this, equation (C.1) is obtained. If the value l is zero in the equation (C.1), then $P_0^l = 1$ and $P_i^l = 0$ (given $i \in [1, m]$). In this case, the equation (C.1) becomes identical to that of legacy nodes presented in [22]. From the equations (4.10) and (C.1), we see equations in (C.2). Using the equations in (C.2), we rewrite (C.1) as (C.3).

$$b_{i,k} = \frac{W_i - k}{W_i} \begin{cases} (1-p)P_i^l \sum_{j=0}^m b_{j,0} & i = 0 \\ pb_{i-1,0} + (1-p)P_i^l \sum_{j=0}^m b_{j,0} & 0 < i < m \\ p(b_{m-1,0} + b_{m,0}) + (1-p)P_i^l \sum_{j=0}^m b_{j,0} & i = m \end{cases} \quad (C.1)$$

$$\begin{aligned}
b_{i,0} &= pb_{i-1,0} + b_{0,0} \frac{P_i^l}{P_0^l} \rightarrow b_{i,0} = b_{0,0} \left(p^i + \sum_{j=0}^{i-1} p^{i-j-1} \frac{P_{j+1}^l}{P_0^l} \right) & 0 < i < m \\
(1-p)b_{m,0} &= pb_{m-1,0} + b_{0,0} \frac{P_m^l}{P_0^l} \rightarrow b_{m,0} = \frac{b_{0,0}}{(1-p)} \left(p^m + \sum_{j=0}^{m-1} p^{m-j-1} \frac{P_{j+1}^l}{P_0^l} \right) & i = m
\end{aligned} \tag{C.2}$$

$$b_{i,k} = b_{0,0} \frac{W_i - k}{W_i} \begin{cases} 1 & i = 0 \\ p^i + \sum_{j=0}^{i-1} (p^{i-1-j}) \frac{P_{j+1}^l}{P_0^l} & 1 \leq i < m \\ \frac{p^m}{1-p} + \sum_{j=0}^{m-1} (p^{m-1-j}) \frac{P_{j+1}^l}{(1-p)P_0^l} & i = m \end{cases} \tag{C.3}$$